



Universiteit  
Leiden  
The Netherlands

## Probing spatial heterogeneity in supercooled glycerol and temporal heterogeneity with single-molecule FRET in polyprolines

Xia, T.

### Citation

Xia, T. (2010, March 25). *Probing spatial heterogeneity in supercooled glycerol and temporal heterogeneity with single-molecule FRET in polyprolines*. *Casimir PhD Series*. Retrieved from <https://hdl.handle.net/1887/15122>

Version: Corrected Publisher's Version

License: [Licence agreement concerning inclusion of doctoral thesis in the Institutional Repository of the University of Leiden](#)

Downloaded from: <https://hdl.handle.net/1887/15122>

**Note:** To cite this publication please use the final published version (if applicable).

Probing spatial heterogeneity in supercooled  
glycerol and temporal heterogeneity with  
single-molecule FRET in polyprolines

PROEFSCHRIFT

ter verkrijging van  
de graad van Doctor aan de Universiteit Leiden,  
op gezag van de Rector Magnificus prof. mr. P. F. van der Heijden,  
volgens besluit van het College voor Promoties  
te verdedigen op donderdag 25 maart 2010  
klokke 11:15 uur

door

**Ted (Tie) Xia**  
geboren te Dalian, China  
in 1977

**Promotiecommissie:**

Promotor: Prof. Dr. M. A. G. J. Orrit  
Overige Leden: Prof. Dr. B. Schuler (Universität Zürich)  
Prof. Dr. J. M. van Ruitenbeek  
Prof. Dr. E. J. J. Groenen  
Prof. Dr. M. van Hecke  
Prof. Dr. T. Schmidt

The presented work is part of the research program of the Stichting voor Fundamenteel Onderzoek der Materie (FOM), which is financially supported by the Nederlandse Organisatie voor Wetenschappelijk Onderzoek (NWO).

Casimir PhD Series, Delft-Leiden, 2010-03  
ISBN: 978-90-8593-068-6

# Contents

<b>1</b>	<b>Introduction</b>	<b>1</b>
1.1	Glass transition and heterogeneity . . . . .	1
1.2	Single-molecule fluorescence and temperature-cycle microscopy	2
1.3	Outline of the thesis . . . . .	5
<b>2</b>	<b>Soft glassy rheology of supercooled liquids</b>	<b>9</b>
2.1	Introduction . . . . .	10
2.2	Experimental methods . . . . .	11
2.2.1	Sample preparation . . . . .	11
2.2.2	Design of the Couette cell . . . . .	12
2.3	Results . . . . .	12
2.3.1	Viscoelastic behavior and yield stress . . . . .	12
2.3.2	Phenomenological model . . . . .	14
2.3.3	Shear thinning and rejuvenation . . . . .	17
2.4	Discussion . . . . .	20
2.5	Appendix . . . . .	24
2.5.1	Viscosities of glycerol and <i>o</i> -terphenyl . . . . .	24
2.5.2	Onset of solid-like behavior in glycerol . . . . .	24
2.5.3	Experimental details . . . . .	26
<b>3</b>	<b>Aging and solidification of supercooled glycerol</b>	<b>29</b>
3.1	Introduction . . . . .	30
3.2	Experimental methods . . . . .	31
3.3	Results . . . . .	32
3.3.1	Viscosity measurements . . . . .	32
3.3.2	Solidification and importance of cooling rate . . . . .	32
3.3.3	Measurements in the plate-plate geometry . . . . .	35
3.4	Discussion . . . . .	39
3.5	Conclusion . . . . .	42
<b>4</b>	<b>Micron-sized structure in a thin glycerol film revealed by fluorescent probes</b>	<b>43</b>
4.1	Introduction . . . . .	44

4.2	Experimental methods . . . . .	45
4.3	Results . . . . .	46
4.4	Discussion . . . . .	52
4.5	Conclusion . . . . .	55
<b>5</b>	<b>Small-angle neutron scattering on supercooled glycerol</b>	<b>57</b>
5.1	Introduction . . . . .	58
5.2	Experimental methods . . . . .	60
5.3	Results and discussion . . . . .	61
5.4	Conclusion . . . . .	66
<b>6</b>	<b>Temperature-cycle microscopy of single-molecule FRET in polyprolines</b>	<b>67</b>
6.1	Introduction . . . . .	68
6.2	Experimental methods . . . . .	72
6.2.1	Sample preparation . . . . .	72
6.2.2	Optical setup . . . . .	73
6.2.3	Heating calibration . . . . .	75
6.2.4	Data analysis . . . . .	76
6.3	Results . . . . .	77
6.4	Discussion . . . . .	85
6.5	Conclusion . . . . .	87
<b>7</b>	<b>Summary</b>	<b>89</b>
7.1	Heterogeneity in supercooled liquids . . . . .	89
7.2	Temperature-cycle microscopy of single-molecule FRET in poly- prolines . . . . .	91
	<b>References</b>	<b>93</b>
	<b>Samenvatting</b>	<b>107</b>
	<b>List of Publications</b>	<b>113</b>
	<b>Curriculum Vitae</b>	<b>115</b>
	<b>Nawoord</b>	<b>117</b>

# 1 Introduction

The work presented in this thesis contains two lines of research. On the one hand, we investigate heterogeneity in supercooled glycerol by means of rheometry, fluorescence imaging, and small-angle neutron scattering. This study was triggered by earlier single-molecule work on supercooled glycerol by Zonderman et al. [1]. On the other hand, we study the conformational dynamics of polyprolines by single-molecule FRET (Förster resonance energy transfer) combined with temperature-cycle microscopy, a novel technique developed in our group, and demonstrate the potential of this new method to address complex molecular dynamics, for example the dynamics of protein-folding, at the single-molecule level.

## 1.1 Glass transition and heterogeneity

A liquid below its standard freezing point will generally crystallize in the presence of a seed crystal or nucleus around which a crystal structure can form. However, lacking any such nucleus, the liquid phase can be maintained all the way down to the temperature at which the system becomes so viscous that it freezes on the accessible experimental time scales, forming an amorphous (non-crystalline) solid, a continuous transition known as the glass transition. Such a liquid-glass transition is not a transition between states at thermodynamic equilibrium. The true equilibrium state is widely believed to be always crystalline. Therefore, the glass transition is considered as a dynamic phenomenon only.

Although glass has been produced for about 3500 years, the full structural description of how a liquid cools down to a glass is still missing. Early models assume the existence of cooperatively rearranging regions (CRR) in glass-forming systems below their critical temperature [2], a temperature at which “normal” and “complex” liquid behaviors are distinctly separated. A “normal” liquid behavior means that the time dependence of the relaxation dynamics can be described by an exponential function, whereas for a “complex” liquid behavior a stretched exponential function is typically employed. Within the CRRs the molecules do not relax independently of one another. Due to a small free volume at low temperatures, close to  $T_g$ , the motion of a particular

molecule depends to a large degree on that of its neighbors [3]. The length scale of CRRs is generally estimated to be a few nanometers [4] and is assumed to increase for decreasing temperatures. Such CRRs are thought to be the origin of the observed dynamic heterogeneities in glass-forming systems [4, 5]. The system is dynamically heterogeneous if it is possible to select a dynamically distinguishable subensemble by experiments or computer simulation [6]. Although such heterogeneities have been reported both experimentally and numerically, the associated length and time scales are still debated. Indirect experiments, mainly from NMR [7, 8] and dielectric relaxation [9, 10], suggest that the length scale of dynamical heterogeneity is on the order of a few nanometers and the time scale comparable to molecular reorientation times ( $\alpha$ -relaxation). However, optical experiments, notably light and X-ray scattering [11, 12], polarized hole-burning [13, 14] and single-molecule spectroscopy [15, 16], reveal much slower relaxations than  $\alpha$ -relaxation and longer length scales, typically 100 nm.

Our group recently investigated the local relaxation of supercooled glycerol at temperatures up to 30 K above its glass transition (190 K) by following the rotational diffusion of individual (fluorescent) probe molecules embedded in the host matrix [1]. These experiments showed that each individual probe molecule rotates at different rates in the supercooled glycerol and that the breadth of rotation times spans nearly one decade, indicating a spatially dynamic heterogeneity. Most strikingly, upon following the rotation of the same molecules as a function of temperature, a long-term memory effect was revealed, i.e., the molecules that rotate faster than the average remain faster and the molecules that rotate slower remain slower than the average, irrespective of the changes of temperature. The associated lifetime is on the order of days, about a million times longer than the  $\alpha$ -relaxation time of the host molecule. Such long-lived heterogeneity strongly suggests that some nearly static structures already develop at temperatures well above the glass transition. Motivated by this surprising finding, we further explored the heterogeneity in supercooled glycerol by different techniques, such as rheometry, fluorescence imaging, and small-angle neutron scattering. This study constitutes the first line of research in this thesis.

## 1.2 Single-molecule fluorescence and temperature-cycle microscopy

Pioneered by Moerner and Orrit [17–19], single-molecule spectroscopy has evolved from a specialized optical spectroscopy at low temperatures in the

early nineties of last century into a versatile and powerful tool to address problems in physics, chemistry, biology, and materials science at present. Because they are inherently free from ensemble averaging, single-molecule approaches can reveal a full variety of nanoscale environments in the system of interest, together with the full extent of the distributions of molecular or local parameters. This makes the techniques highly suitable to study systems in which inhomogeneity is intrinsic to the structure or dynamics of the materials, for example glassy materials and polymers. Examples of such applications in soft and complex matter can be found in a recent review article [20]. Another advantage of single-molecule studies is that since individual molecules can be addressed independently, a synchronization step is no longer required, which makes the design of the single-molecule measurements less troublesome than conventional ensemble experiments.

The application of single-molecule spectroscopy to biological problems is currently expanding rapidly. Hereafter, the discussion will mainly focus on single-molecule fluorescence spectroscopy. Other optical approaches not based on fluorescence such as the detection of photothermal [21–24] or interferometric scattering [25–27] signals from nano-objects (nanogold particles, quantum dots, or even molecules), which play an equally important role in biological applications, are outside the scope of this thesis. Fluorescence has been used for more than one century in many disciplines, ranging from analytical chemistry, biochemistry to medicine. The nearly non-invasive nature of fluorescence is particularly appreciated by cell biologists, who use fluorescence to image labeled biomolecules in a living cell in their daily work. Thanks to the green fluorescent protein and its variants [28, 29] and to advances in genetic engineering, it is now virtually possible to fluorescently label any protein in any organism, which further advances the understanding of some important biological processes such as cell division, gene expression and regulation, and cell signaling at the molecular level. Protein molecules are involved in virtually every biological process. They typically engage in complex and dynamic interactions with other proteins or even other species like DNA/RNA molecules and lipids to fulfill their function. Protein conformations are highly dynamic rather than static, and subtle conformational changes play a crucial role in protein function. Therefore understanding their dynamic behaviors is important for the full description of their functions. However, it is extremely difficult to characterize such heterogeneous dynamics in an ensemble-average experiment, especially when the proteins are involved in multiple-step, multiple-conformation complex chemical interactions and transformations, such as enzymatic reactions, protein-protein interactions and ion-channel membrane pro-



tein processes. Alternatively, single-molecule fluorescence spectroscopy is a powerful approach to probing and analyzing protein conformational dynamics in real time [30–32]. In the design of such experiments, a single dye molecule can be attached to the host biomolecule. By following the temporal fluctuation of the fluorescence intensity, together with the polarization response of the fluorophore, one can obtain the information about the motion and activity of the individual host biomolecule. Probably, the most general approach is to use two fluorophores instead of one, in the form of Förster resonance energy transfer (FRET). The FRET method has proven to be a powerful spectroscopic technique for measuring distances in the range 10 – 75Å [33, 34]. Since the first demonstration of single-molecule FRET by Ha et al. in 1996 [35], there have been many experiments designed for biological applications [36–44]. In the process of FRET, excitation energy of the donor is transferred to the acceptor via dipole-dipole interaction. The efficiency of energy transfer,  $E$ , is given by

$$E = \frac{1}{1 + \left(\frac{R}{R_0}\right)^6} \quad ,$$

where  $R$  is the distance between the donor and acceptor. The distance at which 50 % of the energy is transferred,  $R_0$ , is a function of the properties of the dyes. The distance  $R_0$  contains a contribution from the relative orientation between the two dyes, called  $\kappa^2$ , which may vary from 0 to 4. If the dipole moments of donor and acceptor are free to sample all the possible orientations on a time scale much faster than their radiative lifetimes, a geometric averaging of all the angles will give rise to the value of 2/3 for  $\kappa^2$ . The FRET efficiency,  $E$ , determined through the fluorescence intensities from both the donor and acceptor or the fluorescence lifetime of the donor in the presence and absence of the acceptor, can then be directly related to the inter-dye distance,  $R$ . However, the host molecule may interact with the attached fluorophores, thus restricting their motion. Therefore, one should be cautious when using  $\kappa^2 = 2/3$  for the calculation of  $R$ .

In single-molecule FRET experiments, doubly labeled molecules are either freely diffusing in a solution or immobilized on a surface through a linker. In the former scheme, a confocal microscope is employed to detect photon bursts when the molecule diffuses through the detection volume. The FRET efficiencies from each burst are calculated and the associated distribution can be constructed. However, due to the limited dwell time of the molecules in the detection volume, dynamics on time scales much slower than the characteristic diffusion time of the molecule are not accessible. For this reason, an immobilized scheme is chosen for probing slow dynamics. In this case, indi-

vidual molecules can be addressed one at a time in a confocal configuration or many at the same time via a wide-field imaging setup. Since the molecule is illuminated all the time during the measurements, one limiting factor is the photophysical behavior of the dyes, namely, photoblinking and photobleaching. Photoblinking is the reversible transition of the fluorophore between a fluorescing state and a non- or less-fluorescing state, a “dark” state, which is induced by the excitation light [45]. Photobleaching is the irreversible conversion of a fluorescent molecule into a non-fluorescent entity, which will limit the observation time of the molecules. In addition, since a single molecule can only emit a limited number of photons per second, a certain minimum integration time has to be set in order to detect a signal above the shot noise, which in return restricts the accessible dynamics on the short times. To achieve longer observation windows and access fast dynamics, our group has developed a new type of temperature-cycle microscopy [46]. The method relies on rapid thermal cycling of a microscopic sample to separate the room-temperature conformational evolution of, for example, a single biomolecule from the optical probing of the fluorophore(s), which takes place under cryogenic conditions. That way we want to probe a frozen “snapshot” of the biomolecule at a temperature where the photophysical parameters of the label(s) are more favorable than at room-temperature. The temporal resolution in this case is no longer limited by photon statistics and, instead, is determined by the time it takes to undergo the temperature jump. The second line of research in this thesis involves the first application of this method to study the conformational dynamics of single-molecule FRET-labeled polyprolines.

### 1.3 Outline of the thesis

Chapter 2 describes our first rheological measurements on supercooled glycerol and *ortho*-terphenyl with a home-built rheometer, which is based on a Couette cell (see Figure 2.7). In the experiments, we applied very weak and constant stresses (on the order of 100 Pa) to the sample and the mechanical response was monitored as a function of time. We have identified a solid-like behavior in both materials in the supercooled state, i.e., above the glass transition, suggesting the gradual emergence of an extended solid-like network in the liquid bath. This network stiffens as it ages and can break and melt upon application of large shears, producing all well-known features of soft glassy rheology (yield-stress, shear melting and aging) in the material. The rheological results here are consistent with the earlier single-molecule observation on supercooled glycerol that some nearly static structures already develop at

temperatures well above the glass transition.

Chapter 3 extends the work in Chapter 2 by employing a commercial rheometer to further explore the solidification of supercooled glycerol. The commercial rheometer enables us to perform small strain amplitude oscillatory measurements to avoid the previously observed “breaking event” of the fragile network while measuring its response. We first tried to reproduce the solidification in a Couette cell with similar dimensions as in Chapter 2. We found that an initial slow cooling period was crucial for the formation of the solid-like state. However, as the apparatus compliance, i.e., the deformation of the measurement tools, may limit the maximum measurable rigidity of the sample, we switched to a plate-plate geometry, where gap and plate size were chosen such that the tool compliance is negligible. Another advantage of using the plate-plate configuration is that the sample can be visualized during the measurements. Surprisingly, we could not reliably reproduce the solid-like state in the plate-plate geometry with the thermal profile, which reliably led to the solidification in the Couette cell. Nevertheless, we observed once a slush-like phase that grew from the top plate at the growth speed of the crystal phase. The shear modulus of this slushy phase, however, was two orders of magnitude lower than that of the crystal phase.

Chapter 4 reports on micrometer-sized structures in a thin glycerol film observed by imaging fluorescent probes doped in the host matrix at temperatures close to but above the glass transition temperature. We observed two distinct heterogeneous patterns of the fluorescence intensity, depending on how fast the sample was cooled down. A Swiss-cheese-like pattern in which many micrometer-sized dark spots were nucleated in a bright background was detected in a slowly cooled sample. In contrast, a quickly cooled sample showed a spinodal decomposition pattern where many bright island-like features of micrometer sizes were dispersed in a dark matrix. Those heterogeneous patterns, which are ascribed to differential dye distributions in the glycerol film, can persist for days unless they are heated considerably, pointing to long-lived and micrometer-scale density fluctuations in supercooled glycerol.

Chapter 5 presents the preliminary results of small-angle neutron scattering experiments on solidified glycerol. We have performed two series of experiments on two glycerol samples respectively with thermal histories similar to the one used in Chapter 2. We observed the growth of solid-like structures in one sample only, evidenced by both direct visual inspection and by the scattering spectra. A new peak, centered around  $0.1 \text{ \AA}^{-1}$ , is a hallmark of this solid-like state. It is clearly absent from the pure liquid state and from the crystal at the same temperature.

Chapter 6 reports on the first application of temperature-cycle microscopy in the study of single-molecule FRET in polyprolines. We measured static FRET efficiencies of individual constructs frozen in a thin glycerol film at low temperature, which revealed a broad distribution of FRET efficiency. We tried temperature-cycle measurements on polyproline 6 and we observed the change of FRET efficiency due to the conformational changes induced by the temperature jump. These preliminary results demonstrate that our temperature-cycle microscopy combined with single-molecule FRET labeling has potential for the study of protein-folding dynamics at the single-molecule level.



## 2 Soft glassy rheology of supercooled liquids

**Abstract** – We probe the mechanical response of two supercooled liquids, glycerol and *ortho*-terphenyl, by conducting rheological experiments at very weak stresses. We find a complex fluid behavior suggesting the gradual emergence of an extended, delicate solid-like network in both materials in the supercooled state, i.e., *above* the glass transition. This network stiffens as it ages, and very early in this process it already extends over macroscopic distances, conferring all well-known features of soft glassy rheology (yield-stress, shear thinning, aging) to the supercooled liquids. Such viscoelastic behavior of supercooled molecular glass formers has not been reported before; our results suggest this is because the large stresses in conventional rheology can easily shear-melt the solid-like structure. The work presented here, combined with evidence for long-lived heterogeneity from previous single-molecule studies [Zondervan R, Kulzer F, Berkhout GCG, Orrit M (2007) “Local viscosity of supercooled glycerol near  $T_g$  probed by rotational diffusion of ensembles and single dye molecules”, *Proc Natl Acad Sci USA* 104:12628–12633], has a profound impact on the understanding of the glass transition, since it casts doubt on the widely accepted assumption of the preservation of ergodicity in the supercooled state.

The contents of this chapter have been published:

R. Zondervan, T. Xia, H. van der Meer, C. Storm, F. Kulzer, W. van Saarloos, and M. Orrit, *Proc. Natl. Acad. Sci. USA* **105** (2008) 4993–4998.

## 2.1 Introduction

Many liquids fail to crystallize when they are cooled below their thermodynamic solidification temperature (the melting point of the crystal). Instead, these supercooled liquids become enormously viscous, eventually turning into solid glasses when their glass-transition temperature  $T_g$  is reached. After more than half a century of research, the structural glass transition remains mysterious [47]. It has long been clear that glass formation requires cooperation beyond the molecular scale [4], and is intimately connected with inhomogeneities. The nature, length-scale and timescale of these inhomogeneities are unknown. One may envision them as frozen-in density fluctuations. They cause deviations from pure liquid behavior, and tend to relax by processes known as environmental exchanges. The exchange timescales must be significantly longer than those of the pure liquid. If they exceed experimental times, ergodicity is broken in practice, and the system appears heterogeneous.

Heterogeneity is readily observed in optical experiments on supercooled liquids, notably in light and X-ray scattering [11, 12], polarized hole-burning [13, 14], single-molecule spectroscopy [15, 16], and it appears to relax slowly. Tracking of individual particles in colloidal glasses [48, 49], as well as computer simulations [50–52], provides further evidence for heterogeneity, and confirms that relaxation is driven by collective rearrangements. In parallel, a large body of experimental data [4] from molecular-scale techniques – most importantly NMR [7, 8] and dielectric relaxation [9, 10] spectroscopy – also suggests dynamical heterogeneity, with a length scale that increases upon approaching the glass transition temperature [53]. The latter experiments, however, invariably find relaxation time scales comparable to molecular reorientation times ( $\alpha$ -relaxation), and length scales of a few nanometers only.

Our group has recently studied the local relaxation of supercooled glycerol, up to 30 K above its glass transition, using single-molecule polarization microscopy [1]. The rotational dynamics of individual chromophores provides a nanometer-scale probe of the material in which they are embedded. These experiments showed that different single dye molecules tumble at different rates in the supercooled glycerol in which they are dissolved, with the spread of tumbling times spanning almost one decade. Our most surprising observation was that environmental exchanges were very rare, even over the several hours of a typical measurement. This period is up to about one million times longer than the  $\alpha$ -relaxation time, i. e., the average tumbling time of a glycerol molecule [1]. It is very difficult to reconcile such long exchange times with the picture of a pure liquid, in which all molecules should be equivalent on average. It was therefore suggested [1] that the long memory arises from nearly static

structures, which form a fragile solid-like network dividing the supercooled liquid into heterogeneous “liquid pockets.” Such a scenario naturally explains our previous single-molecule experiments, as well as similar studies in another molecular glass former, *ortho*-terphenyl (OTP) [15]. However, the existence of such static structures is completely at odds with the commonly-held view of supercooled liquids above the rheological glass transition, in which fast environmental exchanges are thought to quickly erase memory effects, and to restore ergodicity. We therefore performed the rheological experiments reported here to test our hypothesis of the presence of an extended solid-like network in supercooled molecular liquids. As it turned out, we indeed found surprising behavior for both supercooled glycerol and OTP.

An embedded solid network can be expected to lead to non-Newtonian rheology, a behavior that is actually the rule in heterogeneous fluid mixtures, gels, suspensions, emulsions, foams, slurries, pastes, quicksand, and surprisingly even in simple fluids close to the critical point [54]. All these systems display distinctly non-liquid-like characteristics such as viscoelasticity, yield stress, shear-thinning, and aging – a combination of features known as “soft glassy rheology” [55]. Similar properties have furthermore been reported in simulations of Lennard–Jones glasses [56]. For the present investigation we chose two archetypal molecular glass formers which were previously studied by single-molecule microscopy [1, 15]: glycerol ( $T_g = 190$  K), which is a comparatively strong glass former due to its extended network of hydrogen bonds, and *ortho*-terphenyl (OTP,  $T_g = 244$  K), whose structure is governed by weaker van der Waals interactions. We indeed find pronounced non-Newtonian behavior, which manifests itself significantly above the glass transition temperature for both of these materials, and we thus demonstrate for the first time that supercooled molecular liquids can exhibit all the hallmarks of soft glassy rheology. The history-dependent behavior shows that such molecular glass formers already exhibit clear signatures of non-ergodic behavior in a significant temperature range above the glass transition temperature.

## 2.2 Experimental methods

### 2.2.1 Sample preparation

Anhydrous glycerol (specified to contain less than 0.1% water) was used as obtained from Sigma-Aldrich, transferred from the newly-opened bottle into the Couette cell (see Figure 2.7) as quickly as possible and then purged repeatedly with dry helium gas. *Ortho*-terphenyl *purissimum* (Fluka, purity greater than 99%) was distilled twice before usage. All rheological samples were kept



under a dry helium atmosphere for the duration of the experiments.

### 2.2.2 Design of the Couette cell

The rheology experiments were conducted with a variable-temperature Couette cell (see Figure 2.7), in which a sample film filled the gap between an inner cylinder and an outer cup. Torque was applied to the cylinder by means of a torsional spring and the viscoelastic response of the sample was deduced from the subsequent movement of the cylinder, which was recorded via the deflection of a laser beam. Additional experimental details can be found in the appendix.

## 2.3 Results

### 2.3.1 Viscoelastic behavior and yield stress

Previous studies of the viscosity of glycerol [57] and OTP [58] throughout the supercooled region down to their respective glass transition temperatures failed to find deviations from Newtonian behavior (apart from the expected observation of viscoelasticity at high frequencies). However, the putative solid-like network is thought to be formed only very slowly, and by limited inhomogeneous compaction of the liquid - not by extended homogeneous crystallization. Therefore we can expect this network to break or shear-melt at the comparatively large stresses ( $> 1$  MPa [57]) that are used in conventional viscosity measurements. Accordingly, we have built a temperature-variable Couette cell that allowed us to apply weak stresses. Furthermore, since the rheological response in yield-stress materials can be highly nonlinear, we did not follow the usual approach of recording the harmonic response with sinusoidal excitation. Instead, in order to discriminate easily between liquid and yield-stress behavior, we applied constant torques (see Experimental methods section and the appendix for details).

We found that both glycerol and OTP continued to behave as seemingly perfect Newtonian liquids during the initial cooldown - even for the smallest stress we could apply ( $\approx 100$  Pa), and all the way down to a few Kelvin above their respective glass transition temperatures. The measured viscosities were in agreement with those previously reported (as can be seen in Figure 2.5 in the appendix). However, the emergence of solid-like behavior could be observed in both materials when the temperature was raised again after a significant waiting period, as shown in Figure 2.1.

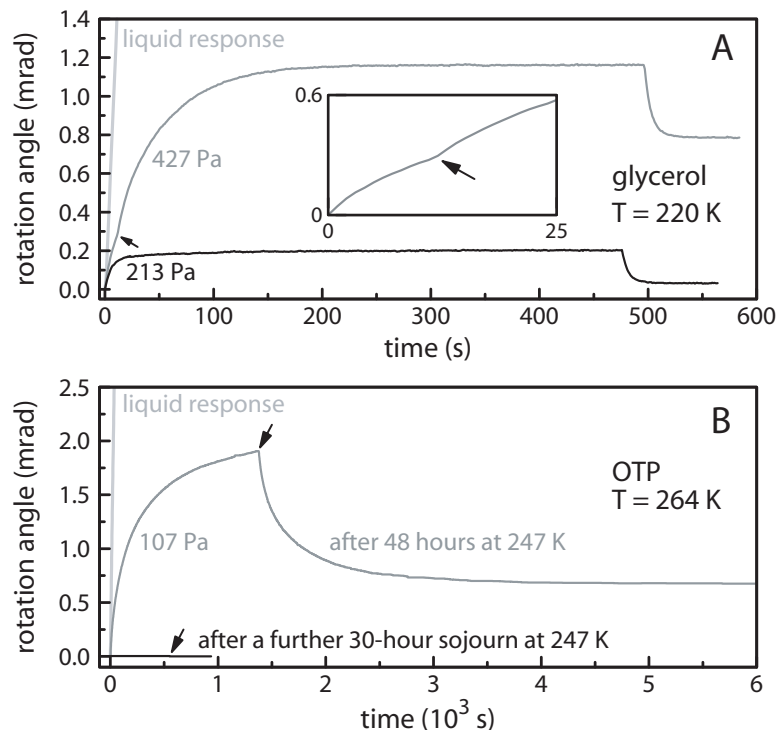


**Figure 2.1:** Viscoelastic behavior of supercooled glycerol and OTP. (A) Shear strain response of supercooled glycerol at 220 K, induced by the application of a constant shear stress at time zero. The plot shows the liquid-like reaction during the initial cooldown (light gray line, at 213 Pa shear stress) and the viscoelastic behavior that could be observed after an excursion to  $197\text{ K} = T_g + 7\text{ K}$  (black curve at 213 Pa, gray curve at 427 Pa). In the case of the latter two curves the torque was released at about 470 s, giving rise to a backward spring motion toward the initial position. The data for 427 Pa exhibits a yielding event (marked by an arrow, see also the enlarged view in the inset) and the initial position is not recovered. (B) Shear strain response of supercooled OTP, measured at 264 K for an applied shear stress of 107 Pa, at three different stages of aging. The light gray line shows the liquid-like response observed during initial cooldown. After 48 hours at 247 K ( $T_g + 3\text{ K}$ ), a clear solid-like response appeared (gray curve). The system sprang back toward its initial position after removal of the applied shear stress (denoted by the arrow). The associated shear modulus was about 10 kPa, 100,000 times smaller than the shear modulus of crystalline OTP. After the next excursion to 247 K (30 hours) the system had become so hard that no response could be measured at 264 K, even at the largest stress we could apply (3 kPa). The associated shear modulus was greater than 10 MPa.

In the case of glycerol, we allowed for aging periods of about one hour at 197 K ( $T_g + 7$  K) and then the material was brought to 220 K. We chose this probing temperature for practical reasons; testing flow properties took only a few minutes at 220 K, whereas reaching the same deformation at a given applied torque would have required 130 times longer at 205 K and 4000 times longer at 197 K. We then repeated this cooling/warming cycle a few times (see Figure 2.6 and accompanying text in the appendix), until a clear solid-like behavior appeared: Upon application of the shearing torque, the angle of the inner cylinder reached a quasi-stationary value (see Figure 2.1 A), which then continued to drift slowly. This observation is the signature of a solid-like connection between the inner Couette cylinder and the outer cup. For larger torques, breaking events occurred at a shear deformation around 0.1 – 0.2 %, as the bottom trace in Figure 2.1 A shows, and the rotation angle did not return to its initial value when the stress was released. This points to the expected yield-stress, and confirms the considerable nonlinearity of the mechanical properties of the supercooled liquid in this regime, already for low stresses (200 Pa) and small deformations (about 0.1 %). Breaking events may arise from shear localization, as found earlier in numerical simulations of glasses [56].

We used the same experimental protocol for OTP, adjusting the parameters to allow for the higher glass transition temperature of OTP ( $T_g = 244$  K) and for the differences in viscosity, which affect the kinetics of the formation of the solid network. Consequently, we cooled the OTP sample down to 247 K, 3 K above the glass transition temperature. After 48 hours at 247 K, the temperature was raised to 264 K within about one hour, and the mechanical properties were tested. Already after less than one hour waiting time at 264 K, the material exhibited a very clear solid-like response, as shown in Figure 2.1 B. As was the case with glycerol, we found that once the solid response had appeared, the system continued aging and became increasingly stiff, at a rate that strongly depended on temperature. This behavior is very similar to that reported for OTP by Patkowski et al. [11,12], who detected the scattering signature of a “supercooled liquid with clusters.”

### 2.3.2 Phenomenological model

To evaluate the angular traces quantitatively, we fitted them with a simple phenomenological model (see Figure 2.2 A). We think of the aged supercooled liquid as a solid-like network that responds elastically for small deformations, and which is embedded in a viscous fluid. A movement of the inner cylinder in the Couette cell gives rise to two torques: a viscous one from the surrounding

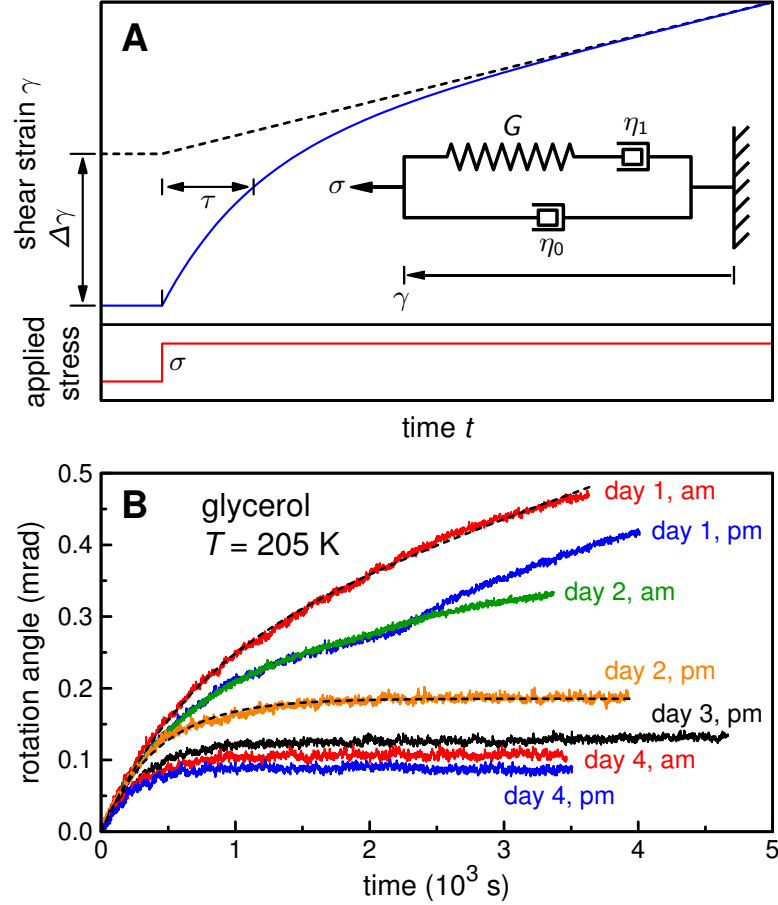


**Figure 2.2:** Rheological response of a solid-like network which is embedded in a liquid. (A) Phenomenological model for the quantitative evaluation of rotation traces, from which three parameters are deduced: the shear modulus  $G$  of the solid network, the viscosity  $\eta_0$  of the embedding liquid, and the effective viscosity  $\eta_1$  representing plastic deformation of the solid network. The constant shear stress  $\sigma$  is suddenly applied at time zero. The expression of the characteristic time  $\tau$  is given in the text and the strain amplitude  $\Delta\gamma$  is the prefactor of the exponential term in Eq. (2.1). (B) Examples of strain traces acquired during the aging and hardening of glycerol, induced by the application of a constant shear stress  $\sigma = 107 \text{ Pa}$  at time  $t = 0$ . The plot shows data taken during the first 4 days of an observation period of 2 weeks. The traces were fitted with Eq. (2.1) resulting from the model described in (A), except when breaking events occurred (e.g., day 1, pm). The dashed lines give two examples of these fits to the data.

fluid, and an (initially) elastic one from the solid network. The solid network will soon undergo microscopic rearrangements and will yield for large enough deformation. We represent this plastic deformation as another viscous response. As a first-order approximation, we neglect a possible strong dependence of this effective viscosity on the applied stress (see next section, Figure 2.4). We therefore represent the solid network as a spring and a dashpot in series (adding deformations), and this viscoelastic system itself is placed in parallel (adding torques) with a dashpot representing the liquid, as shown in Figure 2.2 A. In the spirit of a mean-field approximation, we consider the whole system as a collection of identical cells, all of them with the same elastic modulus and effective viscosities. This oversimplified model obviously fails to represent individual breaking events. The shear strain response  $\gamma(t)$  of the model to a constant stress  $\sigma$  applied at time zero is easily found to be a superposition of a linear drift in a fluid with a total effective viscosity  $\eta = \eta_0 + \eta_1$  (the sum of the viscosity  $\eta_0$  of the liquid and of the effective viscosity  $\eta_1$  of the network), and of an exponential transient:

$$\gamma(t) = \frac{\sigma}{\eta_0 + \eta_1} t + \frac{\sigma}{G} \left( \frac{\eta_1}{\eta_0 + \eta_1} \right)^2 \left\{ 1 - \exp \left( -\frac{t}{\tau} \right) \right\} . \quad (2.1)$$

The latter term corresponds to stretching the springs of the solid-like network, represented by the shear rigidity modulus  $G$ , in the surrounding liquid; this process has a characteristic response time  $\tau$ :

$$\tau = \frac{1}{G} \frac{\eta_0 \eta_1}{\eta_0 + \eta_1} . \quad (2.2)$$

Fitting the experimental trajectories with this model gave us the three rheological parameters of the material,  $\eta_0$ ,  $\eta_1$ , and  $G$  at every temperature and any stage of the aging process. Some examples of fitted traces are shown for glycerol in Figure 2.2 B. We then followed the aging of glycerol at the constant temperature of 205 K for more than two weeks. The evolution of the three parameters  $G$ ,  $\eta_0$ , and  $\eta_1$  during this period is presented in Figure 2.3 A. The effective viscosity  $\eta_1$  was often difficult to determine at later stages of the aging process, because experimental drifts overwhelmed the weak creep signal. Moreover,  $\eta_1$  strongly depended on the applied torque. We nevertheless indicate several values of  $\eta_1$  in Figure 2.3 A to give a feeling for the large increase of effective viscosity correlated with the increase in stiffness of the network. In contrast, the viscosity  $\eta_0$  was found to be constant within experimental error, and consistent with the viscosity of supercooled glycerol obtained in previous rheological measurements [57]. This result suggests that the solid network remained a minor component of the fluid throughout our study of Figure 2.3 A.

The most remarkable feature is the large increase of the shear rigidity modulus  $G$ , by two orders of magnitude over two weeks at 205 K. At the end of this measurement run, the shear modulus had reached about 1 MPa, a value that is, however, still more than three orders of magnitude lower than the modulus of crystalline glycerol [59].

Similarly, we followed the rheological response of the OTP sample as it aged over a period of more than two weeks at a temperature of 256 K. The three parameters  $G$ ,  $\eta_0$ , and  $\eta_1$  were again fitted using the model described in Figure 2.2; these data are shown in Figure 2.3 B. As with glycerol, the liquid viscosity  $\eta_0$  of OTP was comparable to the literature value and to our measurement of the viscosity of the non-aged sample at that temperature (about 10 MPa·s). We again found a pronounced stiffening: The shear modulus increased by more than two orders of magnitude in about 14 days, and did not yet seem to saturate at the end of the measurement. However, the maximum value of about 10 MPa is still two orders of magnitude smaller than the shear modulus of crystalline OTP. The measurements were stopped at that point because, at the maximal torque we could apply, the accuracy of our rheometer was not sufficient to measure smaller deformations.

### 2.3.3 Shear thinning and rejuvenation

We have seen that, when left undisturbed, supercooled glycerol hardens over time, but it shows shear-thinning when strongly perturbed. Figure 2.4 A presents a different run of aging experiments, again indicating hardening at 205 K for days 1 – 4. On day 5, we applied large shears to the sample (more than 10 times the shear previously used for probing) for several minutes. After this strong perturbation, the material presented a liquid-like response with a large amplitude, indicating that the solid connection had been disrupted, possibly by shear banding. This trace was very similar to that of day 1, illustrating the phenomenon of rejuvenation by a strong strain (such shear rejuvenation phenomena are currently attracting interest in other complex fluids as well [60,61]). Nevertheless, if the system is left unperturbed, the solid connection can heal quickly; in our case the hardening process had resumed already during the night between days 5 and 6. Due to experimental limitations in the applied torques, we could not test if the memory of previous aging can be erased permanently by sufficiently energetic stirring.

Figure 2.4 B documents another manifestation of shear thinning. The apparent (total) viscosity of the material during the first waiting period at 197 K after the first cooldown is measured by the long-time drift of the inner cylinder under an applied torque. If the torque is increased, the apparent viscosity

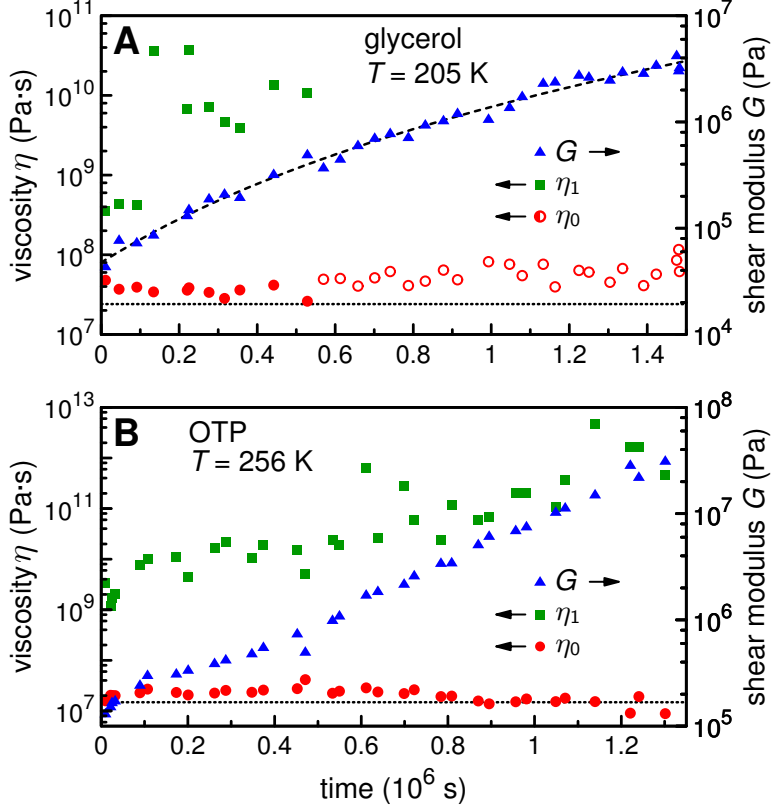


**Figure 2.3:** Aging of glycerol and OTP. (A) Aging of the shear modulus  $G$  (right  $y$ -axis) and of the viscosity parameters  $\eta_0$  and  $\eta_1$  (left  $y$ -axis) of glycerol at 205 K as a function of time over a period of two weeks. Note that the system already presented a weak shear modulus at the beginning of the measurements. The values of the effective viscosity  $\eta_1$  (squares) depend on the applied stress (see Figure 2.4). The measurements up to 0.5 Ms were done at a shear stress of 107 Pa (filled circles representing  $\eta_0$ ), later measurements at 213 Pa and 427 Pa (open circles). The dotted line corresponds to the viscosity derived from the liquid response at large stress, which is close to the literature value. The dashed curve, drawn through the shear modulus data points (triangles) as a guide to the eye, is a fit by a power law of time,  $G(\text{Pa}) = 10^{-18.5} \times [t(\text{s}) + 750,000]^{3.9}$ . (B) Aging of OTP over a period of two weeks at 256 K. The plot shows the evolution of the viscosities  $\eta_0$  (circles, left  $y$ -axis) and  $\eta_1$  (squares, left  $y$ -axis), as well as of the shear modulus  $G$  (triangles, right  $y$ -axis). The dotted line denotes the viscosity value derived from the liquid response during initial cooldown, which is in agreement with previous measurements.

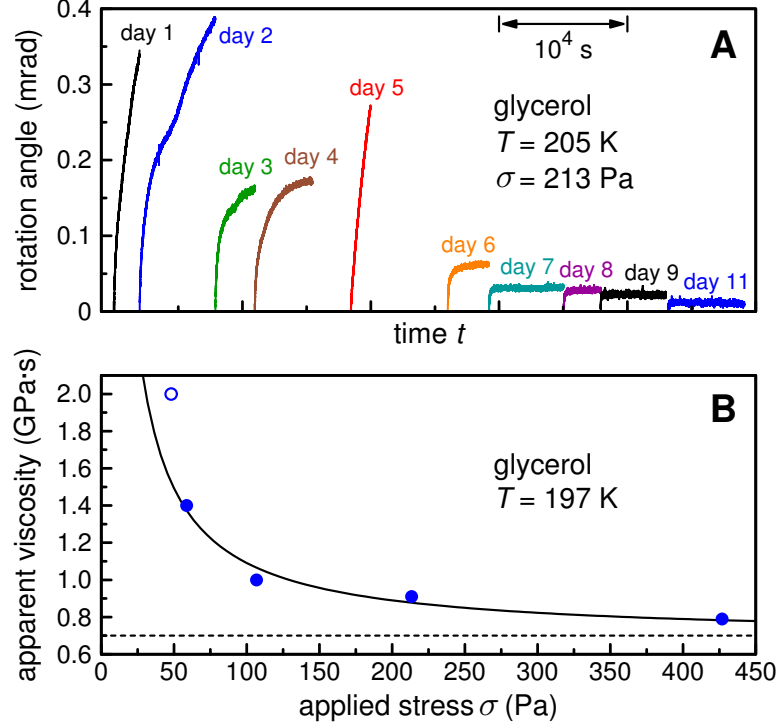


**Figure 2.4:** Shear thinning and rejuvenation of supercooled glycerol. (A) Hardening of glycerol at 205 K, which is interrupted by temporary rejuvenation due to the application of a large shear stress (day 5). (B) Shear thinning at 197 K due to the application of increasingly larger torques.

decreases. We can provide a first-order description of this effect with the following mean-field model: Consider a typical hydrogen bond in the solid network, and suppose that this bond can break under stress or under thermal fluctuations and can also reform with rate  $k_r$ , possibly at a different place. According to Kramers' theory of passage of an activation barrier [62], the rate of bond opening  $k_o$  is modified by the application of an external force  $F$  according to:

$$k_o(F) = K \exp\left(\frac{aF}{k_B T}\right) \equiv K \exp\left(\frac{F}{F_0}\right) \quad , \quad (2.3)$$

where  $a$  is a characteristic bond length,  $k_B$  is the Boltzmann constant, and  $K$  is the rate in the limit of  $F \rightarrow 0$ . Upon deformation of the solid network, an average force develops from stretching the network's springs represented by



the shear-modulus  $G$ . This force acts only during the periods when the bond is closed. The average force, proportional to the deformation rate  $\dot{\gamma}$ , can be represented by an effective viscosity  $\eta_1$ :

$$\eta_1(F) = \frac{1}{2} \frac{G}{k_o(F)} \frac{k_r}{k_r + k_o(F)} \quad , \quad (2.4)$$

which decreases exponentially with the applied force. However, we have to realize that the force  $F$  that acts on the solid network (see the model described in Figure 2.2 A) is not exactly the applied total force  $F_t$ . The difference arises because the network is yielding and there is an additional viscous force from the liquid component. According to the model,  $F$  and  $F_t$  are indeed related by:

$$F = \frac{\eta_1}{\eta_0 + \eta_1} F_t \quad . \quad (2.5)$$

In this expression, the viscosity  $\eta_1$  itself depends on the force  $F$  according to Eq. (2.4). Together, Eqs. (2.4) and (2.5) lead to an implicit equation for the effective viscosity. The exact solution of these equations for forces much larger than  $k_B T/a$  shows that the effective viscosity varies approximately as  $1/F_t$ , i.e., much slower than the exponential decay of Eq. (2.3). This approximation has been used to fit the experimental data in Figure 2.4 B (filled circles). It correctly predicts an asymptotic approach to the viscosity of the liquid for a large applied force (dashed line, value taken from Ref. [57]) and a slow algebraic decay of the effective viscosity (the data point for the lowest torque, i.e., the open circle in Figure 2.4 B, is less reliable, being close to our instrumental limit. This point has therefore been disregarded in the fit).

## 2.4 Discussion

The crucial feature of our experiments is that, once supercooled glycerol and OTP have been kept for some time at temperatures slightly above the glass transition, they show a combination of liquid- and solid-like behaviors: Our force response measurements reveal that, in addition to the expected viscous response, there is a small elastic component whose strength increases steadily with time. The typical shear rigidities that we found were considerably smaller than those of the crystalline materials: the shear rigidity modulus always stayed at least three orders of magnitude below that of the crystal for glycerol, and two orders of magnitude for OTP. We could measure such weak shear rigidities, because we allowed the systems to age and then perturbed them only weakly and rarely. Presumably, in typical viscosity measurements

with conventional oscillatory rheometers, a delicate solid-like network is either shear-melted or prevented from forming altogether. We have been able to shear-melt the network by subjecting it to sufficiently large torques. Their initial fragility explains why such solid-like structures have not been reported earlier.

Observing these signatures of a solid-like network in the macroscopic properties of these glass formers is in agreement with the evidence for long-lived structural heterogeneity on the microscopic scale. Previous studies of single molecules embedded in supercooled OTP [15] and glycerol [1] reported that the probe chromophores locally experience a liquid environment, but that they display a large spread in individual correlation times. The environment of each individual molecule appeared static over time scales that are long compared to both the rotational correlation time of the probe and the  $\alpha$ -relaxation time of the host. This effect was most dramatic for glycerol, with the memory time being at least five orders of magnitude greater than the rotational correlation time of the dye and more than a million times longer than the  $\alpha$ -relaxation time of glycerol. The combined experimental evidence on microscopic and macroscopic scales inevitably leads one to conclude that, after a temperature quench to a few degrees *above*  $T_g$ , supercooled molecular liquids can develop a fragile solid-like elastic matrix that encloses liquid pockets. This scenario was proposed earlier to explain the aforementioned single-molecule results [1]; it is completely consistent with the rheological measurements presented here. The picture that thus emerges is that a supercooled molecular liquid can phase-separate into locally liquid and solid-like regions, leading to the emergence of solid-like yield stresses and elastic moduli, which build up over temperature-dependent time scales. As conjectured earlier [63], we find that a supercooled liquid can exhibit soft glassy rheology well above  $T_g$ , and that the onset of this rheological behavior coincides with the appearance of structural heterogeneity, reminiscent of that found in computer simulations [64] and colloids [48], but associated here with such an extreme separation of scales that ergodicity is effectively broken tens of degrees above the glass transition temperature.

While phase separation is normally characterized by ever-increasing length scales as the domains of each phase coarsen, this apparently is not the case in the systems we investigated. A natural interpretation of this observation is in terms of frustration – either a geometric frustration as proposed by Tarjus *et al.* [65], a dynamic frustration, or both. Such frustration limits the size that domains can attain, and, in an equilibrium system, can indeed lead to an “avoided critical point”. In practice, dynamical arrest will most likely be important: It is natural to assume, and consistent with light scattering, that

the two phases will have different densities. Therefore, any mass transport required for phase separation will be prohibitively slowed down due to the high viscosity and reduced pore size. This scenario indeed agrees with our observation that the aging of the network (which we infer from its increasing shear modulus) proceeds slower at lower temperatures. In this scenario, the previously reported broad distribution of single-molecule rotational diffusion times [1, 15] reflects the differences in densities in the various liquid pockets, as well as, possibly, the pocket size.<sup>1</sup> The ratio  $D\eta/T$  should be constant if the Stokes–Einstein relation holds, but is found to increase sharply as one approaches the glass point [66]. This increase is naturally explained by the large dispersion of local viscosities. The average mobility determination of  $D$  is biased toward the fastest molecules in the low-viscosity liquid lakes, whereas the average viscosity favors the slowest molecules in the high-viscosity lakes [66]. With solid-like parts, this difference between the two averages becomes extreme. This description is similar to Bouchaud’s concept of self-inhibitory dynamics in glasses and granular materials [67], in which an important ingredient is the postulated local conservation of free volume. Free volume conservation would naturally follow from an effective sealing of local areas by a solid-like structure. A related picture is provided by the defect-diffusion model of Shlesinger and colleagues [68], according to which different amounts of free volume can be trapped in different mobility islands. In first approximation, we can relate the concentration of free volume in each island to a local pressure. From the change of the average viscosity with pressure [69] and the spread in local viscosity uncovered in the single-molecule measurements [1], we can estimate the variation of the local pressure to be about 1 – 2 bar for glycerol. Neither the typical scale nor the short-range structure of the solid-like network can be determined directly from our present experimental results. However, the above picture implies long-lived density fluctuations, which should be visible in light scattering experiments. Indeed, a large excess of Rayleigh-scattered compared to Brillouin-scattered light has been observed in the spectra of OTP [12, 70] and other molecular glass formers. Ultrasmall-angle X-ray scattering [11] indicates the presence of slowly-relaxing density fluctuations on even smaller scales. The combined evidence from all these experiments

---

<sup>1</sup>Corrections to the rotational diffusion coefficient of a particle a distance  $r$  from a wall fall off as  $r^{-3}$  due to hydrodynamic interactions. For a confined molecule, this leads to a correction in the diffusion coefficient of the order  $a(S/V)$ , where  $a$  is the molecular size, and  $S/V$  the surface to volume ratio of the confining volume. In the absence of density differences, this would allow one to extract a distribution of pockets sizes from the observed distribution of rotational diffusion times. Presumably, however, the density corrections dominated in our previous single-molecule experiments [1].

points to a broad range of scales for the density inhomogeneities, from about ten to at least a few hundreds of nanometers, with extremely slow relaxation – up to a million times slower than  $\alpha$ -relaxation processes. Furthermore, the excess light scattering depends on the thermal history of the sample, similar to what we observe for the viscoelastic response. (Careful sample preparation and handling can produce specimens in which the excess light scattering is absent or in which its occurrence is significantly delayed [12].) While these light scattering results are thus largely consistent with our measurements (which probe both smaller and larger length scales), their interpretation in terms of isolated clusters in a liquid phase [11,12,70,71] is not supported by the gradual build-up of a finite shear rigidity that we observe. Instead, our results imply the existence of a continuous, system-spanning network [72] that ages over time, as was discussed above. Future study of more supercooled liquids will show whether this feature is generic for molecular glass-formers, or even for glasses in general.

It is noteworthy that extrapolation of the spread in tumbling times of our single-molecule data to higher temperatures suggests that the heterogeneity of the liquid pockets disappears at a temperature somewhat below  $1.2T_g$  [1]. In other words, this type of behavior is found roughly in the same temperature range  $T_g < T < 1.2T_g$  in which fragile glasses are known to show strong non-Arrhenius behavior. One has to wonder whether this is just a coincidence, or the signature of a characteristic property of the supercooled state. In addition to exploring this behavior systematically as a function of temperature and aging for various materials, an important issue for future research is therefore whether the rheological anomalies studied would fail to appear or to grow above some temperature around  $1.2T_g$ . Furthermore, these findings may also clarify a puzzling feature of mode-coupling theory (MCT), its prediction of a sharp transition to a non-ergodic kinetically arrested phase at a critical temperature  $T_c$  significantly larger than  $T_g$ , sometimes called the “best-known failure” of MCT [73]. Our experiments suggest that this supposed failure may only reflect the inadequacy of the widely assumed ergodicity and uniqueness of the metastable supercooled liquid above  $T_g$ . They suggest that the main problem may lie in the association of  $T_c$  with  $T_g$ . Our results show that both supercooled glycerol and supercooled OTP can exhibit all the features commonly found in the soft glassy rheology of a complex fluid: flow, rigidity, yield stress, aging, rejuvenation and shear melting. Rather than either flow or break, these supercooled liquids actually flow and break at the same time, and they do so already at temperatures significantly above their respective glass transition temperatures.

## Acknowledgements

We thank H. S. Overkleeft and A. M. C. H. van den Nieuwendijk for help with the distillation of OTP. This work is part of the research program of the “Stichting voor Fundamenteel Onderzoek der Materie” (FOM), financially supported by NWO.

## 2.5 Appendix

### 2.5.1 Viscosities of glycerol and *o*-terphenyl

The plots in Figure 2.5 show measurements of the viscosities of glycerol and OTP in the temperature range of interest. The filled circles represent experiments that were conducted with our rheometer during initial cooldown, when both substances exhibited purely liquid-like behavior. The solid lines correspond to literature data measured by the drop method for glycerol [57] and by conventional rheology as well as by the beam-deformation method for OTP [58]. The agreement is very good for glycerol. For OTP, our measurements seem to slightly overestimate the viscosity by a factor of about 1.5, most probably due to systematic differences in the determination of the absolute temperature or other calibration effects. Nevertheless, the temperature dependence of the measured values is in very good agreement with the published data.

### 2.5.2 Onset of solid-like behavior in glycerol

An overview of the thermal history of the glycerol sample used in the rheology experiments is given in Figure 2.6. Each individual trace starts at or above room-temperature with an initial overnight cooldown (at a rate of about 5 K/hour) and presents the subsequent temperature variations with time until we observed the onset of a solid-like behavior. The first detection of a shear modulus at 220 K is indicated by the squares which terminate the curves. From that point on we lowered the temperature to 205 K for the aging study presented in Figures 2.3 and 2.4.

The chronological order of the traces in Figure 2.6 is from bottom (oldest) to top (newest) and reflects how we gradually homed in on experimental temperature profiles leading to a solid-like behavior. The thermal history of our previous single-molecule experiments [1] also shows a long period (about 6 days) at 195 K, close to the glass transition, followed by warming up to 205–215 K, when the single molecules were measured. (These studies were con-

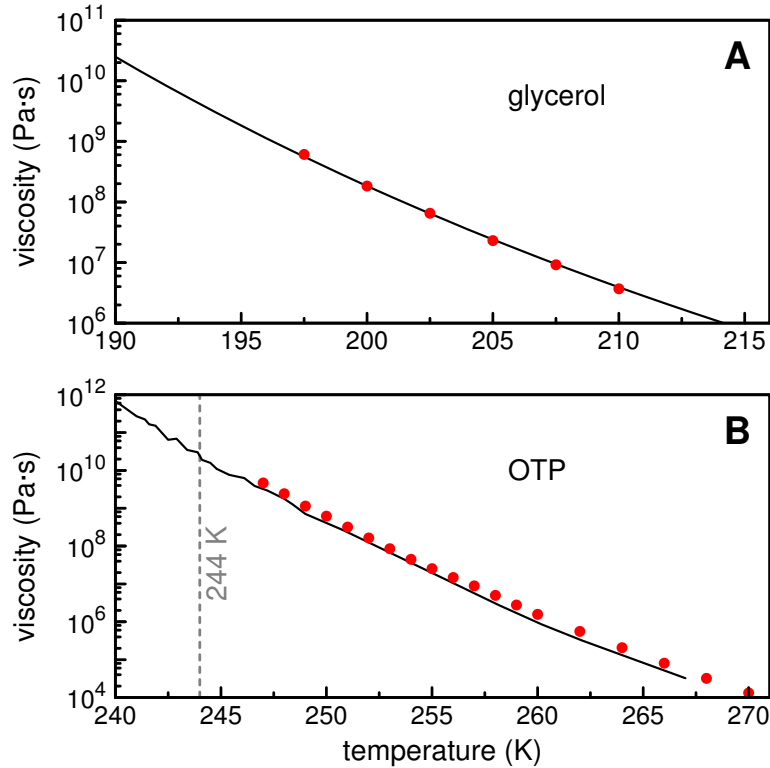


**Figure 2.5:** (A) The viscosity of glycerol ( $T_g = 190$  K) as a function of temperature. The solid line represents reference data taken from the literature [57], the circles show the results of our measurements of the liquid response. (B) The viscosity of OTP ( $T_g = 244$  K) as a function of temperature (circles: our measurements during the initial cooldown; curve: reference data [58]).

ducted several months before the rheology experiments.) Comparison to the traces for bulk glycerol strongly suggests that the extended network was also present in the single-molecule sample at the time the temperature-dependent experiments were performed.

The conclusion of this preliminary study is that the growth of the solid network is initiated after a ripening period of at least a few hours at 197 K, 7 K above the nominal glass transition. Note, however, that a more sensitive probing of elastic properties of the supercooled liquid could perhaps detect the onset of the solid network at earlier stages still. Furthermore, it can be expected that single-molecule measurements already reveal structural heterogeneity long before the solid network has become extended enough to influence the mechanical

properties of a bulk sample. This suggests that a more sensitive probing of the early stages in the development of the solid-like network is possible in future experiments with individual chromophores.

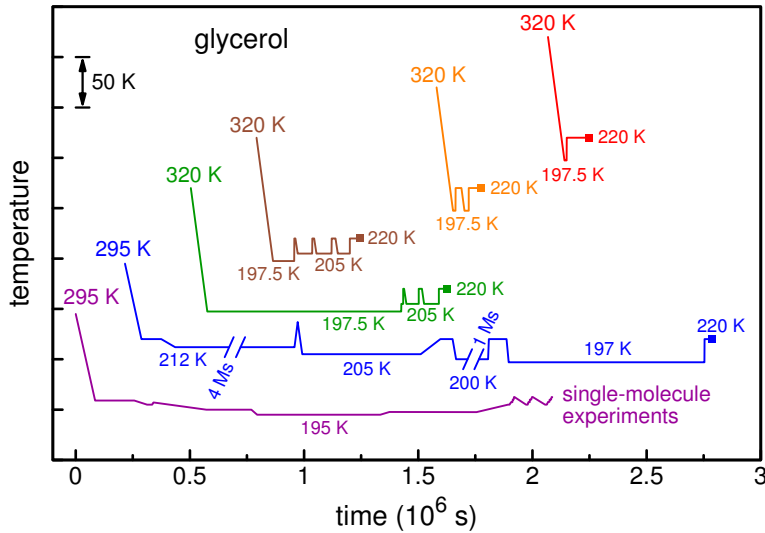


**Figure 2.6:** The thermal history of the glycerol sample in our rheological studies. Each trace is terminated by a square which indicates the first detection of solid-like behavior. The thermal history of the sample in our previous single-molecule experiments [1] is included for comparison (bottom trace).

### 2.5.3 Experimental details

**Design of the Couette Cell.** The design of our rheometer is shown schematically in Figure 2.7. A home-built Couette cell was integrated into a variable-temperature cryostat (Janis SVT-200-5). A film of glycerol or OTP, respectively, with a thickness of two millimeters resided between a movable inner cylinder and a static outer cup. Adjustable torque could be applied with a load lever on top of the cryostat via a bronze wire that acted as a torsional spring. The resulting movement of the inner cylinder was inferred from the deflection of a helium-neon laser beam which was retro-reflected by two mirrors rigidly connected to the cylinder and the cup, respectively. This arrangement, with the two mirrors (initially) perpendicular to each other, helps to ensure that the direction of the reflected laser beam is sensitive only to the motion of the inner cylinder relative to the outer cup. The difference signal of a split photodetector was used as an error indicator to control a galvanometer mirror.

The current fed into the galvanometer mirror was adjusted by a servo loop to compensate for rotation of the inner cylinder, and therefore provided a direct measure for its rotation. The sensitivity limit of the apparatus was found to correspond to a relative deformation of about  $5 \times 10^{-5}$ .

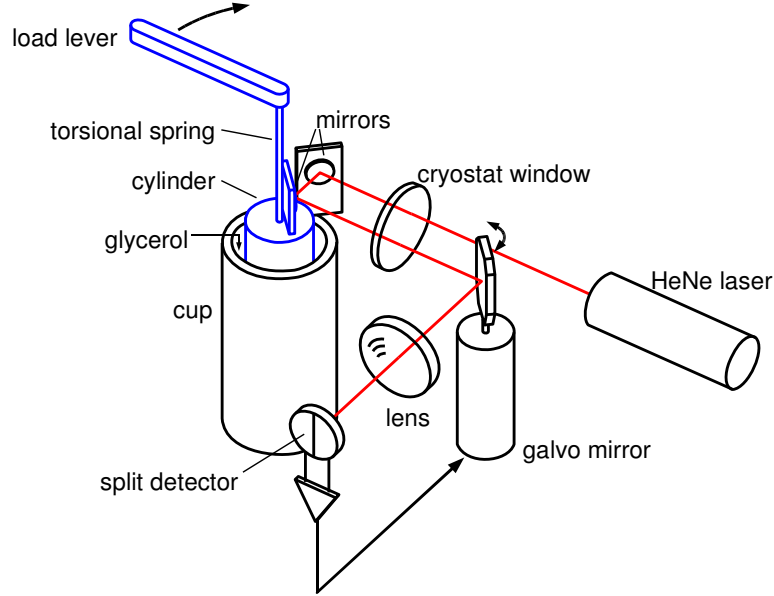


**Figure 2.7:** Schematic drawing of the Couette cell.

**Calculation of Shear Modulus and Viscosity.** The (quasi-)static values of the shear modulus  $G$  and of the viscosity  $\eta$  relate the elastic stress  $\sigma_{el}$  and the viscous stress  $\sigma_{visc}$  to the strain  $\gamma$  and the shear-rate  $\dot{\gamma}$  by:

$$\sigma_{el} = G\gamma \quad \text{and} \quad \sigma_{visc} = \eta\dot{\gamma} \quad . \quad (2.6)$$

The stress and strain are related to the applied torque  $M$  and the rotation angle  $\theta$  of the inner cylinder according to:

$$\gamma = \frac{R\theta}{d} \quad \text{and} \quad \sigma = \frac{M}{2\pi R^2 h} \quad . \quad (2.7)$$

The geometrical characteristics of the cell are the average cylinder radius  $R$ , the height  $h$  of glycerol between the cylinders, and the glycerol film thickness



*d.* We can now relate the intrinsic properties  $G$  and  $\eta$  of the material to the experimental parameters:

$$\eta = C \frac{M}{\dot{\theta}} \quad \text{and} \quad G = C \frac{M}{\theta} \quad \text{with} \quad C = \frac{d}{2\pi R^3 h} \quad . \quad (2.8)$$

The torsion constant of the wire, 0.0767 Nm/rad, which is needed to relate the applied torque to the twist angle of the wire, was determined at room-temperature by incorporating the wire into a torsion pendulum and measuring the oscillation period of a known, variable moment of inertia.

Because of the slight rotation of the inner cylinder, the torque produced by the torsion wire was not kept exactly constant during the deformation. However, the maximum rotation angle of the inner cylinder was very small compared to the twist angle of the wire, less than 0.7% for the weakest shear moduli in Figure 2.3. Even for the qualitative demonstration of the solid-like behavior of OTP (gray trace in Figure 2.1B), the deformation remained below 10% of the applied twist angle. Therefore, to a good approximation, the applied torque can be considered as constant during each individual measurement.

The smallest shear stress that could be applied reproducibly was about 55 Pa. Conducting control experiments under these conditions to check for the presence of solid friction in our apparatus, we could not detect any friction effects above our sensitivity limit.

### 3 Aging and solidification of supercooled glycerol

**Abstract** –We experimentally investigate the solidification of supercooled glycerol during aging that has been observed in Chapter 2. We find that a slow cooling at 5 K/h prior to the aging is required for solidification to take place. Furthermore we show that the time of onset depends strongly on the aging temperature which we varied between 220 K and 240 K. The nature of the solid phase remains unclear. The experiments show that upon heating the solid glycerol melts at the crystal melting point. However, rheology experiments in the plate-plate geometry revealed the growth of a soft, slush-like phase that is distinct from a crystal grown by seeding at the same aging temperature. The slush-like glycerol grows from a nucleation point at almost the same speed as a seeded crystal quenched to the same temperature, but its shear modulus is almost two orders of magnitude smaller than the crystal phase, which we measure independently. While solidification was reproducible in the Couette geometry, it was not in the plate-plate geometry.

The contents of this chapter have been submitted to *J. Phys. Chem. B*: M. E. Möbius, T. Xia, W. van Saarloos, M. Orrit, and M. van Hecke.

### 3.1 Introduction

Recent single-molecule optical experiments on supercooled glycerol near the glass transition have shown evidence for dynamical heterogeneities on the molecular level [1]. Most strikingly, the observed lifetime of the spatial heterogeneity is on the order of days, about six orders of magnitude longer than the typical time for a glycerol molecule to reorient. Moreover, as was shown in Chapter 2 [74], the rheology of supercooled glycerol near the glass transition exhibits a novel viscoelastic behavior after sufficient aging of the sample. This was a surprising finding, given that supercooled liquids are thought to be pure Newtonian liquids whose viscosity diverges at the glass transition temperature  $T_g$ . This non-Newtonian behavior has been conjectured to be a consequence of these microscopic heterogeneities [1].

In this chapter we expand on the work presented in Chapter 2 where our experimental setup was restricted to steady shear measurements which can cause “breaking events” that rejuvenate the sample. Moreover, we did not have optical access to the sample as it aged. In this work we address these shortcomings by performing the experiments in a commercial rheometer.

We employ an Anton Paar MCR 501 rheometer with an environmental chamber that enables us to probe the supercooled glycerol with small strain amplitude oscillatory measurements to avoid the previously observed “breaking events” of the fragile network while measuring its response. We perform experiments first in a Couette geometry with similar dimensions as in Chapter 2. We monitor the linear response of supercooled glycerol as a function of aging time at different aging temperatures above the glass transition. We find that an initial slow cooling period is crucial for the formation of the solid-like state. However, the deformation of the measurement tools (apparatus compliance) may limit the maximum measurable rigidity of the sample [75]. We could not ascertain whether the solid-like structure we measure in the Couette geometry is a crystal growing in a liquid or a solid-like phase distinct from the normal crystal.

We therefore repeated the experiment in a plate-plate geometry, where gap and plate size were chosen such that the tool compliance is negligible. In addition the sample can be optically accessed in this geometry. Surprisingly, we could not reliably reproduce the solid-like state in the plate-plate geometry, although we applied the same temperature history as in the Couette geometry. Nevertheless, we found evidence of a slush-like phase that grows from a nucleation point at the speed of the crystal phase, but has a soft slushy consistency with a shear modulus about two orders of magnitude lower than the crystal phase. The storage modulus of the slushy phase is within an order of magni-

tude of the modulus found in Chapter 2, although the aging temperatures were different (240 K versus 205 K). When slowly heated, the slush-like phase eventually melts at the crystal melting point of glycerol, which indicates that the slush either contains crystallites or turns into a crystal at higher temperatures.

## 3.2 Experimental methods

In order to probe the solidification of glycerol during aging we employed a Anton Paar MCR 501 rheometer with two measurement geometries. The first is a Couette geometry (Anton Paar CC 20) similar in dimensions to that used in Chapter 2. The gap size between inner and outer cylinder is 1 mm. The inner cylinder has a radius of 10 mm and is 30.1 mm long, with a conical bottom. The compliance of the tool and the cup as stated by the manufacturer is 1.65 mrad/Nm and 4.5 mrad/Nm, respectively. The total sample volume is about 7 ml.

Our customized plate-plate geometry (see Figure 3.6A) consists of two parallel discs with an upper disc radius of 1.5 mm and gap sizes between 2.0 and 2.3 mm. The small radius and large gap size ensure that compliance effects are negligible, which we checked explicitly (see Figure 3.5). Another advantage of this geometry is the optical access through the observation window of the chamber. We mounted a camera with a microscope lens outside the chamber which was focused on the sample. The sample was backlit with a LED behind a diffusing plate inside the chamber; the LED was turned on all the time and had no heating effect on the sample. The disadvantage of the geometry is the lower accuracy because of increased edge effects - the sample between the plates is not cylindrical but has a meniscus - and the lower sensitivity. It can only be used for samples with high moduli. Also, the sample volume, about 0.014 ml, is much smaller than in the Couette cell.

Both geometries are placed in a low temperature environmental chamber (Anton Paar CTD 450), which allows cooling down to 173 K. The cooling is provided by a liquid nitrogen evaporation unit (Anton Paar EVU), that coupled with the heating elements in the chamber ensures constant temperature environment with fluctuations of around 0.1 K. The flooding of the chamber with nitrogen vapor also prevents water uptake of the glycerol sample. Due to the high consumption of liquid nitrogen (about 6 l/h), we had to change nitrogen vessels every 15 – 20 hours. Furthermore, we restricted our measurements to aging temperatures of 220 K and above, which is in contrast to our studies in Chapter 2 where the aging temperature was 205 K and the waiting time extended to weeks.

A temperature probe (Anton Paar Pt100) is located at the bottom of both the Couette and plate-plate geometry and allows the rheometer to control the temperature in the chamber (the temperature difference from the center of chamber to the wall can be up to 4 K). A more accurate, better calibrated silicon diode (Lakeshore, DT-670-CU-1.4L) is attached directly to the cup of the Couette cell and the bottom plate of the plate-plate geometry, and was used to measure the absolute temperature.

During the course of the experiment we used two ultrapure samples (99.5% purity) of glycerol from two different suppliers, Invitrogen and Fluka. The bottle of glycerol was sealed with Parafilm and kept in a desiccator. Both samples could be solidified in the Couette geometry.

## 3.3 Results

### 3.3.1 Viscosity measurements

First we measured the viscosity of glycerol as a function of temperature in a Couette cell and a plate-plate geometry, respectively, to test the accuracy of these two different geometries. In both geometries we did strain rate-controlled measurements. It is important to be cautious: when the elastic constant of the sample becomes comparable to that of the measurement cell, the compliance of the measurement device may overwhelm the deformations in the sample [75]. As is shown in Figure 3.1, the measured storage modulus of frozen water with the Couette cell plateaus around  $10^7$  Pa, which is two orders of magnitude below the actual shear modulus of ice (3.9 GPa) [76]. Although this compliance effect is expected in the Couette geometry, it does not affect the viscosity measurements at steady shear [75]. At each data point we waited 10 minutes before the measurement was taken to allow thermal equilibration of the sample. As can be seen in Figure 3.2, the measured values of the viscosity versus temperature are in good agreement with previous measurements by Schröter et al. [57]. In case of the plate-plate geometry the viscosity values are slightly lower, which can be attributed to lower accuracy due to edge effects (see Experimental methods section).

### 3.3.2 Solidification and importance of cooling rate

An initial slow cooling is important for glycerol to develop a solid-like structure. In order to create the solid-like state observed in Chapter 2, we first performed the aging experiments in the Couette Cell. We found that rapidly cooling down the sample to  $T = 192$  K, which is close to the glass transition

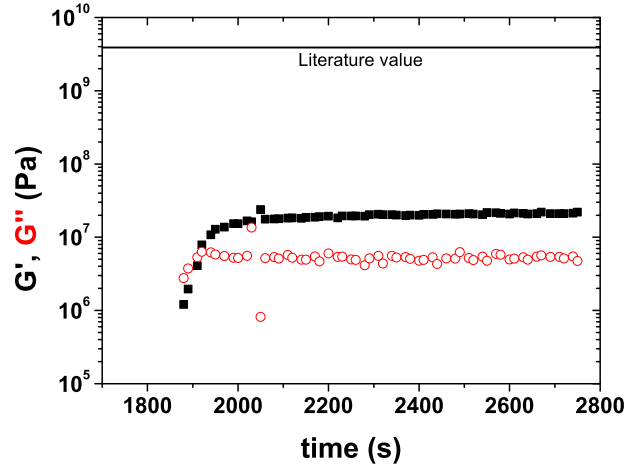


**Figure 3.1:** Measurement artefact in the Couette cell. Oscillation measurement ( $G'$ (■),  $G''$ (○)) of ice in the Couette cell at  $T = 268$  K. The oscillation test yields a storage modulus ( $G'$ ) that is two orders of magnitude lower than the actual shear modulus of ice due to tool compliance, indicating that the upper limit of the measurable shear modulus with the Couette cell is on the order of  $10^7$  Pa.

temperature  $T_g = 190$  K, followed by an aging at a higher temperature, irrespective of the aging temperature, did not lead to solidification reliably. The aging has to be preceded by a slow cooling period at a rate of 5 K/h.

The temperature protocol that leads to reproducible solidification is as follows (see Figure 3.3 A): first, the sample is cooled down to 260 K from room-temperature within about 20 minutes during which the temperature inside the environmental chamber is equilibrated. Then the sample is *slowly* cooled down further at a rate of 5 K/h to 192 K, which is just above  $T_g$ . After 2–3 hours at 192 K, the sample is warmed up to the desired aging temperature  $T_a$  at a rate of 60 K/h. When the  $T_a$  is reached the linear response is probed by oscillation measurements at  $f = 0.1$  Hz and a low strain amplitude  $\gamma = 5.3 \cdot 10^{-4}$ . The low strain amplitude was chosen to disturb the sample as little as possible.

In Figure 3.3 B-D we show the storage and loss modulus as a function of time for the glycerol in the Couette geometry at three different aging temperatures. In all cases, the development of a solid-like structure is evidenced by a steep increase of  $G'$  (and  $G''$ ) at time  $t_s$ . This increase is only observable several hours after the final aging temperature  $T_a$  has been reached. The solidification time  $t_s$  increases with decreasing  $T_a$ . The curves of the moduli as a function of time are not smooth and frequently exhibit kinks, i.e., sudden increases of

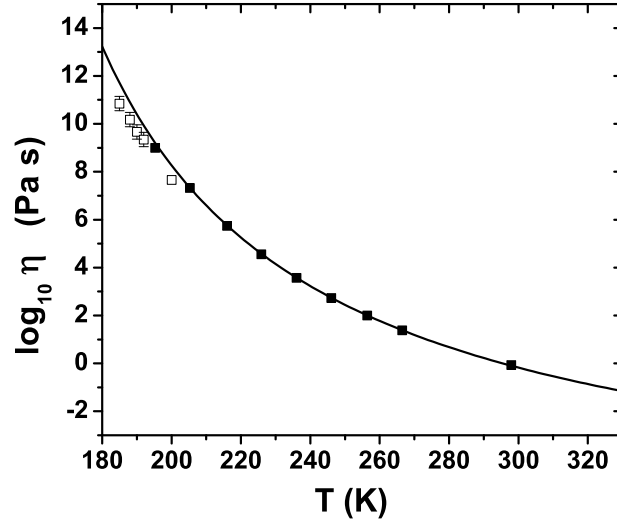


**Figure 3.2:** Dynamic viscosity versus temperature measurements of glycerol. All the measurements are obtained at steady shear (strain rate controlled) on the quickly cooled liquid state of glycerol. The solid symbols (■) are taken in the Couette cell, empty symbols (□) are measurements from the plate-plate geometry. The solid line is the VFTH (Vogel- Fulcher-Tammann-Hesse) fit from Schröter et al. [57]:  $\log_{10}(\eta/Pa \cdot s) = -7.1 + 1260/(T - 118)$ .

the time derivatives of the storage and/or loss moduli. These kinks might indicate meeting or merging events of some macroscopic solid-like clusters as they grow. Since the Couette cell is not transparent, we cannot test this.

Once the solid-like state is formed, it can be molten by heating the sample considerably. Figure 3.4 shows the magnitude of the complex viscosity of solidified glycerol obtained from the aforementioned procedure as a function of temperature. By warming up the sample at a rate of 12 K/h, we first observed a slight increase in the complex viscosity between 220 K and 288 K then a drastic drop when the temperature crossed 291.75 K, the melting temperature of the crystalline glycerol [77]. After that, the values of viscosity followed the literature values of supercooled glycerol. When the solid-like structure has completely molten, the sample was cooled down again from 300 K at a rate of 0.2 K/min and it behaved like a normal supercooled liquid.

The apparent shear modulus of the solid-like state, as shown in Figure 3.3, is two orders of magnitude lower than the modulus of crystalline glycerol, which is about 3.4 GPa, as derived from the transverse sound velocity in the

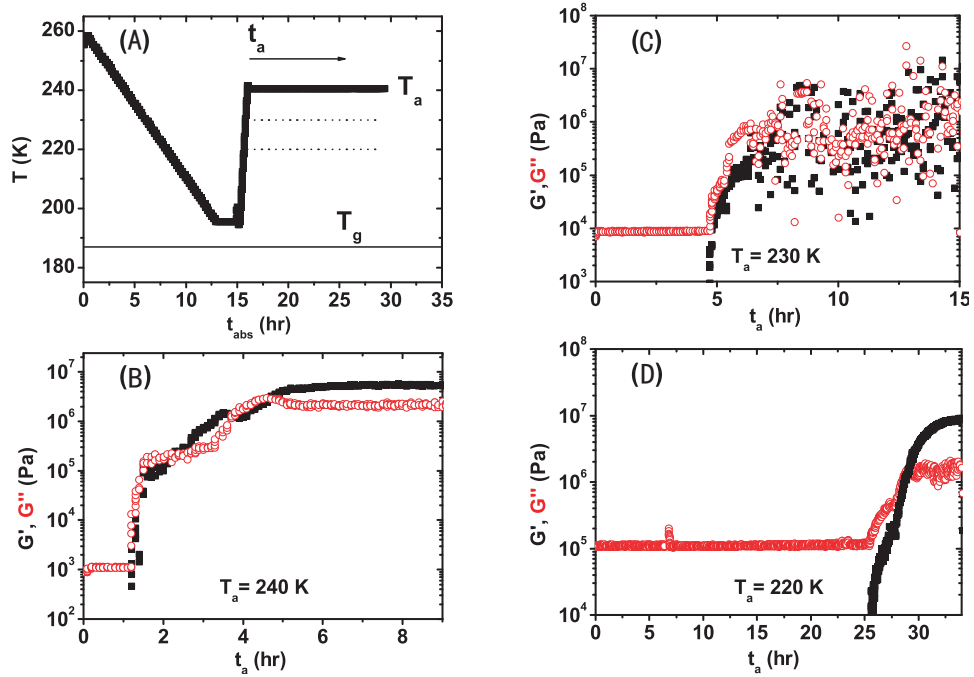


**Figure 3.3:** Aging and solidification of supercooled glycerol. (A) This is the temperature protocol used to create the solid-like state shown in panels (B)-(D). The sample is slowly cooled at 5 K/h from 260 K down to 192 K where it remains for 2 – 3 hours. It is then warmed up at 60 K/h to the desired aging temperature  $T_a$ . Panels (B)-(D) show the linear response,  $G'$  (■) and  $G''$  (○), of the oscillatory measurements during aging at  $f = 0.1$  Hz and a low strain amplitude  $\gamma = 5.3 \cdot 10^{-4}$  at different aging temperatures  $T_a$ : (B)  $T_a = 220$  K, (C)  $T_a = 230$  K and (D)  $T_a = 240$  K. Note: the bump in  $G''$  at  $t_a = 7$  h is due to the changing of the nitrogen vessel.

crystal [59]. Since the control measurements on frozen water have pointed out the compliance issue, the plateau values of the moduli of the aged glycerol in the Couette geometry cannot be trusted.

### 3.3.3 Measurements in the plate-plate geometry

In order to avoid complications due to the compliance of the tool we turned our attention to the plate-plate geometry with a relative wide gap and a small radius [75]. To ensure that the geometry is free of compliance artifacts we measured the  $\alpha$ -relaxation peak of the loss modulus in supercooled glycerol at different temperatures. After a sufficient equilibration period of the sample at



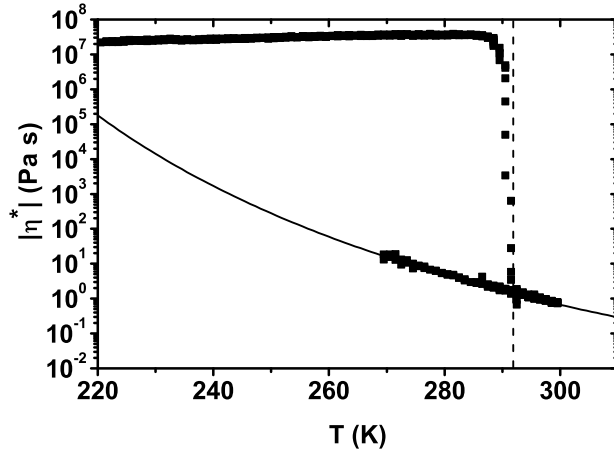


**Figure 3.4:** Modulus of complex viscosity monitored during melting and subsequent cooling. This is the same experimental run as shown in Figure 3.2 D. After aging at 220 K, during which the glycerol has solidified, we slowly heated the sample at 15 K/h while monitoring the linear response. At the melting point of the crystal phase of glycerol  $T_m = 291.75$  K [77], the modulus of the complex viscosity drops down to the values for the dynamic viscosity expected for liquid glycerol. Subsequent cooling from 300 K shows that the Newtonian liquid behavior is restored. The solid line is the same VFHT fit as in Figure 3.2.

each temperature, we performed an isothermal frequency scan of the complex moduli. As can be seen in Figure 3.5 A, there is an asymmetric peak in  $G''$  at a frequency corresponding to the  $\alpha$ -relaxation time similar to the measurements by Jeong [78] and Schröter et al. [57]. Moreover, the storage modulus  $G'$  at high frequencies levels off at  $3.7 \pm 0.1$  GPa, which agrees well with previous results [57, 75]. Furthermore, we probed the temperature dependence of the relaxation peak in  $G''$ . As shown by earlier experiments [78], the complex moduli can be rescaled on a master curve (see Figure 3.5 B), where the peak frequencies are well fit by a VFTH equation.

Surprisingly, the same temperature protocol, which worked reliably in the Couette geometry to create the solid-like state, could not reproduce the solid-like state of glycerol very well in the plate-plate geometry. Out of 6 trials only one run yielded a solid-like state. In addition, a number of cuvette cells (dimensions  $1 \times 9.5 \times 45$  mm<sup>3</sup>,  $2 \times 9.5 \times 45$  mm<sup>3</sup>,  $5 \times 9.5 \times 45$  mm<sup>3</sup>, and  $10 \times 9.5 \times 45$  mm<sup>3</sup>) filled with glycerol were subjected to the same temperature protocol, and none of them showed a cloudy appearance.

As mentioned above, we did observe once the spontaneous solidification of the

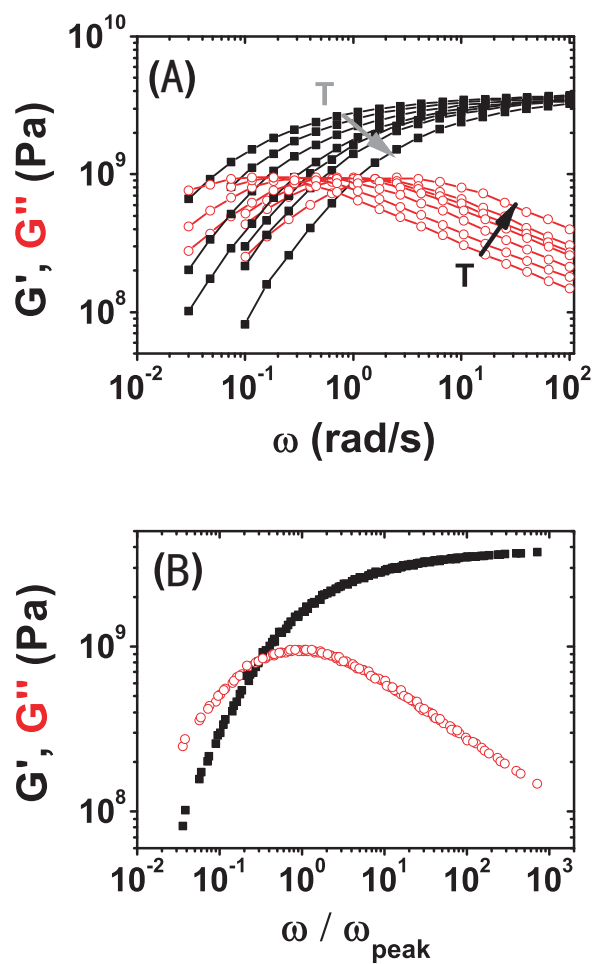


**Figure 3.5:** Relaxation peak of supercooled glycerol near the glass transition ( $G'$  (■) and  $G''$  (○)). (A) Oscillation measurements in plate-plate geometry at strain amplitude  $\gamma = 1.3 \cdot 10^{-4}$  were performed at temperatures  $T=186, 187, 188, 189, 189.5, 190$  and  $191.5$  K. The two arrows indicate the shift of the curves with increasing temperature. (B) Same as (A) with the frequency axis rescaled by the relaxation peak frequency using a VFTH fit:  $\omega_{peak} = 5.7 \cdot 10^{16} \cdot e^{-2856/(T-117)}$  rad/s.

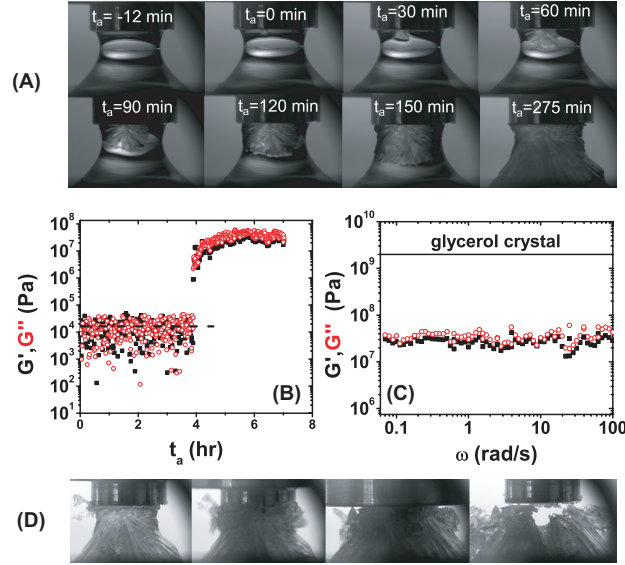


**Figure 3.6:** Emergence of the slushy phase after aging at  $T_a = 240$  K. The same temperature protocol as in Figure 3.2 A was followed. (A) Snapshots of the slushy phase at different times, showing a crystallization-like front moving at  $v = 1.1 \pm 0.2 \cdot 10^{-7}$  m/s. (B)  $G'$  (■) and  $G''$  (○) as a function of time (frequency  $f = 0.1$  Hz, strain amplitude  $\gamma = 7 \cdot 10^{-4}$ ). The noise floor is denoted by the dotted line. (C) Frequency sweep of  $G'$  (■) and  $G''$  (○) at  $t_a = 7$  h, showing a flat frequency response over 3 decades. The line indicates the storage modulus of crystalline glycerol. (D) After the oscillation measurement, a normal force of 10 N is applied and the slushy phase immediately deforms plastically indicating a low rigidity. However, the sample could withstand a normal force of 2 N without plastic deformation.

sample in the plate-plate geometry with our temperature protocol. During that run, a slushy phase formed at  $T_a = 240$  K, as shown in Figure 3.6.  $G'$  and  $G''$  showed a sudden increase once the solidification front spanned the whole gap after about 4 hours aging at 240 K. However, both moduli leveled off around  $3 \cdot 10^7$  Pa — two orders of magnitude below the shear modulus of crystalline glycerol, which is  $2 \cdot 10^9$  Pa (see Figure 3.7).

The measured speed of the solidification ( $v = (1.1 \pm 0.2) \times 10^{-7}$  m/s) front is very close to the growth of the glycerol crystal at the same temperature (see Figure 3.7) in agreement with literature values [79]. In addition, a frequency sweep of  $G'$  and  $G''$  of the solidified sample shows an essentially flat frequency response over three decades in  $\omega$ . The reason for the similar magnitude and fluctuations of  $G'$  and  $G''$  might be slippage at the upper plate. However,

when we applied a moderate normal force of 10 N to the sample in order to reduce slip it immediately deformed and was crushed by the upper plate as shown in Figure 3.6. This is in stark contrast to the crystalline glycerol sample (Figure 3.7) that withstood up to 50 N normal force (the maximum applicable force with our rheometer) without any plastic deformation. This clearly indicates that the slushy phase created through aging has a much lower rigidity than the ordinary crystal.

For comparison, we created an ordinary glycerol crystal and measured its rheological properties. From the previous Couette runs we could harvest crystal seeds that were scratched from the sample before it reached the melting point. These seeds were used to grow large crystals in the freezer at  $T = 253$  K. To compare with the slushy phase, we seeded the glycerol sample in the plate-plate geometry that was quenched at  $T = 240$  K with a few micrograms of the crystal.

By direct imaging we measured the crystallization front that slowly spread from the upper plate through the sample (Figure 3.7) at a speed of  $(9.8 \pm 0.2) \times 10^{-8}$  m/s at 240 K. After two hours, the whole sample has crystallized and the elastic moduli have jumped up. The storage moduli obtained from oscillatory measurements are centered around  $2.2 \pm 0.5$  GPa, which is consistent with previous measurements [59]. A subsequent strain sweep at  $f = 0.1$  Hz at a normal force  $F_N = 20$  N shows that the storage modulus is constant over a range of strain amplitudes, although for larger strain the elastic modulus decreases while the loss modulus increases due to slip. The measurements presented in Figure 3.7 show that we can reliably determine moduli of the solidified glycerol in the relevant GPa range.

### 3.4 Discussion

We have reproduced the solid-like state of glycerol in the Couette geometry at temperatures well above the glass transition as was reported in Chapter 2. We have established that an initial slow cooling period is crucial to create the solid-like state reliably. Perhaps, upon slow cooling, the molecules have enough time to locally rearrange themselves into a configuration that is more favorable for the nucleation of a solid-like structure. This would be more difficult in case of a fast cooling where the molecules are quickly arrested at temperatures close to the glass transition. Once the solid-like structures are formed in the glycerol, the rigidity of the sample increases with time. Both the waiting and the hardening times decrease with increasing aging temperature. However, the maximum moduli we could probe in the Couette geometry are

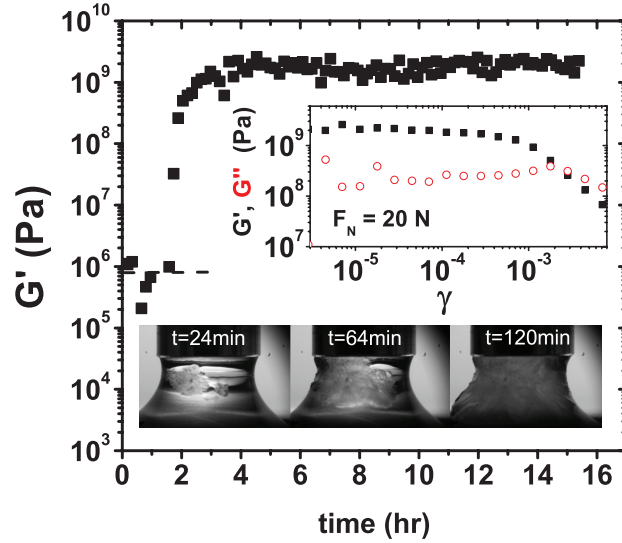


**Figure 3.7:** Measurement of  $G'$  of supercooled glycerol at 240K in the plate-plate geometry seeded with a crystal.  $f = 0.1$  Hz,  $\gamma = 3.5 \cdot 10^{-6}$ , gap is 2.0 mm. The noise floor is denoted by the dotted line. The inset shows strain sweep ( $G'$  (■),  $G''$  (○)) at 0.1 Hz with applied normal force  $F_N = 20$  N measured 15.4 hours after seeding the crystal. Also shown are snapshots of the growing crystal at different times as indicated. The crystal front grows with speed  $v_c = 9.8 \pm 0.2 \cdot 10^{-8}$  m/s. Once the crystal spans the two plates,  $G'$  rapidly increases.

of the order of  $10^7$  Pa due to the compliance of the measuring tool. The measurements on frozen water indeed confirmed this compliance issue, which also leaves the possibility open that the moduli of solidified glycerol may reach the GPa range.

In order to avoid the compliance issue, we switched to the plate-plate geometry, which also allows us to access the sample optically. Surprisingly, the same temperature protocol, which led to a solid-like state in the Couette cell in every run, did not work reliably in the plate-plate geometry. This is not understood yet. However, it should be pointed out that the Couette cell holds about 7 ml of glycerol and has an effective contact area about  $2000 \text{ mm}^2$ , whereas the plate-plate geometry holds about 0.014 ml of glycerol and the contact surface is about  $9.42 \text{ mm}^2$ . If the formation of the solid-like structure is nucleated from clusters whose probability depends on the volume or/and surface, this nucleation may be very unlikely in the plate-plate geometry.

The nature of the solid-like state remains unclear. It is tempting to conclude

that the solid-like behavior is due to a crystal structure growing in a liquid and giving rise to a viscoelastic linear response in the temperature range of our measurements. This scenario is supported by the observations that the growth rate from a nucleation point and the melting temperature of the solid-like structures are similar to those of the crystal. However, the shear modulus of the slushy phase is two orders of magnitude lower than that of the crystal. Moreover, this slushy material can be easily deformed plastically. If the solid-like parts of the slushy phase are small crystallites, their growth appears to be inhibited. This could be because the crystallites are smaller than the nucleation radius, or because of frustration. These crystallites are loosely organized and coexist with a liquid-like fraction, leading to an overall smaller rigidity than the polycrystals (see Figure 3.7). The images of the crushed sample (Figure 3.6 D) also suggest the existence of such crystallites on a larger scale. However, the crystalline structure of this slushy phase is still speculative at this point and would have to be proved by a structural analysis, e.g., X-ray or neutron scattering. It is reasonable to assume that the solid-like states formed in the Couette cell aged at 220 K, 230 K, and 240 K, after undergoing the same temperature protocol, are also slush-like and will turn into a crystal state upon heating, which is evidenced by the observed melting behavior at the crystal melting point. We believe that the solid-like structure formed by seeding a quenched glycerol sample is a crystal since its shear modulus is of the order of GPa, close to that of crystalline glycerol deduced from sound velocity measurements [59]. Moreover, it can be deformed elastically. To our knowledge, this is the first time the shear modulus of polycrystalline glycerol has been directly measured.

A similar solid-like behavior was found earlier in triphenyl phosphite (TPP), another molecular liquid, well known to exhibit an intriguing glacial state, an apparently amorphous state different from the glass and the ordinary liquid [80–83]. There are some striking similarities between the slushy state of supercooled glycerol and the glacial state of TPP. For example, the rheological experiments on the glacial state of TPP show that the maximum  $G'$  is of the order of  $10^6$  Pa [82], close to  $10^7$  Pa of the slushy phase of glycerol. Both moduli are far below their respective crystalline moduli. Upon heating, the glacial state of TPP turns into a crystal [81, 82], which also happens to the solidified glycerol since it melts at the melting point of crystalline glycerol. The structural description of the glacial state of TPP is still under debate. The evidence that the glacial phase is a mixture of micro-crystallites and non-transformed supercooled liquid came from the measurements performed at higher temperatures (216 – 235 K) [84], whereas the experiments at a lower temperature

(213 K) suggest that the glacial state is a homogeneous glassy state of a denser liquid free from micro-crystallites [82, 85]. It would be interesting to do the aging measurements on glycerol at lower temperatures. However, the kinetics associated with this aging process for glycerol appears to be much slower than that of TPP, which makes the experiments e.g. at  $T = 205$  K [74] impractical. It still remains an open question if the scenario of the glacial phase in TPP carries over to supercooled glycerol. If so, the timescales of forming the glacial state are vastly different.

## 3.5 Conclusion

We can reproduce the solid-like state of glycerol in the Couette geometry reliably with our temperature protocol which involves an initial slow cooling period prior to the aging, but not in the plate-plate geometry (except for one run out of six). The observed viscoelastic behavior seems to be related to a crystal-like structure growing in a liquid in the probed temperature range, 220 – 240 K. However, this crystal-like structure can vary considerably in its rheology. The slushy phase, which grew from a nucleation point after slow cooling and subsequent aging at 240 K behaved quite differently from the crystal that was created by seeding a glycerol sample quenched to the same aging temperature. The slushy phase is two orders of magnitude softer and can easily be deformed plastically, whereas the seeded sample has a shear modulus of  $\approx 2$  GPa and can only be elastically deformed. Whether the slushy state of glycerol shares the same structural origin as the glacial state of TPP remains an open question. Nevertheless, the cooling rate emerges as a crucial parameter in studies of glycerol at temperatures near the glass transition and appears to affect the structure and dynamics on the molecular level.

## Acknowledgements

This work is part of the research program of the “Stichting voor Fundamenteel Onderzoek der Materie” (FOM), which is financially supported by the Netherlands Organization for Scientific Research.

## 4 Micron-sized structure in a thin glycerol film revealed by fluorescent probes

**Abstract** – We report on micrometer-sized structures in supercooled glycerol observed by imaging fluorescent probes at temperatures close to, but above, the glass transition temperature (190 K). Two distinct heterogeneous patterns of the fluorescence intensity were detected, depending on how fast the sample was cooled down. In a slowly cooled sample, we observed a Swiss cheese-like pattern in which many micrometer-sized dark spots were nucleated in a bright background. A quickly cooled sample resulted in a spinodal decomposition pattern where many bright island-like features on micrometer scale were dispersed in a dark matrix. Similar patterns were seen earlier in triphenyl phosphite, another molecular liquid, which shows solid-like behavior at temperatures above its glass transition. Once the heterogeneous patterns are formed in the glycerol, they can persist for days, unless the samples are heated above 260 K for more than 10 hours. Such heterogeneous patterns are ascribed to differential dye distributions in the glycerol film, pointing to long-lived and micrometer-scale density fluctuations in supercooled glycerol. The observation of such heterogeneity may provide additional understanding on how supercooled glycerol behaves before it turns into a glass.

The contents of this chapter have been published:  
T. Xia, L. Xiao, and M. Orrit, *J. Phys. Chem. B* **113** (2009) 15724–15729.



## 4.1 Introduction

Many liquids can be cooled below their melting points without being crystallized and remain liquid-like until their glass transition temperatures  $T_g$  are reached. Along this cooling down, their viscosities increase enormously. The structural mechanism, through which the dynamics of supercooled liquids are slowed down and finally arrested, has been a mystery for more than half a century [71]. It is widely accepted that rearranging many molecules locally in a cooperative manner (forming locally favored structures) plays a key role in dynamical heterogeneity and glass formation [4]. Heterogeneity has been observed in many glass forming systems by both experiments and computer simulations [51, 52, 86]. However, there is no consensus on the structural origin, time, and length scales of those inhomogeneities. Molecular-scale spectroscopic techniques like NMR [7, 8] and dielectric relaxation [9, 10] invariably find the relaxation time of heterogeneity comparable with molecular reorientation times in supercooled liquids and the length scales of a few nanometers. However, optical experiments, notably light and X-ray scattering [11, 12], polarized hole-burning [13, 14], and single-molecule spectroscopy [15, 16], reveal much slower relaxation and longer length scales.

Recent single-molecule rotational diffusion measurements in a thin glycerol film showed that different single-probe molecules rotate at different rates in the supercooled regime and that the distribution of rotation rates broadens upon approaching the glass transition temperature (190 K) [1]. This is consistent with previous observations of dynamical heterogeneity in supercooled glycerol by various techniques [9, 10, 87–89]. In addition, Zondervan et al. [1] found surprisingly long-lived inhomogeneity at temperatures well above  $T_g$ . The time scale is on the order of hours, which is about six orders of magnitude longer than the typical time for a glycerol molecule to reorient. Such long-lived heterogeneity strongly suggests that some nearly static structures already exist at temperatures above  $T_g$  and form a solid-like network percolating in the supercooled liquid. Indeed, later rheological measurements on glycerol confirmed the existence of a solid-like network at temperatures well above the glass transition temperature as shown in Chapter 2.

Fluorescence imaging has been widely used to study phase separation in polymer blends [90–92] and membrane-like systems [93–95] where fluorescent probes are either chemically attached to the molecules of interest or doped directly into materials under investigation. When the phase separation is initiated, for example by a temperature change, this process can be monitored by following the evolution of the fluorescence pattern [95]. Here, we used fluorescent dyes to image thin glycerol films at temperatures close to, but above,  $T_g$

and we found two distinct heterogeneous dye distribution patterns, depending on the cooling rate applied to the sample. A Swiss cheese-like pattern in which many micrometer-sized dye-depleted regions are nucleated in a thin glycerol film can be observed upon slow cooling, whereas quick cooling gives rise to a spinodal decomposition pattern where micrometer-sized dye-enriched droplets are dispersed in a dye-depleted matrix.

## 4.2 Experimental methods

Solutions of Alexa 488, Rhodamine 6G (R6G), and *N,N'*-bis(2,5-di-*tert*-butylphenyl)-3,4,9,10-Perylenedicarboximide (PDI) in glycerol were prepared at  $10^{-7}$  M. Alexa 594 and Alexa 488 - polyproline 40 mer - Alexa 594 (dual-labeled) construct were prepared in glycerol at  $10^{-8}$  M and  $10^{-9}$  M, respectively. The structures of the fluorophores and glycerol are shown in Figure 1. Anhydrous glycerol and PDI were purchased from Sigma-Aldrich Chemie BV (Netherlands). Alexa 488 and Alexa 594 were ordered from Invitrogen (Netherlands). R6G was purchased from Radiant dye Laser (Germany). Dual-labeled proline 40 mer was synthesized in the Department of Biochemistry, University of Zurich. The glycerol solution was directly spin-coated at 6000 rpm on a round glass substrate with a diameter of 20 mm. To improve wetting, the glass substrates were first treated in a UV-ozone cleaner (model 42-220, Jelight, Irvine, CA). The resulting thickness of the glycerol film from this procedure was 0.5–2  $\mu\text{m}$ , as deduced from examination in a home-built Michelson Interferometer. To minimize water content in glycerol solution, the samples were dried in the cryostat by repeatedly pumping and flushing with helium gas at room-temperature and kept under dry helium throughout all experiments.

The experiments were conducted with a home-built laser-scanning confocal microscope that allows for the optical experiments in the full temperature range from 1.5 K to room-temperature. This setup is described in detail in ref. [46]. The slow cooling was done by cooling the sample from room-temperature without precooling the cryostat, which leads to a nearly constant cooling rate of 5 K/h between 295 K and 208 K. The quick cooling rate was achieved by quickly putting the sample from room-temperature into the pre-cooled cryostat whose temperature was 220 K. In this way, the sample experienced a very sudden temperature drop in the very beginning and the cooling rate then decayed with time. Since the temperature went through the freezing point of water very fast, the drying procedure was not applied to the quickly cooled sample. Although the water content in this case is probably higher than that in the slowly cooled sample, we don't believe that the water traces change the

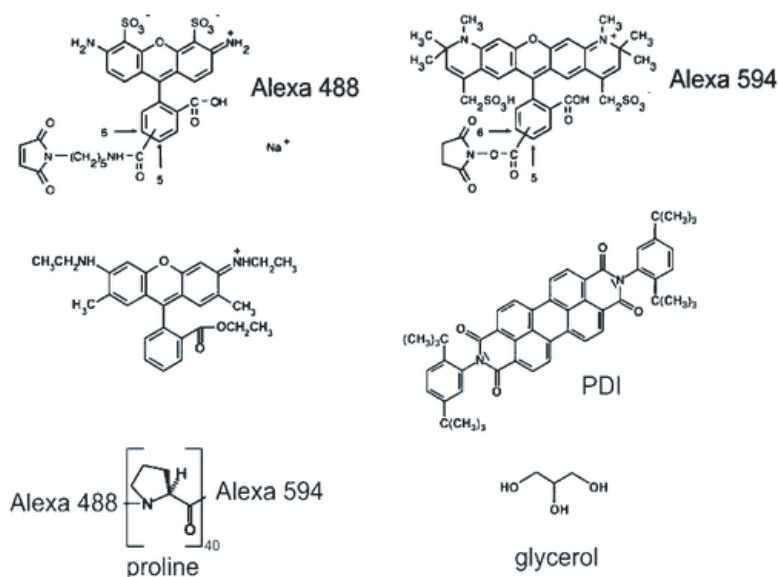


**Figure 4.1:** Structures of the fluorophores and glycerol.

properties of glycerol significantly (see Discussion section).

We excited the fluorescence at 488 nm with an Argon-ion laser (Spectra-Physics Stabilite 2017) and at 594 nm with a yellow HeNe laser (Melles Griot, 25LYP173-230). All the images of  $100 \times 100 \mu\text{m}^2$  were scanned with 200 by 200 pixels, a dwell time of 10 ms, and an excitation power of  $2.0 \text{ kW}/\text{cm}^2$  for the fluorescence and  $60 \text{ W}/\text{cm}^2$  for the scattering measurements.

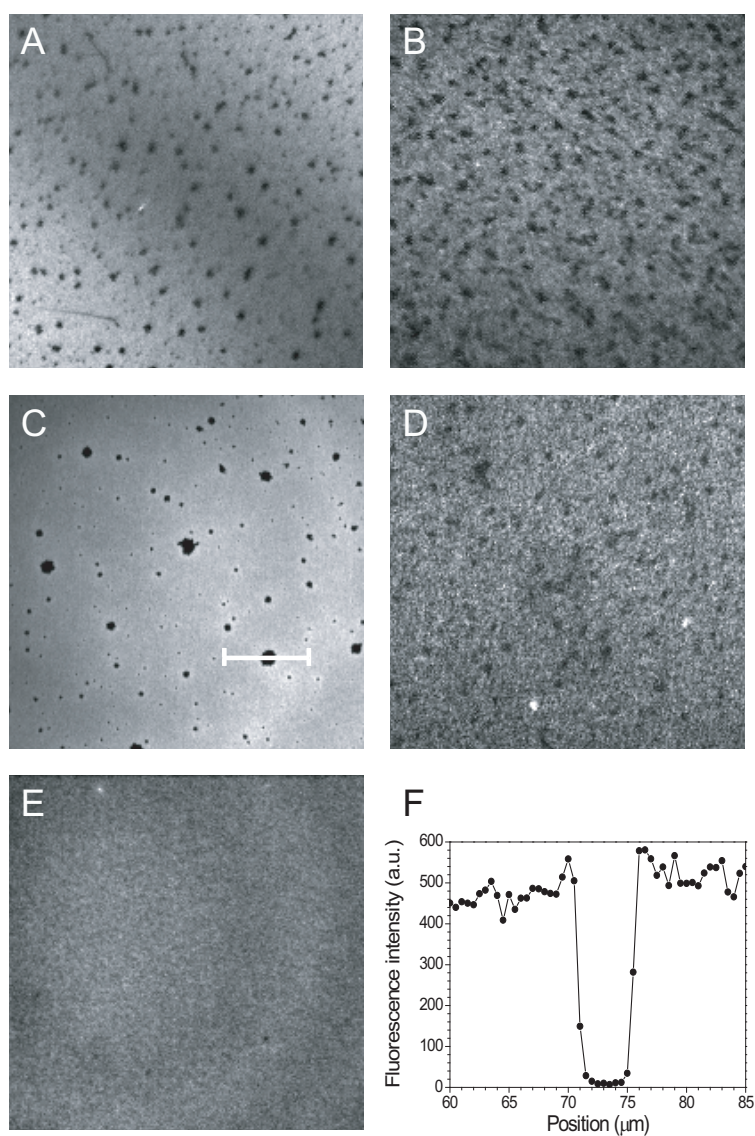
### 4.3 Results

In this work, five different fluorescent probes (see Figure 4.1) were used to image thin glycerol films. All the probes, except Alexa 488, showed a conspicuous long-lived heterogeneous pattern of the fluorescence intensity (Figure 4.2 A-D) in glycerol at temperatures 15–18 K above  $T_g$ . This pattern is characterized by many micrometer-sized dark spots with a roughly circular shape, dispersed in a bright background, which resembles a cross section of a Swiss cheese with many holes. Although the shape and size of dark spots differ among and even within those samples, the bright and dark regions are quite distinguishable. Such cheese-like patterns become first detectable at temperatures around 220 K (data not shown), which is 30 K above the glass transition temperature

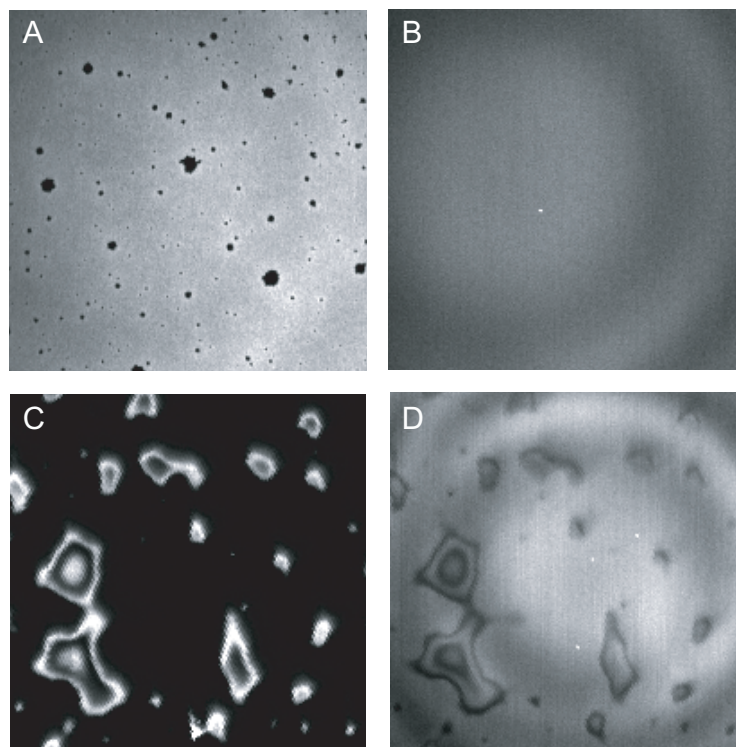
of glycerol. However, the cheese-like pattern was not clearly seen in the glycerol when doped with Alexa 488 (Figure 4.2 E) where the fluorescence intensity was nearly homogeneous in the scanned field in the same temperature range. Once the cheese-like pattern is formed, it can persist for days unless the sample is heated up to 260 K and kept at this temperature for about 10 hours. After this treatment, the pattern disappears and the fluorescence intensity becomes homogeneous (data not shown). If the heated sample is cooled down again toward glassy temperature, the cheese-like pattern will reappear reliably.

Figure 4.2 F shows the one-dimensional fluorescence intensity profile of a dark spot of Figure 4.2 C. The fluorescence intensity drops almost to the background level in the center of the dark region. If we assume that the probe molecules are homogeneously distributed in the sample, the fluorescence intensity would then be correlated to the thickness of the glycerol film. The observed dark spots should therefore stem from steep variations in the film thickness, resulting from the formation of physical holes, tentatively due to local dewetting. Another assumption would be that the thickness of the film is more or less uniform within the scanned area and that either the local probe concentration or the fluorescence emissivity of the probe are not homogeneous on the length scale of a few micrometers. To test the first assumption, we imaged the sample directly with the laser light scattered from the surface. If there were any physical holes or morphological structure present in the sample, the incident light should be strongly scattered by the holes, resulting in a position-dependent signal in the scanned image. It should be noted that the scattering measurements here differ from conventional light scattering. In the latter method, an incident beam with a high power usually illuminates a sample with a thickness of some millimeters. Additionally, the intensity, angular dependence, or dynamical fluctuations of the scattered intensity provide information about refractive index fluctuations in the material. Here, we used a relatively weak laser beam to scan a thin film of glycerol (see Experimental methods section), so that only strong index fluctuations or morphological structures such as holes in the film would give rise to a measurable signal. Figure 4.3 A again shows the fluorescence image of Rhodamine 6G (R6G) in glycerol (Figure 4.2 C) revealing the cheese-like pattern. The right image was taken from the scattering measurement in the same area. The intensity of the scattered light is more or less homogeneous in the field of view (except for concentric interference fringes due to multiple reflections in the cryostat windows, which modulate the power of the incident light during the beam scanning). Since the scattering image does not show any sign of morphological features, the cheese-like pattern is not likely due to the formation of physical holes resulting from dewetting, but rather to a differential

#### 4 Micron-sized structure in a thin glycerol film revealed by fluorescent probes



**Figure 4.2:** Confocal scanning images of different fluorescent probes in thin glycerol films at temperatures close to, but above,  $T_g$ . All the images recorded are  $100 \times 100 \mu\text{m}^2$ . (A) The fluorescence image of Alexa488-polyproline 40 mer-Alexa594 construct ( $10^{-9}$  M) excited by 594 nm laser at 206 K. (B)  $10^{-7}$  M PDI excited by 488 nm laser at 208 K. (C)  $10^{-7}$  M R6G in glycerol at 207 K. (D)  $10^{-8}$  M Alexa594 in glycerol at 205 K (E)  $10^{-7}$  M Alexa488 in glycerol at 208 K. (F) One-dimensional fluorescence profile of a dark spot in (C) indicated by the white bar.



**Figure 4.3:** Comparison of fluorescence and scattering images ( $100 \times 100 \mu\text{m}^2$ ). (A) The fluorescence image of  $10^{-7}$  M R6G in glycerol reveals the cheese-like pattern at 207 K. (B) The scattering image of the same area in (A) doesn't show any physical features, indicating that the thickness and index of refraction of the glycerol film are rather uniform in the scanned area. (C) This fluorescence image was taken from the sample ( $10^{-7}$  M PDI in glycerol) at 295 K, which was first heated up to 295 K from 208 K and then kept at 295 K for 24 hours. The image reveals many isolated bright features with irregular droplet and ring-like shapes, suggesting that the glycerol film is completely ruptured after long time at room-temperature due to dewetting. (D) The scattering image of the same region shows the same features as seen in (C). Physical features can be detected by both fluorescence and scattering imaging. The concentric interference pattern seen in (B) and (D) is due to multiple reflection of the incident beam from the cryostat windows, which modulates the incident power during the beam scanning. This profile can be weakly seen in (A) as well.

dye distribution or to a variable fluorescence brightness due to photophysics of the dyes (see Discussion section) in glycerol films. Control experiments shown in Figure 4.3 C and D show that the rupture of the glycerol film resulting from dewetting at room-temperature can be reliably detected by both fluorescence and scattering imaging.

As was demonstrated in Chapter 2, the behavior of supercooled glycerol is strongly dependent on the thermal history, in particular the cooling rate is one of the important factors. The above mentioned cheese-like pattern was observed from the samples that had an average cooling rate of 5 K/h starting from room-temperature. If the sample was cooled down to 208 K with a quick cooling rate (see Experimental methods section), it showed a quite different pattern (see Figure 4.4 A). Instead of a cheese-like pattern in which many dark spots are nucleated in the bright matrix, bright micrometer-sized and island-like features are formed in a dark matrix, which resembles a spinodal decomposition pattern. The bright features in the left part of the image are more circular in shape and smaller, whereas features in the right part of the image are more branched, elongated, and bigger. Such a gradient across the sample may originate from a slight variation of the film thickness from the right (thin) to the left (thick). Because the cheese-like pattern disappeared upon heating the slowly cooled sample at 260 K for more than 10 hours, the same thermal treatment was also applied to the fast cooled sample. Figure 4.4 (A-F) shows sequential fluorescence images of PDI in glycerol as a function of temperature and the thermal history of the sample is indicated in (G). Upon heating up from 208 K, the isolated bright features first coarsened, then neighboring small features started to contact with one another and fused to bigger ones. Meanwhile, the dark area kept shrinking along with this heating process. Finally, all the big bright features merged into one uniform bright area at 260 K and the dark area vanished completely. This evolution of the fluorescence pattern mainly takes place at higher temperatures. Annealing the sample at a fixed temperature well below 260 K does not give any significant change of the pattern on the time scale of hours (data not shown). The bright island-like features observed at 208 K disappeared upon heating the sample to 260 K. However, the cheese-like pattern formed again from the same sample upon slow cooling down (5 K/h) to 208 K. Clearly, the cooling rate influences the pattern of the fluorescence intensity in supercooled glycerol.

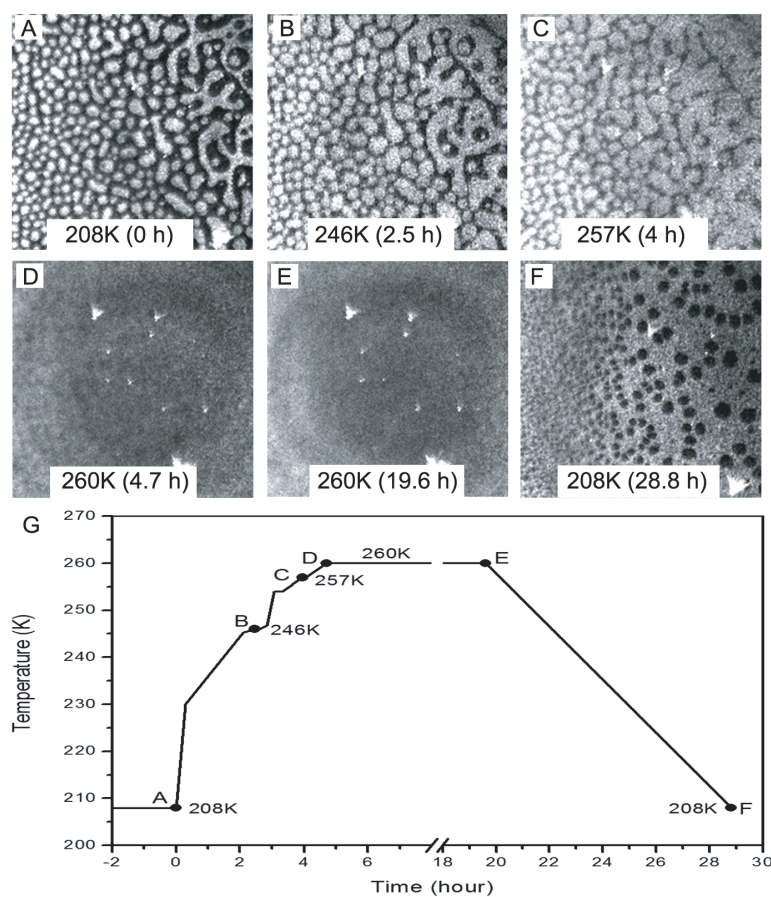


**Figure 4.4:** Sequential fluorescence images ( $100 \times 100 \mu\text{m}^2$ ) of  $10^{-7}$  M PDI in glycerol during first warming up (A-D) and then slow cooling down (E, F). The employed thermal history is shown in (G) where the solid circles indicate the fluorescence measurements of A-F. Upon the initial quick cooling from room-temperature, bright island-like features are separated by a dark matrix. The isolated bright features coarsen upon warming up and neighboring features start to fuse into bigger ones. Finally, all bright features merge into one uniform bright region at 260 K and the dark region disappears completely. After one night at 260 K, the sample was cooled slowly (5 K/h) down to 208 K and the cheese-like pattern appeared.



## 4.4 Discussion

We have chosen five fluorescent probes to image supercooled glycerol and the cheese-like pattern was observed with dual-labeled polyproline 40 mer, PDI, Alexa 594 and R6G, but not with Alexa 488. The dark areas in the cheese-like patterns revealed by those different probes are quite different in terms of size, shape and density. We tentatively attribute those differences to the different experimental conditions (e.g., the thickness of the films, the concentration of the dyes, and the chemical nature of the probes). Scattering measurements on the cheese-like pattern indicate no obvious morphological features in the glycerol film, which leaves two other possible origins responsible for the heterogeneous pattern of the fluorescence intensity. i) The dye distribution is heterogeneous. ii) The dye distribution is homogeneous, but its fluorescence brightness is not uniform in the sample due to its photophysics (e.g., the photophysics of a long-lived dark state). Early work shows that R6G can form a radical ion from the triplet state in polyvinyl alcohol, which leads to a long-lived dark state [96]. Similar photophysics were seen in R6G/glycerol, where the lifetime of this dark state has a strong temperature dependence between 280 K and 200 K [46]. However, PDI is rather photostable and its fluorescence emissivity is almost independent of temperature [1]. If the photophysics of R6G are the cause of the cheese-like pattern in R6G/glycerol sample, then PDI should give a much lower contrast. Both R6G and PDI showed the cheese-like pattern, suggesting that such a pattern is unlikely to be due to photophysics of the dyes. Therefore, we assume that a non-uniform dye distribution in the sample is responsible for the observed cheese-like pattern.

One obvious question is whether the observed cheese-like pattern is probe-induced or an intrinsic property of supercooled glycerol that can be sensed by the probes. The following arguments can rule out the probe-induced hypothesis: first, the concentrations of all five probes used in this work are rather low, ranging from  $10^{-7}$  to  $10^{-9}$  M. Such low concentrations of probes are not expected to influence the properties of glycerol significantly. Secondly, dual-labeled polyproline 40 mer, PDI, Alexa 594 and R6G differ in many aspects, such as size, structure, and chemical properties (Figure 4.1), but they all show similar dye distribution patterns. Therefore, the observed cheese-like pattern is probably not induced by the probes, but rather an intrinsic property of supercooled glycerol made visible by the probes.

Light and X-ray scattering experiments have indicated that density fluctuations occur in supercooled liquids when they are cooled toward their glass transition temperatures [11, 12, 70]. When supercooled glycerol is cooled close to  $T_g$ , the system may start to develop (or nucleate) regions that have higher

density than their surroundings. It is then natural to assume that the observed heterogeneous pattern of the fluorescence intensity at temperatures close to  $T_g$  is related to density fluctuations in the glycerol film. Since the system begins in the pure liquid state in which the fluorescence is homogeneous over the sample, it is very likely that bright areas have a close-to-normal density and the dark areas a higher density. The local glycerol structures in such denser and darker regions may be less disordered or more solid-like. When the probes are added into the glycerol, they may be less easily incorporated into such local ordered structures and therefore are segregated out of these regions. Segregation results from a lower solubility of probes in solid-like parts than in liquid-like regions with the normal liquid density, provided that translational diffusion of the probes is fast enough during the cooling process. Similar segregation is also seen in membrane [93, 94] and other 2D systems [97]. According to this interpretation, the size of dark areas in the fluorescence image corresponds to the size of solid-like domains. We propose that the relatively strong polarity of Alexa 488 is the reason why it did not show the cheese-like pattern in glycerol, because it would interact more strongly with glycerol through hydrogen bonds.

Since the coexistence of liquid and solid-like structures in supercooled glycerol above  $T_g$  has been confirmed by rheological experiments (Chapter 2), it is not very surprising to see distinct dark (solid-like) and bright (liquid) regions in the same temperature range. However, a further growth of the solid-like network in glycerol, which was seen in the rheology was not observed from the fluorescence images at temperatures between 220 K and 190 K. Namely, the size of dark spots remains fairly constant in this temperature range. Experimental conditions (e.g., sample volumes, thickness of films, and contact surfaces) in these two experiments are quite different. In the rheological experiments, the glycerol resided in a 2 mm gap of Couette cell, which was made of brass and held about 9 ml of sample. Here, a glycerol film with a thickness of a few micrometers was coated on a glass substrate with a diameter of 20 mm. Therefore, the behavior of glycerol in these two experiments could be different as well. The picture we have in mind is the following. The solid-like structures appear already at temperatures above 220K. Since the fluorescence is homogeneous at 260 K, the nucleation and growth of solid-like structures perhaps take place between 260 K and 220 K where the viscosities of glycerol are not large enough to prevent the probes from being pushed away from the growing solid-like structures. However, between 220 K and 190 K, this redistribution of the probes due to the growth of the solid-like structures is slowed down and even arrested because of the extremely large viscosities in this temperature

range. Therefore, the size of the dark spots remains nearly the same even at temperatures below  $T_g$  (data not shown).

Another interesting finding is that the fluorescence patterns resulting from slow and quick cooling are quite distinct. In the slowly cooled samples, nucleated micrometer-sized dark spots are dispersed in a bright background. In the quickly cooled sample, however, bright micrometer-sized features are isolated by a dark matrix. Such phenomena are very analogous to nucleation and spinodal decomposition behaviors of phase separation in a two-component system, respectively. [98] Triphenyl phosphite (TPP), another molecular glass-former, was also found to show solid-like behavior at temperatures above its glass transition [80, 81]. This apparently amorphous phase was denoted as the glacial phase, a new amorphous phase distinct from both the glass and crystal. Moreover, two types of phase transformation have been seen in TPP as well, depending on the annealing temperature. The nucleation-growth type of phase transformation was observed at higher annealing temperature ( $T_g+15$  K) and the spinodal decomposition type of transformation happened at lower temperature ( $T_g+8$  K) [82, 83]. These observations from TPP are very similar to what we found here for glycerol. However, these two molecular liquids also show several dissimilarities. First, both types of phase transformation in TPP are more or less complete and lead to the glacial phase [80, 81]. In contrast, the cheese-like and spinodal decomposition patterns are rather stable in glycerol at a fixed temperature below 260 K. Secondly, whereas in TPP the temperature alone determines the phase, in glycerol, the cooling rate plays an equally important part. Lastly, the heterogeneous fluorescence patterns in glycerol from both quick and slow cooling became homogeneous again upon heating at 260 K for more than 10 hours, which suggests that the solid-like structures formed at low temperature in both cases are free from large microcrystallites since the growth of a crystal is more favored at higher temperature once large enough seeds are formed. In the case of TPP, the glacial phase resulting from spinodal decomposition is free from microcrystallites, whereas the final state of nucleation-growth transformation is a mixture of the new amorphous phase and microcrystallites. When heated up above 240 K, TPP from both types of transformation turns into a crystal.

More interestingly, the cheese-like pattern in glycerol can be observed in a previously quickly quenched sample upon heating to 260 K and slow cooling again, indicating that keeping the sample at 260 K for a long period can effectively melt the dense or solid-like structures. This observation not only confirms that the glycerol remained liquid-like at 260 K, but also excludes the possibility that water traces are responsible for the observed heterogeneous

patterns, since the fluorescence intensity became homogeneous at 260 K (see Figure 4.4 E), 12 K below the freezing point of water. Additionally, the cheese-like pattern appeared again upon slow cooling of the quickly quenched sample (see Figure 4.4 F). This additional “melting point” suggests the existence of a “liquid-liquid phase transition” or LLP in a single-component liquid [82,83,99] although the observations here are not the same. Whether the observed solid-like structure in glycerol is related to the glacial phase of TPP or to Fischer clusters is not yet clear. The length-scale of heterogeneity in supercooled glycerol revealed by fluorescence imaging is on the order of micrometers, bridging the gap between the millimeter scale of rheological measurements (Chapter 2) and the nanometer scale of single-molecule fluorescence [1].

## 4.5 Conclusion

We observed a heterogeneous fluorescence pattern in supercooled glycerol doped with fluorescent probes. Such a heterogeneous pattern resulting from a differential dye distribution reveals micrometer-sized structures with an extremely long lifetime, and appears to be connected to the long-lived density fluctuations on the micrometer scale in supercooled glycerol postulated earlier. Moreover, the structure of the heterogeneous pattern is clearly influenced by the cooling rate. A slow cooling leads to a Swiss cheese-like pattern, whereas a quick cooling results in a spinodal decomposition pattern. More work is needed to characterize such heterogeneous patterns, for example, a study of the mobility of probes in the dark and bright regions will give more local structural information, which may help to better understand the complex behavior of supercooled molecular liquids.

## Acknowledgements

We thank Prof. Benjamin Schuler for kindly providing us with dual-labeled polyproline samples. This work is part of the research program of the “Stichting voor Fundamenteel Onderzoek der Materie” (FOM), which is financially supported by the Netherlands Organization for Scientific Research.

4 Micron-sized structure in a thin glycerol film revealed by fluorescent probes

## 5 Small-angle neutron scattering on supercooled glycerol

**Abstract** – We investigate aging of supercooled glycerol by means of small-angle neutron scattering. Two samples are prepared in cuvette cells with thermal histories similar to the previously established one (Chapter 2). We observe the growth of solid-like structures in one sample only, evidenced by both direct visual inspection and the scattering spectra. A new peak appeared around  $0.1 \text{ \AA}^{-1}$  after annealing at 240 K for hours. It is a hallmark of this solid-like state, for it is clearly absent from the pure liquid spectrum of glycerol at the same temperature and from the crystal spectrum.

## 5.1 Introduction

Understanding supercooled liquids and their glass transition is still an open problem in material science. Early concepts for the explanation of the liquid to glass transition postulate the existence of cooperatively rearranging regions (CRR), which are believed to be responsible for the observed spatial and dynamical heterogeneities in many glass-forming systems [4]. Although heterogeneity is readily detected experimentally, its characteristic length scales still remain unclear. The scale of a few nanometers was found by NMR [7, 8] and dielectric relaxation spectroscopy [9, 10]. However, light and X-ray scattering experiments have detected correlation lengths on the order of 100 nm [11, 12]. Glycerol, an archetypal glass-former, has been investigated extensively by many different methods [9, 10, 57, 87–89], but nonergodic behavior in the supercooled regime was never reported until in a recent single-molecule study of local relaxation of supercooled glycerol. This study revealed an extremely long-lived heterogeneity at temperatures well above its glass transition [1]. The associated time scale is on the order of days, about one million times longer than the alpha-relaxation time. Later complementary rheological studies of supercooled glycerol also uncovered a novel viscoelastic behavior at temperatures above  $T_g$  (Chapter 2), consistent with the single-molecule observation that some solid-like structures already developed above the glass transition. To explore the structural origin of this solid-like state, we perform small-angle neutron scattering (SANS) experiments on supercooled glycerol. This technique has proved to be a powerful tool in materials science, which can provide structural information on length scales of 1–100 nm. The technique of ultra small-angle neutron scattering (USANS) further raises the upper resolution limit for structural studies by two orders of magnitude (up to 50  $\mu\text{m}$ ) [100, 101] and hence overlaps with light scattering and microscopy. Similar to the often complementary techniques of small-angle X-ray scattering (SAXS) and light scattering, SANS is very useful because many materials, substances and biological systems possess interesting and complex features in their structure, which match the length ranges that the technique can access. On the other hand, unlike X-ray photons, which interact with the electron cloud surrounding the nucleus, neutrons interact with atomic nuclei and because they are electrically neutral particles, they are deeply penetrating, and are therefore more able to probe bulk materials. As a consequence, SANS enables the use of a wide range of sample environments that are sometimes difficult to use with synchrotron X-ray sources. Another advantage of neutrons over X-rays is that for neutrons the scattering cross section does not vary with the number of nuclei as for X-rays, but is completely different from an element to another.

For instance, H, C, N and O have non negligible scattering cross sections for neutrons, which is not the case with X-rays.

In neutron scattering, the scattering cross-section for the nucleus is the sum of two terms,

$$\sigma = \sigma_c + \sigma_{inc},$$

where  $\sigma_c$  is the cross-section for coherent scattering and  $\sigma_{inc}$  for incoherent scattering. It is the former one that can produce interference and determine the intensities of the Bragg reflections of crystals for neutrons. The latter one in contrast only leads to an isotropic (flat) background. Hydrogen, for instance, has a very large total scattering cross-section ( $\sigma_H = 81.5 \times 10^{-24} \text{ cm}^2$ ) among elements and isotopes. However, the coherent contribution ( $\sigma_{Hc}$ ) is only  $1.8 \times 10^{-24} \text{ cm}^2$ , less than 3% of the total scattering cross-section, which means that the signal from coherent scattering will almost completely drown in the background of incoherent scattering when performing neutron scattering on hydrogenated samples. This, however, is not the case for deuterium, because its total scattering cross-section ( $\sigma_D = 7.4 \times 10^{-24} \text{ cm}^2$ ) has a large coherent component ( $\sigma_{Dc} = 5.4 \times 10^{-24} \text{ cm}^2$ ).

The remarkable difference in scattering contrast between hydrogen and deuterium makes deuterium-labeling techniques practically very useful since partial substitution of deuterium for hydrogen in molecules can increase the signal from the coherent scattering, thus competing with the isotropic background due to the incoherent scattering from hydrogens. This, for example, has been used in polymer studies to specifically “stain” certain polymer chains by replacing the relevant hydrogens with deuteriums during the synthesis and make them “visible” in concentrated solutions and the condensed states [102]. Such selectivity or the enhanced contrast could not be achieved without working in dilute solutions by light and small-angle X-ray scattering. This unique feature of SANS also makes it particularly useful for the biological sciences [103, 104], since biological molecules are usually dissolved in water, and hydrogens which are loosely associated with these molecules are able to exchange with any deuteriums in the solvent. This usually has minimal functional effect on the sample but has dramatic effects on the scattering.

Here we use fully deuterated glycerol samples for SANS measurements for the reason mentioned above. We apply thermal treatments, similar to the previously established one (Chapter 2), to two glycerol samples and the scattering signal is monitored during annealing at 240 K. In one sample, we observe the growth of the solid-like structures at 240 K and the scattering spectrum shows a distinct peak appearing around  $0.1 \text{ \AA}^{-1}$ , which is not seen in the pure liquid



state of glycerol nor in the crystal.

## 5.2 Experimental methods

The small-angle neutron scattering experiment was performed on instrument D11 at the Institut Laue-Langevin (ILL) in Grenoble, France. A neutron beam with a wavelength of 6 Å was used for the scattering measurements. The small and large angle range was chosen to cover the  $Q$  range from 0.008 to 0.431 Å<sup>-1</sup> by changing the detector distance. The deuterated glycerol (DLM-558-5, Cambridge Isotope Laboratories, Inc) was loaded into two quartz cells (100 QS-2 mm, Hellma). These two samples have been measured. The first one (sample A) was prepared in a cryostat with a slow cooling (5 K/h) from 300 K to 194 K followed by a long waiting time (about 43 hours) at a fixed temperature (194 K). During the installation of the cryostat on D11, the temperature regulation was off for about one hour and the sample temperature dropped down to 113 K. The neutron scattering measurements were started when the sample temperature was stabilized again at 194 K. The sample was then heated up to 240 K with a rate of 60 K/h and kept at this temperature for about 16 hours. Due to an unexpected technical problem on the data acquisition, the data during the second half of the aging at 240 K were not saved. We therefore only measured the beginning and the end of the last part of aging. After that, we further heated up the sample to 328 K (30 K/h) to record the spectrum of the normal liquid state and then applied a fast cooling (60 K/h, from 328 K to 240 K) to the sample to obtain the signal arising from the usual supercooled liquid state of glycerol, as a control.

The second sample (sample B) was prepared in a different cryostat with the same slow cooling profile, but it was kept at 194 K for 4 hours before transfer into the D11-cryostat. It is clear that this transfer procedure is not satisfying, due to sudden temperature changes during transfer into liquid nitrogen of a fragile sample. The annealing at 244 K was then monitored for 16 hours.

A deuterated polycrystalline glycerol sample prepared in a quartz cell (100 QS-1 mm, Hellma) was also measured at 243 K as an additional control.

The raw 2D data were treated with a standard procedure in Large Array Manipulation Program developed at the ILL. Because the raw 2D data show strong anisotropy in the scattering signal (see Figure 5.1), which is partly attributed to the reflection from the cryostat, additional care has been taken for the data treatment.

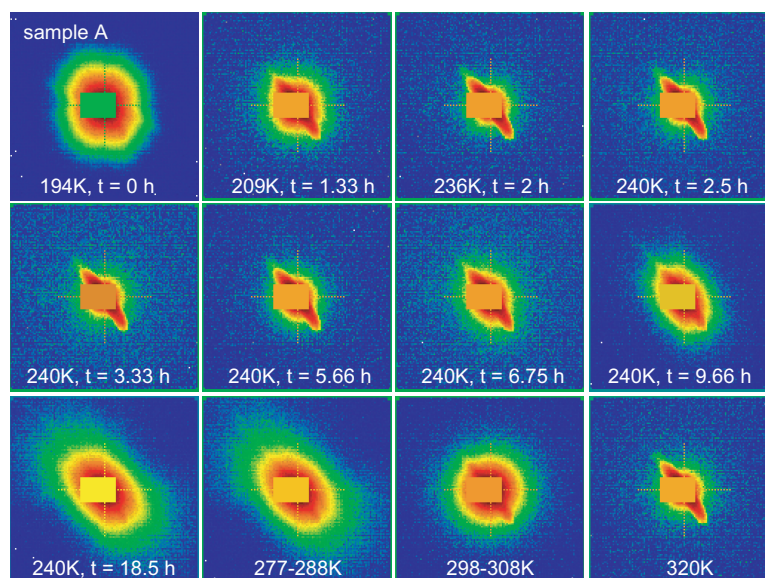


**Figure 5.1:** The raw 2D scattering data of sample A as a function of temperature measured in the small angle range. The diagonal elongated spot (for example on the third image at 236 K) is partly due to a parasitic reflection from the cryostat. The one dimensional scattering spectrum was obtained by radial averaging of the reduced raw 2D data. The rectangle shade in each image indicates the region in which the data have not been taken for radial averaging.

### 5.3 Results and discussion

The work presented in Chapter 3 has shown that the behavior of glycerol has a strong thermal history dependence and an initial slow cooling period appears to be crucial for the development of the solid-like structure. We therefore applied this slow cooling procedure to the two samples measured in this work. Figure 5.2 shows their actual thermal histories and they both, to different extents, deviate from the desired thermal profile because of practical reasons (see Experimental methods section). Nevertheless, we observed the solid-like structures developed in sample A after annealing at 240 K for about 8 hours, which was even visible by eye (data not shown). The whitish material started to grow from one side of the wall in the cuvette cell and it expanded with time. The raw 2D data of this sample also showed a steady increase in the radius of the scattering signal during aging at 240K (see the images at 240K in Figure 5.1). The 1D scattering spectra of this sample are plotted in Fig-

ure 5.3. Figure 5.3 A shows the control spectra of the pure liquid state of glycerol (sample A) at 240 K ( $T_g + 50$  K) obtained by a fast cooling (60 K/h, from 300 to 240 K) into the supercooled regime and at 328 K ( $T_m + 36$  K) in the normal liquid regime, in comparison with the spectrum of the crystal sample recorded at 243 K. Upon heating the sample to 240 K after a long period of quenching at 194 K, the small angle scattering signal between  $0.008 \text{ \AA}^{-1}$  and  $0.07 \text{ \AA}^{-1}$  first decreased dramatically with increasing temperature, whereas the signal in the large angle range remained unchanged (see Figure 5.3 B), suggesting a pronounced rearranging process taking place mainly on the large scales (9-63 nm). However, after annealing at 240 K for a few hours the signal started to recover, indicating that a restructuring can occur after incubating at a higher temperature. Meanwhile, in the large angle range, a new peak appeared around  $0.1 \text{ \AA}^{-1}$  during this annealing process (see Figure 5.3 C), corresponding to a characteristic length scale of 6 nm approximately. The  $0.1 \text{ \AA}^{-1}$  peak is a hallmark of the solid-like state of glycerol, which is clearly absent in the pure liquid state obtained by a fast cooling (see the inset in Figure 5.3 C). This peak is also absent from the crystal sample. Upon further heating the solidified glycerol to temperatures below 292 K, the shape of the spectra did not change much except for a slight increase of the overall signal (data not shown). When the temperature crossed the melting point of the crystalline glycerol, the scattering signal dropped and the peak disappeared (see the molten spectrum in Figure 5.3 A), indicating the melting of the solid-like structures.

Sample B, however, was transparent all the time at 240 K and the spectra revealed no changes at this temperature for 16 hours (see Figure 5.4). It is not clear why the solidification did not happen to this sample. However, it should be noted that the thermal histories of the two samples are not the same. For example, sample A had a period of 43 hours at 194 K, about 10 times longer than that of sample B (about 4 hours). Sample B experienced a much lower temperature (77 K) than sample A and was annealed at 244 K, instead of 240 K. All these differences may contribute to the failure of partial solidification in sample B. A similar problem was also seen in the rheological measurements of glycerol in the plate-plate geometry (in Chapter 3) where only one out of six runs showed the solid-like behavior, even though the thermal history was well controlled. It seems that solidification of supercooled glycerol has a random nature and its onset is influenced by many external parameters. Some of them are controllable in practice, such as the thermal history and the sample geometry. Some are difficult to control, like the purity of the sample and the properties of the interface between the sample and the measurement device. This somehow coincides with a general scenario of crystallization of

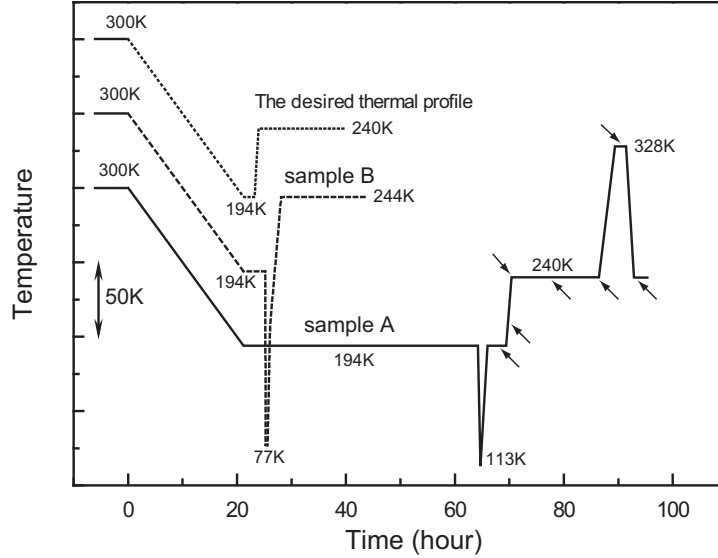


**Figure 5.2:** The thermal histories of the two samples in comparison with the established thermal profile. The lines are vertically shifted for clarity. The dotted line is the desired thermal profile, which we would like to reproduce. The solid and dashed lines are the actual thermal profiles for sample A and sample B, respectively. The initial slow cooling rate is about 5 K/h. The sudden drops of temperature far below the glass transition (190 K) in sample A and B are due to the practical reasons (see Experimental Methods). The arrows indicate when the spectra of sample A in Figure 5.3 were taken.

melts where the number of nuclei in the melt, crucial to the final crystallization, is greatly influenced by the size and history of the sample and the condition of the container. The effect of amount of materials on the frequency of nucleation has been investigated by many people. Tammann, for instance, noted that 6 g of phenol required, on the average, 2810 s to crystallize, whereas 30 g took only 33 s under the same conditions [105]. The stochastic nature of crystal nucleation can also be seen in crystallization of polymers in a confined geometry [106].

Is solidification of supercooled glycerol related to a crystallization process? Based on the preliminary results from sample A, this is still an open question since the spectra of the solidified glycerol are different from that of the crystal sample. In addition, the Q range used in this work is outside the range where

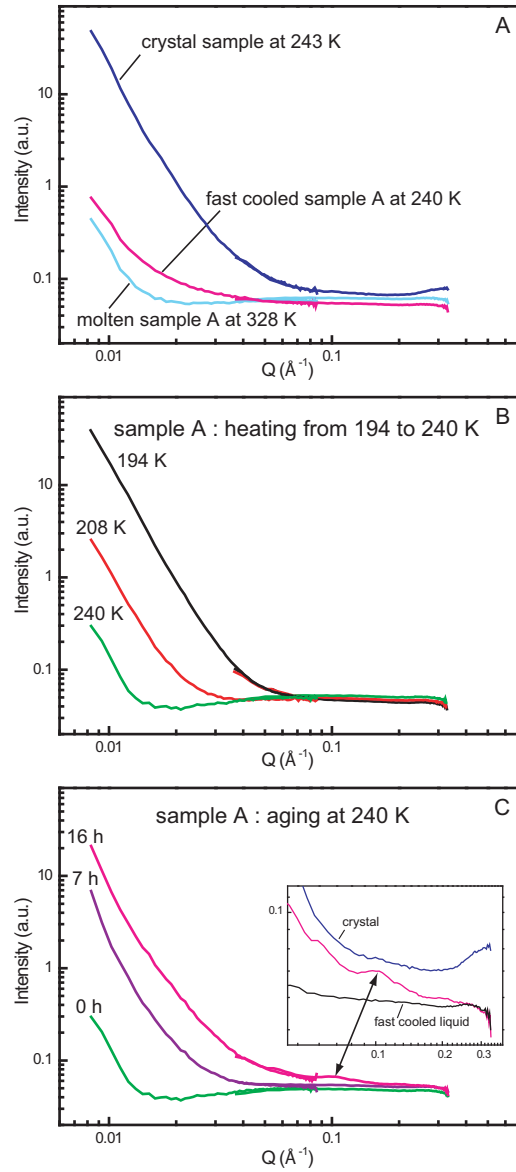


**Figure 5.3:** The scattering spectra of sample A at different stages. (A) Pure liquid state of sample A at 240 K (by a fast cooling) and 328 K, in comparison with a crystalline state of a control sample. (B) Heating from 194 to 240 K. (C) Aging at 240 K. The inset is the enlarged view of the region in which a new peak centered around  $0.1 \text{ \AA}^{-1}$  was clearly identified after 16 hours at 240K, which was not seen in the liquid and crystalline states of glycerol in this temperature range.

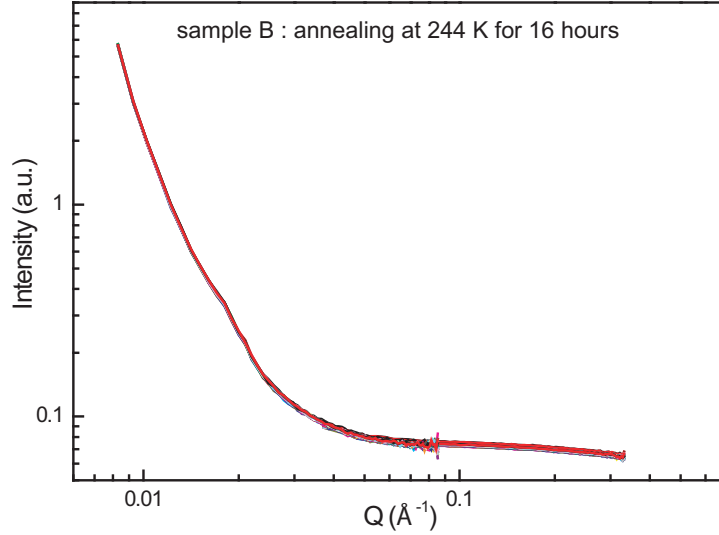


**Figure 5.4:** 24 spectra of sample B measured every 40 min at 244 K for a period of 16 hours. They are all perfectly overlapped

the Bragg peaks are normally seen, i.e., between  $0.5 \text{ \AA}^{-1}$  and  $5 \text{ \AA}^{-1}$ . Nevertheless, the steady increase of the scattering signal around  $0.1 \text{ \AA}^{-1}$ , leading to the formation of a well defined peak, during the aging at 240 K is a unique feature for the solid-like state of supercooled glycerol. Schwickert et al. have recently performed a similar study on supercooled triphenyl phosphite (TPP) [107], a molecular liquid that shows an anomalous solid-like behavior at temperatures above its glass transition [80, 81]. They characterized the early stages of cluster growth in supercooled TPP by using small-angle neutron scattering and they found a pronounced increase of the scattering signal around  $0.07 \text{ \AA}^{-1}$  during annealing in the temperature range of 210 K to 214 K, which is very similar to what we observed from the solidified glycerol here. The solid-like state of glycerol, therefore, seems to be closely related to the solid-like state of TPP, also known as the glacial state [80, 81]. The structural description of this glacial state is still under debate. The experiments performed at higher temperatures (216 K-235 K) indicate that the glacial state of TPP is a mixture of micro-crystallites and non-transformed supercooled liquid [84], whereas the measurements at a lower temperature (213 K) suggest that the glacial state is a homogeneous glassy state of a denser liquid free from micro-crystallites [82, 83].

The sample (thermal) history is therefore an important experimental parameter, which should be carefully taken into account before any interpretation of own results or comparison with others' is made, especially in the study of viscous molecular liquids whose behaviors have a strong thermal history dependence.

## 5.4 Conclusion

We studied the aging of supercooled glycerol by small-angle neutron scattering. Two samples were measured and we only observed the solid-like structures in one sample where a new peak formed around  $0.1 \text{ \AA}^{-1}$  in the scattering spectrum after aging at 240 K for hours. This peak was absent in both the liquid and crystalline states of glycerol at the same temperature. Because the Q range chosen in this work does not cover the range in which the Bragg peaks normally appear, we do not know whether the solid-like structures contain crystals or not. Future studies in the large Q range at a lower temperature, for example at 220 K or even 205 K, combined with different cooling rates shall give more insight into the structural origin of this solid-like state in supercooled glycerol.

## Acknowledgements

We thank Marie Plazanet and Isabelle Grillo for the local assistance at the ILL and David Bowyer for the technical support on the D11 machine.

## 6 Temperature-cycle microscopy of single-molecule FRET in polyprolines

**Abstract** –We investigate the conformational dynamics of polyprolines by single-molecule Förster resonance energy transfer (FRET) combined with a temperature-cycle microscopic technique developed in our group. We first measure the static FRET efficiency of individual frozen constructs in a thin glycerol film at a low temperature. The measurements on polyproline 6 and polyproline 20 reveal a broad FRET distribution. The broadening stems from the wide distribution of the orientation factor and the fluctuation of the interdye distance. In the fluorescence time traces of the individual constructs, we study variation of the donor and acceptor signals and observe 3 types of events. (1) A correlation between the two signals, i.e., the acceptor intensity is positively correlated with the donor intensity, is observed when the donor is in a dark state or bleached. (2) A noncorrelation, i.e., the acceptor intensity changes independently of the donor intensity, is seen when the acceptor is in non-fluorescing states and it could still accept the excitation energy from the donor. (3) An anticorrelation between the donor and acceptor intensity is detected if a non-fluorescing form of the acceptor is not able to quench the donor emission. We performed our first temperature-cycle measurements on polyproline 6 molecules and we could indeed detect the conformational changes induced by temperature jumps by measuring the FRET efficiency. These preliminary results demonstrate that temperature-cycle microscopy combined with single-molecule FRET has potential for studies of protein-folding dynamics at the single-molecule level.



## 6.1 Introduction

The study of single molecules in biological systems has been booming in the last decade. Because single-molecule techniques are intrinsically free from ensemble averaging, they are particularly appealing in addressing biological processes in which heterogeneity is native to the structure or dynamics of the systems, such as enzymatic reactions, protein-DNA or -RNA interactions, and protein-folding. Single-molecule techniques can be divided into two categories in general. One category gathers force-based approaches, which typically involve an atomic force microscope (AFM), or optical/magnetic tweezers, and allow to study mechanical properties of single biomolecules, like DNA molecules [108–111] and proteins [112–114], or interactions between biomolecules, such as protein-DNA interactions, e.g., in nucleosomes [115,116] and chromatin [117,118]. The other class is based on single-molecule optical detection, which requires microscopes to detect optical signals by absorption, emission (fluorescence), scattering, or a combination of these using labeled systems. The information from the detected optical signals has to be related to the underlying molecular process. These two approaches provide molecular information about different aspects and thus are complementary. If they are employed in the same experiment, one will uncover more details about biological processes under investigation than with either of them alone. This will further extend the capability of single-molecule methods to address more complicated processes, e.g., the transcriptional machinery. Indeed, several groups have demonstrated the feasibility of combining force measurements with fluorescence to study protein-DNA interactions *in vitro* [119–122].

Among the optical-based methods, single-molecule fluorescence spectroscopy has been widely used in biological applications because of its high sensitivity, selectivity and versatility [123–125]. A single dye-labeling typically allows to probe translational and/or rotational diffusion of individual labeled biomolecules and thus to gain the information on their mobility in certain environments. This has been used, for instance, to study the mobility of cAMP-receptor on the plasma membrane of chemotacting cells in directional sensing [126]. Labeling with two different dyes enables to study inter- or intramolecular interactions on the length scale of 10 – 75 Å by Förster resonance energy transfer (FRET), [33,34]. The length scale is about one to two orders of magnitude smaller than the wavelength of visible light. The FRET technique thus proves to be a powerful “spectroscopic ruler”. Since the first demonstration of single-molecule FRET by Ha et al. in 1996 [35], many experiments have been designed for biological applications [36–41,43,44,127]. In the FRET process, excitation energy from a donor is transferred to an acceptor

via a near-field dipole-dipole interaction. The efficiency of energy transfer,  $E$ , is given by

$$E = \frac{1}{1 + \left(\frac{R}{R_0}\right)^6} \quad ,$$

where  $R$  is the distance between the donor and acceptor and  $R_0$  is the Förster radius, at which 50 % of the energy is transferred. It is a function of the properties of the dyes. The distance  $R_0$  (in Å) is calculated in the Förster theory according to the following equation [128]:

$$R_0 = 9.78 \times 10^3 (\kappa^2 n^{-4} \phi_D J(\lambda))^{1/6} \quad ,$$

$$J(\lambda) = \int_0^\infty F_D(\lambda) \epsilon_A(\lambda) \lambda^4 d\lambda \quad ,$$

where  $J(\lambda)$  is the normalized overlap integral between the donor emission,  $F_D(\lambda)$ , and the acceptor absorption,  $\epsilon_A(\lambda)$ .  $\phi_D$  is the donor's fluorescence quantum yield and  $n$  is the refractive index of the medium between the dyes. The factor  $\kappa^2$  depends on the relative orientation between the two dyes and can vary from 0 to 4. If the dipole moments of donor and acceptor are free to rotate isotropically on a time scale much faster than their radiative lifetimes, a geometric averaging of all the angles will result in a value of 2/3 for  $\kappa^2$ . The FRET efficiency,  $E$ , determined through the fluorescence intensities from both the donor and acceptor or the fluorescence lifetimes of the donor in the presence and absence of the acceptor, can then be related to the inter-dye distance,  $R$ . However, since the fluorophores may interact with the host molecule to which they are attached and this interaction will restrict their motion, the averaged angular factor may differ from 2/3 and should be checked carefully for the proper calculation of  $R$ .

When performing single-molecule FRET experiments on biological systems, one can detect dual-labeled molecules in two different ways. One way is to detect freely diffusing molecules in a solution with a confocal microscope. When the molecule diffuses through the confocal volume, a photon burst from the labels can be detected. The FRET efficiency from each burst is calculated and the associated histogram can be constructed. In addition, fast dynamics on the time scale of microseconds can be probed by performing Fluorescence Correlation Spectroscopy (FCS). The detection of freely diffusing molecules is relatively easy to perform and there are no complications resulting from immobilization procedures. However, as the molecules only reside in the detection volume for a limited time period, the slow dynamics on time scales much larger

than the characteristic diffusion time of the molecules are not accessible. To probe such slow dynamics, one normally immobilizes the molecules on a surface. The molecule can be attached directly through a linker or encapsulated within a surface tethered vesicle [129]. Individual molecules can then be studied one at a time via a confocal configuration or in parallel via a wide-field imaging setup. Although immobilization enables to access slow dynamics, in practice it often involves sophisticated surface preparations and tethering chemistries, which sometimes can introduce artifacts into the dynamics or affect the structure of the molecules of interest. In addition, since the molecule is illuminated all the time during the measurements, one limiting factor is the photophysical behavior of the dyes, namely, photoblinking and photobleaching. Photoblinking is the reversible transition of a fluorophore between a fluorescing state and a non-fluorescing state, a “dark” state, which is induced by the excitation light [45] and can sometimes complicate the interpretation of the FRET results [44]. Photobleaching is the irreversible conversion of a fluorescent molecule into a non-fluorescent entity, which limits the observation time of the molecules. Moreover, since a single dye molecule can only emit a limited number of photons per second, a certain minimum integration time has to be chosen in order to obtain a reasonable signal-to-noise ratio, which restricts the accessible dynamics on the short times. The above mentioned limitations are generic in room-temperature single-molecule fluorescence measurements.

To achieve longer observation windows and access fast dynamics from single-molecules, our group has developed a new type of temperature-cycle microscopy [46]. The method relies on (a) rapid freeze-thaw cycle(s) of a microscopic sample to separate the conformational evolution of a single molecule at room-temperature from the optical probing of the fluorescent label(s), which takes place at low temperature where the photophysical parameters of the label(s) are more favorable than at room-temperature. The temporal resolution in this case is only determined by the time it takes to undergo the temperature jump, which has been shown to be as short as a few microseconds [46]. This leads to an improvement in time resolution of about three orders of magnitude compared to conventional single-molecule experiments at room-temperature. In addition, the temperature at which dynamics take place and the duration of dynamics can be well controlled by tuning the heating power and heating period, respectively. The control of temperature opens the possibility of manipulating some reactions or processes in which the temperature determines the probability to pass activation barriers. Hence, temperature variation allows not only to determine the height of an activation barrier (Arrhenius law),

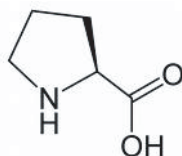
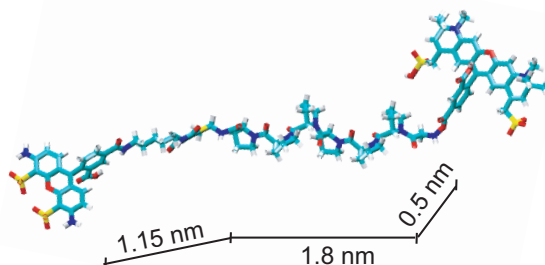


**Figure 6.1:** Structure of the amino acid proline.

but also to selectively block certain pathways involved in a process. These features are particularly useful to study complicated multi-pathways processes, such as protein-folding, since the associated potential-energy landscape in principle can be mapped out with our proposed temperature-cycle microscopy and thus can help to understand how a 1D polypeptide chain folds into a functional 3D structured protein.

To prove the principle of temperature-cycle microscopy, we apply this new method to the investigation of the conformational dynamics of single-molecule FRET labeled polyprolines in a thin glycerol film. Proline is one of the 20 amino acids that build up proteins. Unlike the other 19 amino acids, the side chain of proline is connected back to its backbone (see Figure 6.1), so the overall structure is considerably restricted. The oligomer of proline or polyproline can form two types of helix, a left-handed poly-Pro II helix due to the *trans* isomer of its peptide bond and a right-handed poly-Pro I helix due to the *cis* isomer. Both helices are stable and stiff. In aqueous solution polyproline usually adopts a *trans*-form poly-Pro II helix, which is energetically more favorable than a poly-Pro I helix. However, it has been shown that *cis* isomerization can take place within a poly-Pro II helix [130–132]. Since polyproline was first used as “a molecular ruler” to calibrate distances from FRET measurements by Stryer and Haugland in 1967 [34], much more effort has been devoted to characterizing its behavior in buffer solutions at room-temperature [43, 127, 131–137], providing ample reference for our low-temperature measurements on this model molecule. In our experiments, we choose glycerol as solvent for polyprolines because of the following reasons. First, glycerol is not harmful to proteins and is often added to buffer solutions in low temperature measurements to prevent ice formation during the cooling, which sometimes can disturb the structure of bio-macromolecules significantly. Second, glycerol has a very high viscosity at room-temperature, thousand times more viscous than water. Its viscosity varies by about 10 orders of magnitude from room-temperature to the glass transition (190 K) [57], and can be used to calibrate our heating for temperature-jumps [46]. In ad-



Alexa 488 - Cys - [Pro]<sub>6</sub> - Gly - Alexa 594

**Figure 6.2:** Structure of dual-labeled polyproline 6. The contour length of polyproline 6 is about 1.8 nm. The lengths of two linkers are about 1.15 nm and 0.5 nm, respectively. If the molecule is fully stretched, the interdye distance is around 3.45 nm. If the two linkers fold back to the backbone, the interdye distance is approaching to 0.15 nm.

dition, owing to its viscous nature, glycerol hardly evaporates in a dry environment, which makes the sample preparation much easier than working with normal buffer solutions. The latter typically requires a cover slip or a closed cell to prevent the sample solution from evaporating.

## 6.2 Experimental methods

### 6.2.1 Sample preparation

Alexa 488 & Alexa 594 dual-labeled and Alexa 488 single-labeled polyprolines were synthesized in the Department of Biochemistry, University of Zurich. The structure of dual-labeled polyproline 6 is shown in Figure 6.2. The labeled polyprolines were dissolved in glycerol solution at concentrations ranging from  $10^{-11}$  to  $10^{-13}$  M. The glycerol solution was directly spin-coated at 6000 rpm on a round glass substrate, which has a diameter of 20 mm and is coated first with a thin absorbing metal film (thickness 50 nm, Chromium) and then a layer of silica (thickness 50 nm). To improve wetting, the glass substrates were first treated in a UV-ozone cleaner (model 42-220, Jelight, Irvine, CA). The resulting thickness of the glycerol film from this procedure was 0.5–2  $\mu$ m, as deduced from examination in a home-built Michelson interferometer. To

minimize the water content of glycerol, the samples were dried in the cryostat by repeatedly pumping and flushing with helium gas at room-temperature and kept under dry helium throughout all experiments.

### 6.2.2 Optical setup

The setup combined a low-temperature home-built confocal microscope with single-molecule sensitivity and a heating path for the fast temperature cycles. It has been described in detail in ref. [46]. The key optical components inside the cryostat are schematically shown in Figure 6.3. Briefly, the probing beam from either the 488 nm line of an Argon-ion laser (Spectra-Physics Stabilite 2017) or a 594 nm yellow HeNe laser (25LYP173-230, Melles Griot) enters the cryostat through the bottom window and is focused by a custom-made low-temperature microscope objective (NA=0.85) onto the sample. The fluorescence emitted from the sample is collected through the same objective and then spatially filtered with a 100  $\mu\text{m}$  pinhole. After additional filtering to remove scattered laser (Semrock NF01-488U-25 & LP02-488RU-25 for the 488 nm laser, NF01-594U-25 for the 594 nm laser, and Thorlabs FES0700, a short-pass filter for blocking the NIR heating laser), the fluorescence is separated into donor and acceptor components by a dichroic mirror (585DCXR, AHF Analysentechnik) and three final filters (AHF Analysentechnik HQ535/50X for the donor and HQ615LP & HQ638/95M for the acceptor). Each component is focused onto a photon-counting avalanche photodiode (SPCM-AQR, Perkin-Elmer). The NIR heating beam from a 785 nm single-mode diode laser (XTRA, TOPTICA Photonics AG) enters the cryostat through one of its side windows, is directed downward by a 45° mirror and focused onto the metal film by an aspheric singlet lens (NA=0.68). The sample plate and the NIR lens (together with the 45° mirror) are separately held by a home-built cryostat insert. This insert allows us to adjust both elements in three dimensions so that the visible and NIR foci can be overlapped.

To achieve alternating illumination with probing or heating light, a mechanical shutter (VS14S2Z0-7070, UNIBLITZ) and an acousto-optical modulator (AOM) (MT100A1.5-IR, AA Opto-Electronic) were used to gate the probing (488 nm) and heating (785 nm) beam, respectively. The employed alternating-cycle is shown in Figure 6.4. A full cycle begins with the optical probing at a low temperature for a period  $t_1$  (300 ms), then followed by a delay  $t_2$  (100 ms) produced by the response of the mechanical shutter (10 ms). After this short break, the NIR heating laser is switched on for a very short time  $t_3$  (10  $\mu\text{s}$ ) during which the temperature quickly jumps to a high temperature. At the end of the cycle another delay  $t_4$  (100 ms) after the heating is inserted to en-

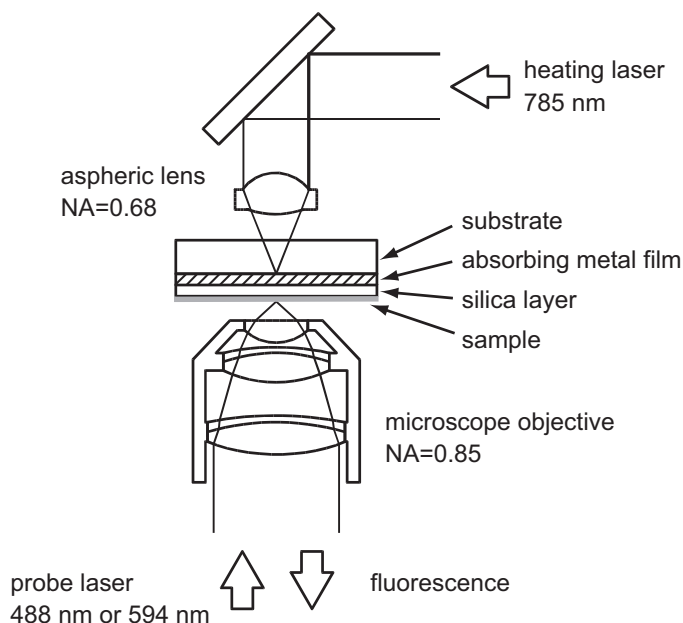


**Figure 6.3:** Scheme of the key optical elements around the sample plate inside the cryostat (not to scale). The figure shows the absorbing sample plate required for sufficient NIR laser absorption, which consists of a glass substrate (thickness 0.17 mm), a thin absorbing metal film (thickness 50 nm, Chromium), and a silica layer (thickness 50 nm). The fluorescent sample is spin-coated on the silica surface. Fluorescence is excited by a probe laser (488 nm or 594 nm) and collected by the custom-made ten-lens objective (NA=0.85, represented by a simplified scheme) beneath the sample. Above it, a 45° mirror and an aspheric singlet lens (NA=0.68) direct and focus the NIR heating beam (785 nm) onto the metal film above the visible focus.

sure that the temperature relaxes back to the original point before the next cycle starts. This alternating scheme was controlled by the ADwin-Gold system (Jäger Computergesteuerte Messtechnik GmbH) via our data-acquisition software written in Labview.

The confocal scanning images,  $20 \times 20 \mu\text{m}^2$  in size, were scanned with 200 by 200 pixels, a dwell time of 10 ms, and an excitation power of  $2.0 \text{ kW}/\text{cm}^2$  for both 488 nm and 594 nm excitations. The fluorescence time traces were recorded with an integration time of 100 ms and an excitation power varying from  $0.4$  to  $2.0 \text{ kW}/\text{cm}^2$ .

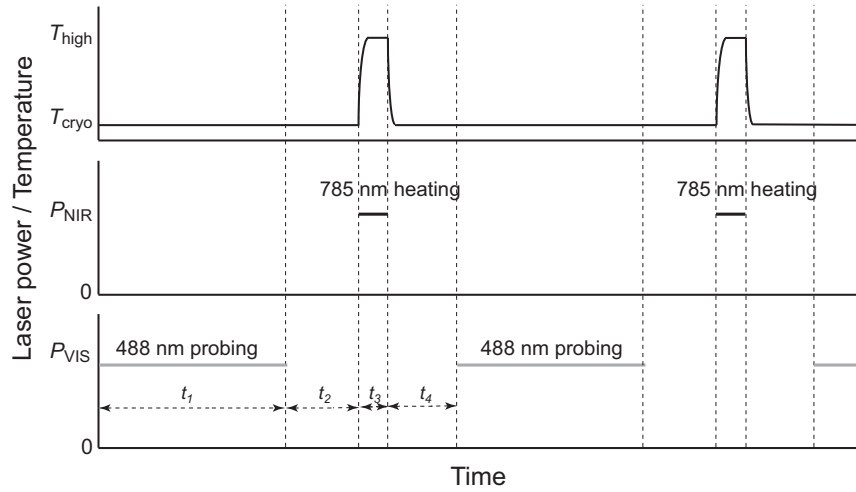


**Figure 6.4:** The alternating scheme of the probing and heating beams. A full cycle starts with  $t_1$  (300 ms) during which only the probing beam is on and the fluorescence measurements take place at low temperature. Then a short delay  $t_2$  (100 ms) follows to wait for the response of the mechanical shutter to fully block the probing beam. After this short interval, the NIR heating beam is switched on for a very short period  $t_3$  (10  $\mu\text{s}$ ) during which the temperature rapidly jumps to a high temperature. Another break  $t_4$  (100 ms) is set at the end of the cycle to allow the temperature to relax back to the initial low temperature before the new cycle begins.

### 6.2.3 Heating calibration

Temperature calibration of the heating spot on the metal film with the NIR laser (785 nm) was performed in the same way as described in ref. [46]. Briefly, the photoblinking of Rhodamine 6G in glycerol has a strong temperature dependence between 200 and 280 K, which gives rise to a positive sublinear relationship between the fluorescence anisotropy and the temperature. At temperatures above 280 K, the anisotropy decreases with increasing temperature according to Perrin's law [138]. The center temperature of the heating spot, therefore, can be calibrated from the fluorescence anisotropy of Rhodamine 6G ( $10^{-5}$  M) in glycerol as a function of NIR power in a series of images at varying heating power. The resulting local temperature calibration is shown in Figure 6.5 where a linear fit gives a slope of 10 K/mW, which is in good agreement with the previous calibration (10.3 K/mW) [46].



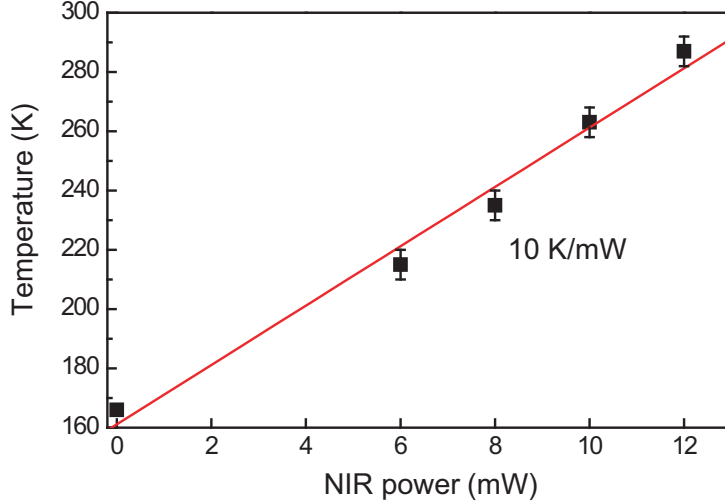


**Figure 6.5:** Actual temperature calibration with anisotropy in the center of the heating spot as a function of heating power. The temperature scales linearly with applied power with a slope of 10.0 K/mW (solid line). The first data point is given by the cryostat temperature and the accuracy of the calibration is  $\pm 5$  K, indicated by error bars.

#### 6.2.4 Data analysis

The FRET efficiency from the fluorescence intensity traces was calculated by means of the following equation:

$$E = \frac{I_A}{I_A + \gamma I_D} \quad ,$$

Where,  $I_A$  and  $I_D$  are acceptor and donor intensity (after background subtraction and crosstalk correction) respectively, and  $\gamma = \frac{\Phi_A \eta_A}{\Phi_D \eta_D}$  is a parameter correcting for the photophysical properties of the dyes.  $\Phi_A$  and  $\Phi_D$  are acceptor and donor quantum yield, and  $\eta_A$  and  $\eta_D$  are acceptor and donor detection efficiency respectively. For the optical setup and the fluorophores used in this study,  $\gamma$  is estimated to be close to unity.

A Labview-based analysis routine was used to facilitate automatic FRET calculation from the raw intensity traces recorded with temperature cycles. The analyzing algorithm involves a selection step to take only the signals above a predefined threshold for further calculation in each channel, which sometimes

leads to no FRET value in some cycles if the associated signals are below the threshold.

## 6.3 Results

In dual-labeled polyproline constructs, Alexa 488 and Alexa 594 were chosen as the FRET pair. These two dyes are frequently used in fluorescence measurements, however there are no detailed studies of their photophysical properties available from literature neither at room-temperature nor at low temperature. Therefore, before we performed the FRET measurements on the full constructs, we first checked the photophysical behavior of the donor from Alexa 488-labeled polyproline10 molecules in glycerol. Figure 6.6 A shows a fluorescence image of this donor-only labeled construct. Most of the bright spots in the image originate from single emitters, as evidenced by a single step bleaching behavior in the relevant fluorescence time traces measured afterwards. Examples of two traces taken from two bright spots in this image are shown in Figure 6.6 B and C, respectively. Both traces show a clear single step bleaching, and additionally trace B has a fluorescence intermittence, the fingerprint of photoblinking, for about 20s before the molecule is bleached. The blinking events sometimes can be seen in the scanned image as well. For instance, the spot in the middle of the right edge has a clear black stripe in it, indicating a dark state of the fluorophore during raster scanning that line. We also measured single Alexa 594 alone in glycerol at low temperature and the photoblinking was observed as well (data not shown). Here, we did not intend to do systematic photophysical studies of these two dyes. Rather we wanted to have a general impression about their photophysics in glycerol at temperatures below the glass transition (190 K).

We performed static FRET measurements first on dual-labeled polyproline 6 molecules at temperatures below the glass transition of glycerol where the molecules were frozen in the host matrix. Figure 6.7 shows a fluorescence image of this construct recorded at 170 K by exciting the donor. Representative fluorescence time traces from some of these molecules are shown in Figure 6.8. Because of the interplay of the photophysics of the donor and acceptor, the behaviors of their fluorescence time traces were very different from what we expected. In an ideal situation, the two signals from the donor and acceptor should be anticorrelated, i.e., when the acceptor is bleached or in a dark state, the signal from the donor is increased to a new level before it is bleached. This was indeed observed (see trace A after  $t=50$  s and trace D at  $t=60$  s), but very rarely. Frequently, we saw the acceptor intensity was positively correlated with

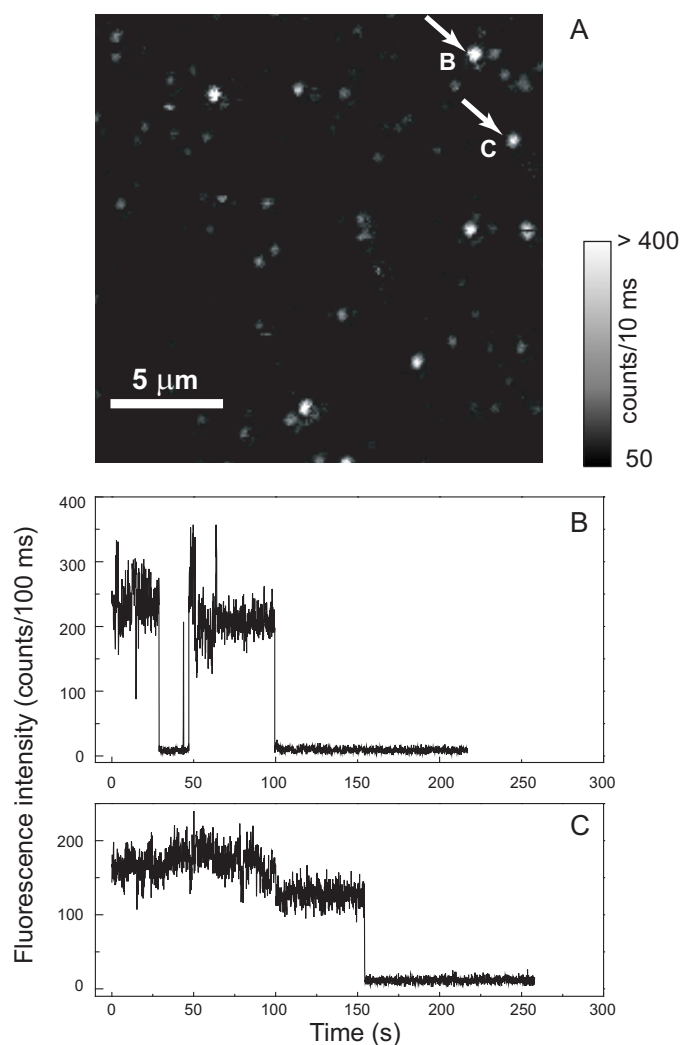


**Figure 6.6:** A confocally scanned fluorescence image of Alexa488-labeled polyproline10 molecules in glycerol recorded at 159 K (A) and examples of fluorescence time traces taken from two bright spots in this image (B&C). (A) The image was scanned by  $200 \times 200$  pixels, an integration time of 10 ms, and an excitation power of  $2.0 \text{ kW/cm}^2$ . The scale bar is  $5 \mu\text{m}$ . The two bright spots indicated by the arrows from the image were further analyzed by recording their time traces with a time resolution of 100 ms and an excitation power of  $100 \text{ W/cm}^2$ , which are shown in (B) and (C), respectively. Both traces show a single-step bleaching behavior, indicating the origin of a single emitter. In addition, there was a dark period of about 20 s in trace B, showing the photobleaching of the fluorophore. Blinking events can also be seen in the image, for example the spot in the middle of the right edge has a clear black stripe in it, indicating a temporary dark state of the fluorophore during raster scanning that line. Most of the bright spots in the image stem from single polyproline constructs.

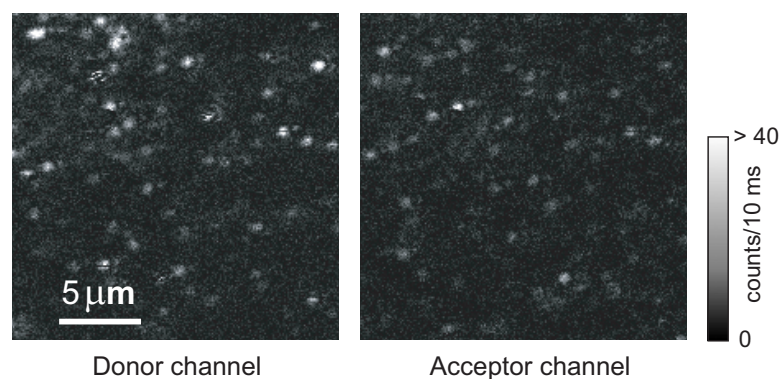


**Figure 6.7:** A confocally scanned fluorescence image of dual-labeled polyproline 6 molecules in glycerol excited with the 488nm laser at 170 K. The images were scanned by  $200 \times 200$  pixels, an integration time of 10 ms, and an excitation power of  $2.0 \text{ kW/cm}^2$ . The bright spots in the acceptor channel indicate the occurrence of FRET.

the donor intensity as shown in trace B and C. This correlated behavior can be explained by the photoblinking and bleaching of the donor, which prevents energy transfer from the donor, hence emission from the acceptor. Sometimes, we observed that a non-fluorescing state of the acceptor did not trigger the increase of the donor signal (see trace D before  $t=40$  s), indicating that this dark state of the acceptor can still accept the excitation energy from the donor. This non-fluorescing quenching could even happen when the acceptor was bleached (see trace E).

The static FRET efficiencies were calculated from the fluorescence time traces of frozen molecules. Figure 6.9 A shows the histogram of the FRET efficiencies of 80 molecules. Instead of the narrow peaked distribution observed at room-temperature [43], our low temperature measurements revealed a very broad distribution spanning the full range of the FRET values. According to the Förster theory, the FRET efficiency,  $E$ , depends not only on the interdye distance,  $R$ , but also on the relative orientation of the two dyes,  $\kappa^2$ . In first approximation, the dual-labeled polyproline 6 construct can be considered as a short rigid spacer (about 1.8 nm) flanked by a FRET pair of dyes, assuming  $R$  is constant. This leaves  $\kappa^2$  as the only variable for the FRET efficiency. In this approximation, the observed broad distribution of FRET efficiency therefore reflects the distribution of  $\kappa^2$ . If the dye molecules were frozen into various angular configurations randomly at a fixed distance, the distribution of the

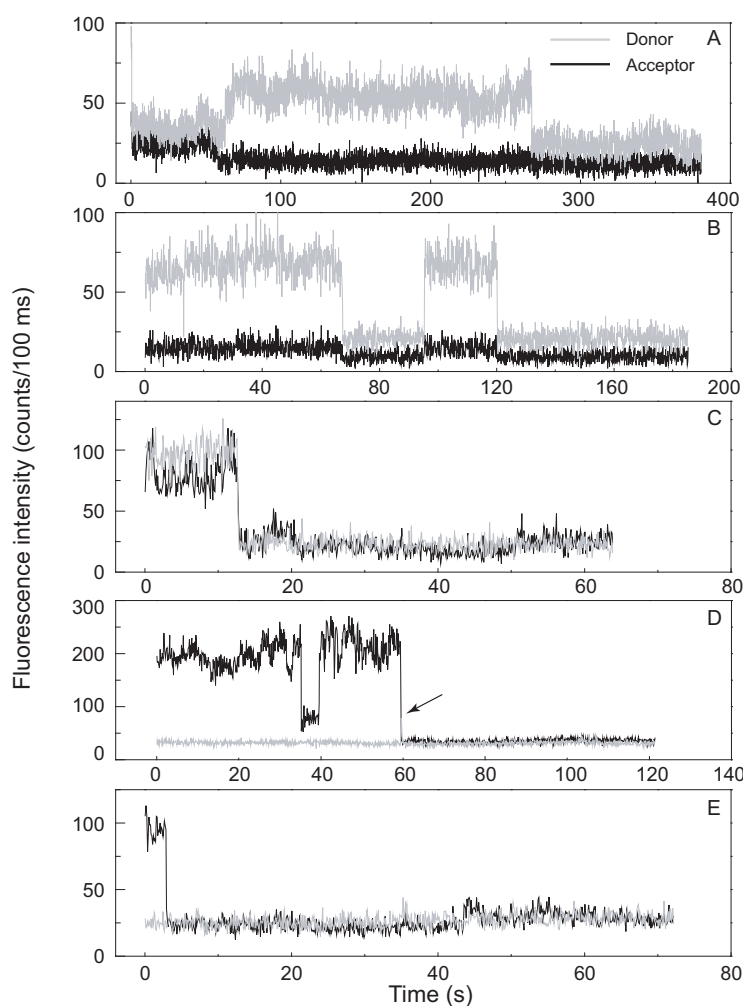


**Figure 6.8:** Representative fluorescence time traces from frozen dual-labeled polyproline 6 molecules. All the traces were recorded by the donor excitation with an integration time of 100 ms and an excitation power of  $1 \text{ kW/cm}^2$  except for trace D  $2 \text{ kW/cm}^2$ . (A) The two intensities varied in phase in the first 60 s. Then the acceptor intensity went down to the background level and the donor intensity went up to a new level before it was finally bleached. (B & C) The intensities of the donor and acceptor changed in a correlated manner. (D) The donor intensity was on the background level in the first 60 s, whereas the acceptor intensity was relatively high, indicating a high FRET efficiency. However, the acceptor had a period of low emission during which the donor intensity did not recover. When the acceptor was bleached, the donor intensity simultaneously jumped up, indicated by the arrow, but went down to the background level very quickly. (E) The traces showed a high FRET efficiency in the beginning. When the acceptor was bleached, the donor intensity still remained the same.

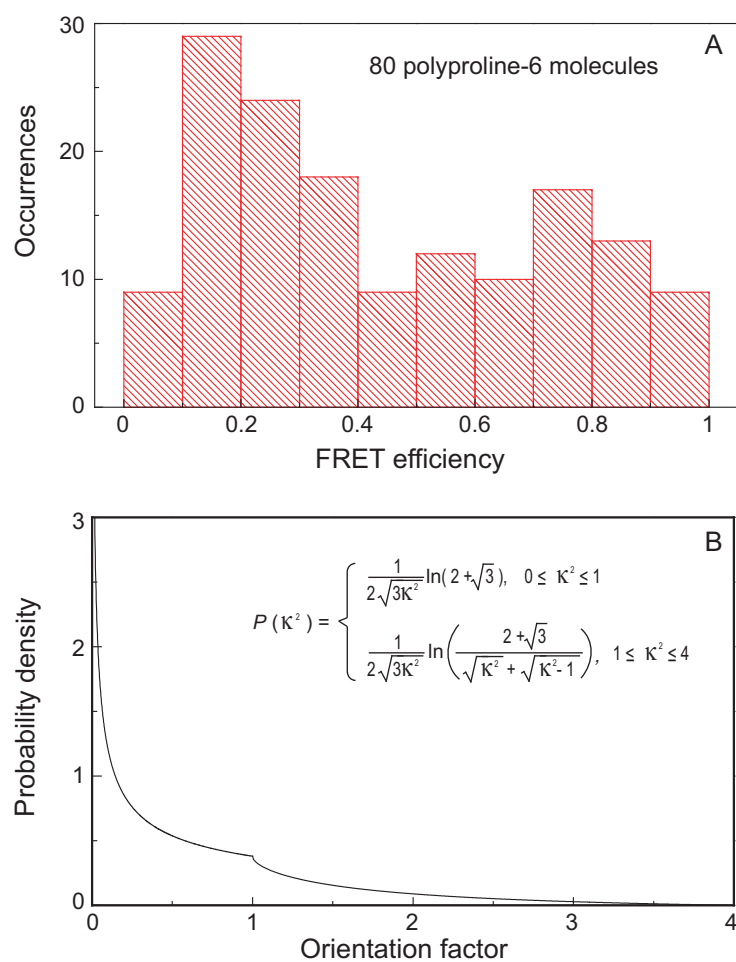


**Figure 6.9:** Histogram of the FRET efficiencies measured from 80 polyproline 6 molecules (A) and probability density function of  $\kappa^2$ , the orientation factor, for the freely rotating dyes (B).

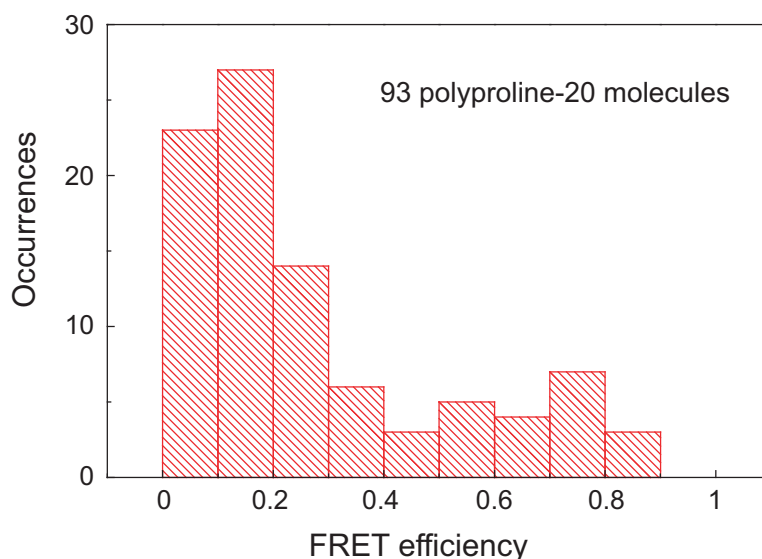


**Figure 6.10:** Histogram of the FRET efficiencies of 93 polyproline 20 molecules.

FRET efficiency would just follow the probability density function of  $\kappa^2$  as shown in Figure 6.9B. According to this probability density function, there is a high probability of identifying a low FRET efficiency and a low chance of finding a high FRET value. The measured FRET distribution is partially consistent with this prediction, i.e., many molecules have low FRET values. However, there are still a number of molecules that have relatively high FRET efficiencies, for example in the peak formed around 0.8 in the histogram. The distribution of the FRET efficiency uncovered from dual-labeled polyproline 6 constructs suggests that the donor and acceptor molecules were not free to sample all the possible orientations. This non-isotropic behavior might be due to the choice of the solvent, glycerol. Since the polyproline 6 molecules were dissolved in this viscous matrix, some configurations may be thermodynamically restricted during slow cooling (5 K/h). Static FRET measurements were also tried on the dual-labeled polyproline 20 construct. They again revealed a broad distribution of the FRET efficiency in which many molecules have FRET values below 0.5, the averaged FRET efficiency measured from the same construct at room-temperature [43], and very few have relatively high values between 0.5 and 0.9 (see Figure 6.10).

We carried out our first temperature-cycle FRET measurements on polyproline 6 molecules. The employed temperature-cycle scheme is shown in Fig-

ure 6.4. In each cycle, we started with exciting the donor only with the probing laser (488 nm) at low temperature for a period of 300 ms during which the FRET from a frozen molecule was probed. A short delay (100 ms) then followed to wait for the full closure of the probing beam. The heating beam was switched on after this delay for a very short time (10  $\mu$ s) during which the local temperature quickly jumped to a high temperature at which the conformation of the molecule was expected to change. When the heating was off, the molecule was frozen into a new conformation, which would be probed in the next cycle. A second delay was put at the end of the cycle to ensure that the temperature relaxed back to the original low temperature before the next probing began. As mentioned before, for polyproline 6 molecules, the FRET efficiency, in first approximation, can be related to the relative orientations of the two dyes, we therefore expect to see a variation of the FRET efficiency due to reorientations of the donor and acceptor in the temperature-cycle measurements. This indeed can be detected. Figure 6.11 shows two such examples of the fluorescence time traces with temperature cycles recorded at 171 K. Each peak in the traces is a probing event and what is in between is the heating period together with the two delays. With 10 mW heating power, the local temperature is estimated to be around 271 K. Considering the associated viscosity (about 13.6 Pa·s) and the heating period (10  $\mu$ s), we expect to detect reorientations of the labels, occurring on the time scale of a few microseconds (assuming a hydrodynamic radius of 0.5 nm for the two labels). The rotation time of the whole molecule is about 50  $\mu$ s at 271 K (assuming a hydrodynamic radius of 1.5 nm for dual-labeled polyproline 6). In panel A, the FRET efficiency probed from the first 11 cycles fluctuated around  $0.33 \pm 0.1$ , which might suggest that there were no significant conformational rearrangements within the molecule when it was cycled to a high temperature. However, in the 13th cycle ( $t=11.5$  s), the FRET value suddenly jumped to 0.82 and then went down to 0.73 and 0.61 in the following two cycles. After that, the efficiency went up again to 0.9 and then dropped back to 0.3 before the donor was finally bleached. These consecutive large variations of the FRET efficiency clearly indicate pronounced reorientations of the two labels within the molecule during these temperature cycles. Panel B shows another example in which the molecule with low FRET configurations in the first 30 s suddenly switched to high FRET conformations and persisted for about 63 s before the acceptor was bleached. Thus, fast thermal cycling between a low and high temperatures can induce conformational changes of dual-labeled polyproline 6 molecules, which can be probed by measuring the FRET efficiency.



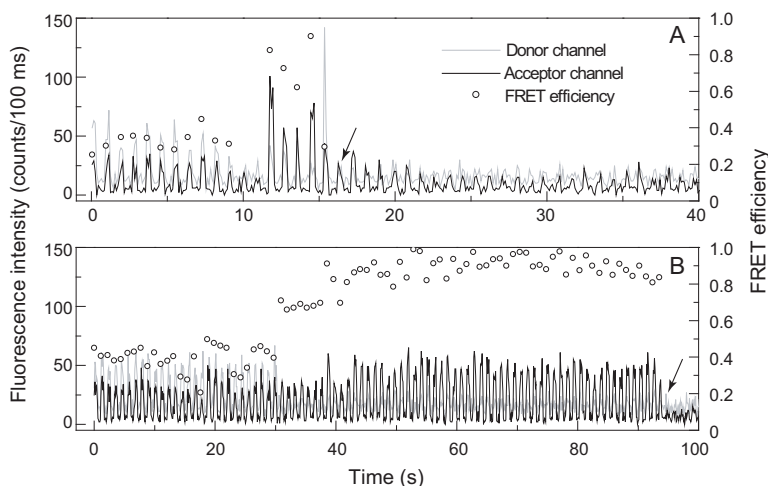


**Figure 6.11:** Two examples of the fluorescence time traces of polyproline 6 with temperature cycles. The fluorescence time traces were recorded at 171 K with a bin time of 100 ms. In each cycle, the molecule was first excited by the 488 nm laser for 300 ms with a power of  $400 \text{ W/cm}^2$ . This probing event manifested as a peak in each channel. The associated FRET efficiency (empty circle) was calculated from the two peaks in the donor (gray line) and acceptor (black line) channels, respectively. The molecule was then heated up to a high temperature (about 271 K) by the 785 nm NIR laser for  $10 \mu\text{s}$  with a heating power of 10 mW. The heating event, which was flanked by the two delays (100 ms each), took place between the peaks in the traces. (A) The FRET efficiencies probed in the first 11 cycles fluctuated between 0.25 and 0.45. In the next two cycles, the two signals were very close to the background levels and thus no FRET was calculated according to the selection criteria (see Data analysis in Experimental methods section). In the 13th cycle, the FRET efficiency suddenly increased to 0.82 and went down to 0.73 and 0.61 in the following 2 cycles. It jumped back again to 0.9 in the new cycle and then dropped to 0.3 before the donor was finally bleached (denoted by the arrow). These large consecutive changes of the FRET efficiency clearly indicate pronounced conformational changes within the molecule during these cycles. (B) The molecule began with low FRET configurations ( $\leq 0.5$ ) and changed to high FRET conformations around  $t = 30 \text{ s}$ . These high FRET conformations lasted for about 63 s before the acceptor was bleached (denoted by the arrow).

## 6.4 Discussion

We first briefly looked at the photophysics of the donor (from Alexa 488-labeled polyproline 10) and the acceptor (Alexa 594 alone) in glycerol respectively at temperatures below the glass transition. We found that both of them showed photoblinking. This is not very surprising since these two dyes are derivatives of Rhodamine 6G (R6G) and R6G has been shown to have a long-lived dark state in polyvinyl alcohol [96] and glycerol [46] due to formation of a radical ion from the triplet state. The same mechanism might apply to Alexa 488 and Alexa 594 in glycerol as well.

When we recorded the fluorescence time traces from individual dual-labeled polyprolines, we observed three types of relations between the donor and acceptor signals due to the interplay of their photophysics. (1) A correlation between the two signals was often detected, i.e., the acceptor fluorescence intensity was positively correlated with the donor intensity, when the donor molecule was in a dark state or photobleached. (2) A noncorrelation, i.e., the donor intensity remained constant even when the acceptor stopped emitting photons, was frequently seen when the acceptor was in a non-fluorescing state, either a temporary dark or bleached state. This noncorrelated behavior suggests that the non-fluorescing form(s) of Alexa 594 can still quench the emission of Alexa 488. This is probably because the absorption spectrum associated with such non-fluorescing form(s) is very similar to or even identical with that of the fluorescing state of the acceptor although its fluorescence is extinguished. The energy transfer between the two molecules therefore remains more or less the same efficiency. (3) An anticorrelation, which we expected, was found in rare cases. When the acceptor ceased emitting photons, the fluorescence intensity of the donor simultaneously increased to a new level until the donor was finally bleached. This may be due to the blue shifted absorption spectrum of the acceptor after its photobleaching. Since a dark state of the acceptor can lead to a zero FRET efficiency and this should be distinguished from a null FRET resulting from a zero  $\kappa^2$ , one possibility would be to insert another probing event in each temperature cycle to check the photophysical state of the acceptor, as often used in room-temperature single-molecule FRET measurements [139,140], and the integrity of the constructs, e.g., the presence of constructs without acceptor.

The static FRET measurements on frozen polyproline 6 molecules revealed a broad FRET distribution. This is in big contrast to the narrow peaked distribution observed at room-temperature [43]. The interdye distance ( $0.15 \text{ nm} < R < 3.45 \text{ nm}$ ) of this construct is rather short and thus high FRET efficiencies are expected from the measurements. However, since the molecules were frozen

in the host matrix, the orientation factor ( $\kappa^2$ ), which normally is assumed to be  $2/3$  in room-temperature FRET measurements, would vary between 0 and 4 if the two dyes were free to rotate. The observed broad FRET distribution therefore partially reflects the distribution of  $\kappa^2$ . However, this distribution is different from the one predicted for an isotropic reorientation of the dyes, suggesting that the motion of the two labels was somehow hindered within the construct. This may be due to the chemical differences between glycerol and water molecules. The water molecule is much smaller and more polar than glycerol, therefore it could easily break possible hydrogen bond(s) formed within the construct, making the labels free to reorient. Such a lubricating role of water molecules has been reported in the studies of rotaxane, a hydrogen bond-assembled synthetic molecular machine [141, 142]. This lubrication might be difficult if the labeled molecules are dissolved in glycerol because the glycerol molecules are rather large, resulting in steric hindrance for disrupting hydrogen bonds. In addition, glycerol molecules themselves can form an extended network of hydrogen bonds, which reduces the mobility of both glycerol and the construct. Therefore, some configurations of the molecules with high free energy, which can form transiently in a normal buffer solution, may be forbidden in glycerol at room-temperature. In addition, more energetically unfavorable configurations will be excluded during the slow cooling (5 K/h). A computer simulation may help us to understand how glycerol influences the dynamics of the polyproline 6 construct. In the future, we would also like to repeat static FRET measurements on this construct in a normal buffer solution, which is more physiologically relevant. Such measurements may uncover a different FRET distribution and more dynamics at a desired high temperature ( $T_{high}$ ) in temperature cycles. For polyproline 20, we also observed a broad FRET distribution. Although the broadening was also seen in the room-temperature measurements where the well-defined peak was centered around 0.5 in the histogram, our low-temperature measurements showed that most of the molecules have FRET efficiencies below 0.5 and only a few of them have high FRET values between 0.5 and 0.9. This broad FRET distribution again originated from the interplay of the orientation factor ( $0 \leq \kappa^2 \leq 4$ ) and the interdye distance ( $4.35 \text{ nm} < R < 7.65 \text{ nm}$ ). All the data in these two histograms were taken from the full constructs with non-zero FRET efficiencies. Due to the limitation of the employed detection scheme, populations of full constructs with zero FRET and donor-only constructs may be missing in the histograms. As discussed before, an alternating-laser excitation will be incorporated in our setup to eliminate this limitation [139, 140].

The dynamic FRET measurements on polyproline 6 with temperature cycles

clearly demonstrate that conformational changes of the molecules, which take place at a high temperature, can be probed at low temperature by measuring the FRET efficiency. Due to the limited time available for finishing this thesis, we have not tried to play around with the experimental parameters, such as the heating power and heating period in temperature cycles. The relatively stable FRET efficiencies in Figure 6.11 B indicate that the conformational memory has not been removed completely in glycerol with the applied heating power. Perhaps a higher heating power or replacing glycerol with a normal buffer solution would lead to more detectable dynamics. In addition, to better characterize how the orientation factor influences the FRET efficiency, a well defined model system is needed, for example a double-stranded DNA molecule flanked by two labels with linkers much shorter than the length of the molecule. Even though we only performed few temperature-cycle measurements, we can obtain snapshots of a fast dynamic process of single-molecules with temperature-cycle microscopy. This is not possible with conventional single-molecule spectroscopy at room-temperature. Thus temperature-cycle microscopy will be a new platform on which different probing approaches can be adapted to study fast molecular dynamics at the single-molecule level.

## 6.5 Conclusion

We studied the conformational dynamics of polyprolines by single-molecule FRET combined with a new type of temperature-cycle microscope developed in our group. We first characterized the static FRET efficiency of individual frozen constructs in a thin glycerol film at low temperature. Both the measurements on polyproline 6 and polyproline 20 revealed a broad FRET distribution. The broadening was ascribed to the interplay of the orientation factor and the interdy distance. Additionally, in the fluorescence time traces of the individual constructs, we saw that the donor and acceptor signals varied in three different manners due to their photophysics. (1) A correlated behavior, i.e., the acceptor intensity was positively correlated with the donor intensity, was detected when the donor was in a dark state or bleached. (2) A noncorrelated behavior, i.e., the change of the acceptor signal was independent of the donor signal, was seen when the acceptor was in non-fluorescing states and it can still accept the excitation energy from the donor. (3) An anticorrelated behavior, i.e., a decrease in the acceptor intensity was coupled to an increase of the donor intensity, was observed if a non-fluorescing form of the acceptor was not able to quench the donor emission. We performed our first temperature-cycle measurements on polyproline 6 molecules and we could indeed detect the con-

formational changes of the individual molecules induced by temperature jumps by following the variation of the FRET efficiency. These preliminary results show that our proposed temperature-cycle microscopy combined with single-molecule FRET labeling has potential for studies of protein-folding dynamics at the single-molecule level.

## **Acknowledgements**

We thank Prof. Benjamin Schuler for kindly providing us with dual-labeled polyproline samples.

## 7 Summary

### 7.1 Heterogeneity in supercooled liquids

Understanding how a liquid becomes a glass is the central topic in glassy studies. Early models postulate the existence of cooperatively rearranging regions (CRR) in glass-forming systems at temperatures close to the glass transition. Such CRRs are believed to be intimately connected to heterogeneity and characteristic of the glass transition. Understanding heterogeneity is, therefore, a key step to the full structural description of the glass transition. Motivated by earlier single-molecule studies on supercooled glycerol, which uncovered a long-lived heterogeneity at temperatures well above the glass transition, we further investigated the heterogeneity in glycerol by rheometry, fluorescence imaging, and small-angle neutron scattering.

In Chapter 2, we described our first rheological measurements on supercooled glycerol and *ortho*-terphenyl, respectively. The experimental setup was a home-built rheometer based on a Couette cell. It allowed us to apply small and constant shear stresses (on the order of 100 Pa) to the sample and to monitor the mechanical response as a function of time. We have detected a solid-like response in both materials at temperatures well above their respective glass transitions. We found that a proper thermal treatment was necessary to observe such a solid-like behavior. The thermal treatment involved an initial cooling to a temperature just a few Kelvin above the glass transition, followed by annealing at that temperature for a few hours, and aging at a higher temperature. We also realized that the thermal history of earlier temperature-dependent single-molecule rotation measurements in glycerol was very similar to those used for the rheological measurements here. Consistent with the single-molecule observation, supercooled glycerol already develops a solid-like network percolating in the liquid bath at temperatures well above the glass transition. The network becomes stiff with time, responds elastically for a small shear, and breaks with large shears, conferring to the material all well known features of soft glassy rheology, such as aging, yield-stress, and shear thinning.

In Chapter 3, we expanded the work on supercooled glycerol discussed in Chapter 2 by employing a commercial rheometer, which allowed us to per-

form oscillatory measurements with very small strains to avoid disturbing the fragile solid-like network as much as possible during the experiments. We first reproduced the solidification of glycerol in a Couette cell as was observed in Chapter 2. We found that an initial slow cooling (5 K/h) prior to annealing at a higher temperature was crucial for the onset of the solid-like behavior. The associated waiting time for such onset decreased with increasing annealing temperature. Upon heating, the solid glycerol melted at the melting point of crystalline glycerol. However, due to the apparatus compliance, i.e., the deformation of the measurement tools, the maximum measurable rigidity of glycerol in the Couette cell was only on the order of  $10^7$  Pa. We therefore switched to a plate-plate geometry, where gap and plate size were chosen such that the tool compliance was negligible. Additionally, this configuration allowed us to access the sample optically during the measurements. To our surprise, the thermal profile which led to the solidification in the Couette cell could not reliably reproduce the solid-like state of glycerol in the plate-plate geometry. We detected the solid-like behavior only in one run (out of six). In that run, a slush-like phase grew from the top plate at the growth speed of the crystal phase. The shear modulus of this slushy phase, however, was two orders of magnitude smaller than that of the crystal phase, which we measured independently from the seeded sample.

In Chapter 4, we studied the thin film of glycerol doped with fluorescent probes by fluorescence imaging. We detected two distinct heterogeneous patterns of the fluorescence intensity, depending on the cooling rate applied to the sample. A slowly cooled sample showed a Swiss-cheese-like pattern in which many micrometer-sized dark spots were nucleated in a bright background, whereas a quickly cooled sample resulted in a spinodal decomposition pattern where many bright island-like features of micrometer sizes were dispersed in a dark matrix. These two heterogeneous patterns, due to inhomogeneous dye distributions in the glycerol films, could persist for days if they were not heated considerably, suggesting long-lived and micrometer-sized density fluctuations in supercooled glycerol.

The results from Chapters 2 and 3 raise one important question: what is the structural origin of the solid-like state of glycerol. The observed viscoelastic behavior seems to be related to a crystal growth in supercooled glycerol, since the solid-like structures grew at more or less the same speed as the crystal and melted upon heating to the melting point of crystalline glycerol. On the other hand, the rigidity of the solidified glycerol is two orders of magnitude smaller than that of the crystal. Moreover, the measurements in Chapter 4 suggested that the glycerol film was free from large microcrystallites no matter how

slowly it was cooled.

In Chapter 5, we tried to understand the structural origin of the solid-like state of glycerol by performing small-angle neutron scattering experiments. We did two series of measurements on two glycerol samples, respectively, with thermal histories similar to the one used in Chapter 2. We saw the growth of solid-like structures in one sample only, evidenced by both direct eye visualization and by the scattering spectra. A new peak, centered around  $0.1 \text{ \AA}^{-1}$ , in the spectra is a hallmark of this solid-like state, since it is clearly absent from the pure liquid state and from the crystal at the same temperature. However, as the Q range ( $0.008$  to  $0.431 \text{ \AA}^{-1}$ ) chosen for the measurements did not cover the range ( $0.5$  to  $5 \text{ \AA}^{-1}$ ) where the Bragg peaks are normally seen, we could not confirm whether the solidified glycerol has a crystalline identity or not. Future measurements in the large Q range should give more insight into the nature of this solid-like state in supercooled glycerol.

## 7.2 Temperature-cycle microscopy of single-molecule FRET in polyprolines

Observing a single dye molecule for an infinitely long time and probing fast dynamics from single molecules without accumulating photon events from different individual molecules are the dreams of experimentalists working with single-molecule fluorescence spectroscopy. Although it is now possible to observe an immobilized dye molecule for minutes at room temperature in a solution by adding triplet quenchers and oxygen scavengers, the time resolution is still limited to the range of a few milliseconds in order to have a reasonable signal to background ratio. To achieve a longer observation time without immobilizing single molecules and to probe fast dynamics from these molecules in the submillisecond or even microsecond range, we have recently proposed a new type of temperature-cycle microscopy. In Chapter 6, we demonstrated how to use this new method to study the conformational dynamics of polyprolines with single-molecule FRET. We first measured the static FRET efficiency of frozen polyproline 6 and polyproline 20 molecules at low temperature in glycerol, respectively. Both of the measurements revealed a broad distribution of FRET efficiencies. The broadening originated from the wide distribution of the orientation factor and the fluctuation of the interdye distance. In the fluorescence time traces of individual constructs, we studied the variations of the donor and acceptor signals and observed 3 types of events. (1) A correlation between the two signals, i.e., the acceptor intensity was positively correlated with the donor intensity, was observed when the donor was in a dark state



or bleached. (2) A noncorrelation, i.e., the change of the acceptor intensity is independent of the donor intensity, was seen when the acceptor was in non-fluorescing states and it could still quench the donor emission. This is probably because the absorption spectrum associated with such non-fluorescing form(s) is very similar to or even identical with that of the fluorescing state of the acceptor although the fluorescence is extinguished. The energy transfer between the two molecules therefore remains unchanged. (3) An anticorrelation between the two signals was detected if a non-fluorescing form of the acceptor did not accept the excitation energy from the donor. We performed our first temperature-cycle measurements on polyproline 6 and we could indeed detect the conformational changes induced by temperature cycles by following the FRET efficiency. These preliminary results show that temperature-cycle microscopy combined with single-molecule FRET has potential for studies of protein-folding dynamics at the single-molecule level.

## References

- [1] R. Zondervan, F. Kulzer, G. C. G. Berkhout and M. Orrit, “Local viscosity of supercooled glycerol near  $T_g$  probed by rotational diffusion of ensembles and single dye molecules”, *Proc. Natl. Acad. Sci. U. S. A.* **104** (2007) 12 628–12 633.
- [2] G. Adam and J. Gibbs, “On the temperature dependence of cooperative relaxation properties in glass-forming liquids”, *J. Chem. Phys.* **43** (1965) 139–146.
- [3] S. Glarum, “Dielectric relaxation of isoamyl bromide”, *J. Chem. Phys.* **33** (1960) 639–643.
- [4] H. Sillescu, “Heterogeneity at the glass transition: A review”, *Journal of Non-Crystalline Solids* **243** (1999) 81–108.
- [5] E. Donth, “The glass transition”, Springer-Verlag (2001).
- [6] R. Böhmer, R. V. Chamberlin, G. Diezemann, B. Geil, A. Heuer, S. C. Hinze, G. and Kuebler, R. Richert, H. Schiener, B. and Sillescu, H. W. Spiess, U. Tracht and M. Wilhelm, “Nature of the non-exponential primary relaxation in structural glass-formers probed by dynamically selective experiments”, *J. Non-Cryst. Solids* **235-237** (1998) 1–9.
- [7] G. Diezemann, R. Böhmer, G. Hinze and H. Sillescu, “Reorientational dynamics in simple supercooled liquids”, *J. Non-Cryst. Solids* **235** (1998) 121–127.
- [8] U. Tracht, M. Wilhelm, A. Heuer, H. Feng, K. Schmidt-Rohr and H. W. Spiess, “Length scale of dynamic heterogeneities at the glass transition determined by multidimensional nuclear magnetic resonance”, *Phys. Rev. Lett.* **81** (1998) 2727–2730.
- [9] B. Schiener, R. V. Chamberlin, G. Diezemann and R. Böhmer, “Non-resonant dielectric hole burning spectroscopy of supercooled liquids”, *J. Chem. Phys.* **107** (1997) 7746–7761.

- [10] U. Schneider, P. Lunkenheimer, R. Brand and A. Loidl, “Dielectric and far-infrared spectroscopy of glycerol”, *J. Non-Cryst. Solids* **235** (1998) 173–179.
- [11] A. Patkowski, T. Thurn-Albrecht, E. Banachowicz, W. Steffen, P. Bösecke, T. Narayanan and E. W. Fischer, “Long-range density fluctuations in orthoterphenyl as studied by means of ultrasmall-angle x-ray scattering”, *Phys. Rev. E: Stat. Phys., Plasmas, Fluids, Relat. Interdiscip. Top.* **61** (2000) 6909–6913.
- [12] A. Patkowski, E. W. Fischer, W. Steffen, H. Gläser, M. Baumann, T. Ruths and G. Meier, “Unusual features of long-range density fluctuations in glass-forming organic liquids: A Rayleigh and Rayleigh-Brillouin light scattering study”, *Phys. Rev. E: Stat. Phys., Plasmas, Fluids, Relat. Interdiscip. Top.* **63** (2001) 061 503.
- [13] M. T. Cicerone and M. D. Ediger, “Enhanced translation of probe molecules in supercooled o-terphenyl: Signature of spatially heterogeneous dynamics?”, *J. Chem. Phys.* **104** (1996) 7210–7218.
- [14] M. D. Ediger, “Spatially heterogeneous dynamics in supercooled liquids”, *Annu. Rev. Phys. Chem.* **51** (2000) 99–128.
- [15] L. A. Deschenes and D. A. Vanden Bout, “Heterogeneous dynamics and domains in supercooled o-terphenyl: A single molecule study”, *J. Phys. Chem. B* **106** (2002) 11 438–11 445.
- [16] A. Schob, F. Cichos, J. Schuster and C. von Borczyskowski, “Reorientation and translation of individual dye molecules in a polymer matrix”, *Eur. Polym. J.* **40** (2004) 1019–1026.
- [17] M. Orrit and J. Bernard, “Single pentacene molecules detected by fluorescence excitation in a p-terphenyl crystal”, *Phys. Rev. Lett.* **65** (1990) 2716–2719.
- [18] W. E. Moerner and L. Kador, “Optical detection and spectroscopy of single molecules in a solid”, *Phys. Rev. Lett.* **62** (1989) 2535–2538.
- [19] W. E. Moerner and M. Orrit, “Illuminating single molecules in condensed matter”, *Science* **283** (1999) 1670–1676.
- [20] F. Kulzer, T. Xia and M. Orrit, “Single molecules as optical nanoprobe for soft and complex matter”, *Angew. Chem., Int. Ed.* **49** (2010) 854–866.

- 
- [21] D. Boyer, P. Tamarat, A. Maali, B. Lounis and M. Orrit, “Photothermal imaging of nanometer-sized metal particles among scatterers”, *Science* **297** (2002) 1160–1163.
- [22] S. Berciaud, D. Lasne, G. A. Blab, L. Cognet and B. Lounis, “Photothermal heterodyne imaging of individual metallic nanoparticles: theory versus experiment”, *Phys. Rev. B* **73** (2006) 045 424.
- [23] F. Kulzer, N. Laurens, J. Besser, T. Schmidt, M. Orrit and H. P. Spaink, “Photothermal detection of individual gold nanoparticles: Perspectives for high-throughput screening”, *ChemPhysChem* **9** (2008) 1761–1766.
- [24] P. M. R. Paulo, A. Gaiduk, F. Kulzer, S. F. G. Krens, T. Schmidt, M. Orrit and H. P. Spaink, “Photothermal correlation spectroscopy of gold nanoparticles in solution”, *J. Phys. Chem. C* **113** (2009) 11 451–11 457.
- [25] K. Lindfors, T. Kalkbrenner, P. Stoller and V. Sandoghdar, “Detection and spectroscopy of gold nanoparticles using supercontinuum white light confocal microscopy”, *Phys. Rev. Lett.* **93** (2004) 037 401.
- [26] H. Ewers, V. Jacobsen, E. Klotzsch, A. E. Smith, A. Helenius and V. Sandoghdar, “Label-free optical detection and tracking of single virions bound to their receptor in supported membrane bilayers”, *Nano Lett.* **7** (2007) 2263–2266.
- [27] P. Kukura, M. Celebrano, A. Renn and V. Sandoghdar, “Imaging a single quantum dot when it is dark”, *Nano Lett.* **9** (2009) 926–929.
- [28] F. G. Prendergast and K. Mann, “Chemical and physical properties of aequorin and the green fluorescent protein isolated from *Aequorea forskalea*”, *Biochemistry* **17** (1978) 3448–3453.
- [29] R. Tsien, “The green fluorescent protein”, *Annu. Rev. Biochem.* **67** (1998) 509–544.
- [30] H. P. Lu, L. Y. Xun and X. S. Xie, “Single-molecule enzymatic dynamics”, *Science* **282** (1998) 1877–1882.
- [31] G. Harms, G. Orr, M. Montal, B. Thrall, S. Colson and H. Lu, “Probing conformational changes of gramicidin ion channels by single-molecule patch-clamp fluorescence microscopy”, *Biophys. J.* **85** (2003) 1826–1838.

## References

---

- [32] H. Lu, “Probing single-molecule protein conformational dynamics”, *Acc. Chem. Res.* **38** (2005) 557–565.
- [33] T. Förster, “Modern Quantum Chemistry”, Academic Press, New York (1965).
- [34] L. Stryer and R. Haugland, “Energy transfer: A spectroscopic ruler”, *Proc. Natl. Acad. Sci. U. S. A.* **58** (1967) 719–726.
- [35] T. Ha, T. Enderle, D. F. Ogletree, D. S. Chemla, P. R. Selvin and S. Weiss, “Probing the interaction between two single molecules: Fluorescence resonance energy transfer between a single donor and a single acceptor”, *Proc. Natl. Acad. Sci. U. S. A.* **93** (1996) 6264–6268.
- [36] J. Schütz, G. W. Trapesinger and T. Schmidt, “Direct observation of ligand colocalization on individual receptor molecules”, *Biophys. J.* **74** (1998) 2223–2226.
- [37] Y. Ishii, T. Yoshida, T. Funatsu, T. Wazawa and T. Yanagida, “Fluorescence resonance energy transfer between single fluorophores attached to a coiled-coil protein in aqueous solution”, *Chem. Phys.* **247** (1999) 163–173.
- [38] T. Ha, A. Y. Ting, J. Liang, W. B. Caldwell, A. A. Deniz, D. S. Chemla, P. G. Schultz and S. Weiss, “Biophysics single-molecule fluorescence spectroscopy of enzyme conformational dynamics and cleavage mechanism”, *Proc. Natl. Acad. Sci. USA* **96** (1999) 893–898.
- [39] S. Brasselet, E. J. G. Peterman, A. Miyawaki and W. E. Moerner, “Single-molecule fluorescence resonant energy transfer in calcium concentration dependent cameleon”, *J. Phys. Chem. B* **104** (2000) 3676–3682.
- [40] A. A. Deniz, T. A. Laurence, G. S. Beligere, M. Dahan, A. B. Martin, D. S. Chemla, P. E. Dawson, P. G. Schultz and S. Weiss, “Single-molecule protein folding: diffusion fluorescence resonance energy transfer studies of the denaturation of chymotrypsin inhibitor 2”, *Proc. Natl. Acad. Sci. U. S. A.* **97** (2000) 5179–5184.
- [41] X. W. Zhuang, L. E. Bartley, H. P. Babcock, R. Russell, T. J. Ha, D. Herschlag and S. Chu, “A single-molecule study of RNA catalysis and folding”, *Science* **288** (2000) 2048–2052.

- 
- [42] B. Schuler, E. A. Lipman and W. A. Eaton, “Probing the free-energy surface for protein folding with single-molecule fluorescence spectroscopy (vol 419, pg 743, 2002)”, *Nature* **421** (2003) 94.
- [43] B. Schuler, E. A. Lipman, P. J. Steinbach, M. Kumke and W. A. Eaton, “Polyproline and the ‘spectroscopic ruler’ revisited with single-molecule fluorescence”, *Proc. Natl. Acad. Sci. U. S. A.* **102** (2005) 2754–2759.
- [44] W. Koopmans, R. Buning, T. Schmidt and J. van Noort, “spFRET using Alternating Excitation and FCS reveals progressive DNA unwrapping in nucleosomes”, *Biophys. J.* **10** (2009) 195–204.
- [45] T. Basché, S. Kummer and C. Bräuchle, “Direct spectroscopic observation of quantum jumps of a single molecule”, *Nature* **373** (1995) 132–134.
- [46] R. Zondervan, F. Kulzer, H. van der Meer, J. A. J. M. Disselhorst and M. Orrit, “Laser-driven microsecond temperature cycles analyzed by fluorescence polarization microscopy”, *Biophys. J.* **90** (2006) 2958–2969.
- [47] P. G. de Gennes, “A simple picture for structural glasses”, *C. R. Phys.* **3** (2002) 1263–1268.
- [48] E. R. Weeks and D. A. Weitz, “Properties of cage rearrangements observed near the colloidal glass transition”, *Phys. Rev. Lett.* **89** (2002) 095704.
- [49] J. C. Conrad, P. P. Dhillon, E. R. Weeks, D. R. Reichman and D. A. Weitz, “Contribution of slow clusters to the bulk elasticity near the colloidal glass transition”, *Phys. Rev. Lett.* **97** (2006) 265701.
- [50] M. M. Hurley and P. Harrowell, “Kinetic structure of a 2-dimensional liquid”, *Phys. Rev. E* **52** (1995) 1694–1698.
- [51] C. Bennemann, C. Donati, J. Baschnagel and S. C. Glotzer, “Growing range of correlated motion in a polymer melt on cooling towards the glass transition”, *Nature* **399** (1999) 246–249.
- [52] J. D. Stevenson, J. Schmalian and P. G. Wolynes, “The shapes of cooperatively rearranging regions in glass-forming liquids”, *Nat. Phys.* **2** (2006) 268–274.
- [53] L. Berthier, G. Biroli, J. P. Bouchaud, L. Cipelletti, D. El Masri, D. L’Hôte, F. Ladieu and M. Pierno, “Direct experimental evidence of

- a growing length scale accompanying the glass transition”, *Science* **310** (2005) 1797–1800.
- [54] R. F. Berg, M. R. Moldover and G. A. Zimmerli, “Viscoelasticity of Xenon near the critical point”, *Phys. Rev. Lett.* **82** (1999) 920–923.
- [55] P. Sollich, F. Lequeux, P. Hébraud and M. E. Cates, “Rheology of soft glassy materials”, *Phys. Rev. Lett.* **78** (1997) 2020–2023.
- [56] F. Varnik, L. Bocquet, J. L. Barrat and L. Berthier, “Shear localization in a model glass”, *Phys. Rev. Lett.* **90** (2003) 095 702.
- [57] K. Schröter and E. Donth, “Viscosity and shear response at the dynamic glass transition of glycerol”, *J. Chem. Phys.* **113** (2000) 9101–9108.
- [58] W. T. Laughlin and D. R. Uhlmann, “Viscous flow in simple organic liquids”, *J. Phys. Chem.* **76** (1972) 2317–2325.
- [59] F. J. Bermejo, A. Criado, A. de Andrés, E. Enciso and H. Schöber, “Microscopic dynamics of glycerol in its crystalline and glassy states”, *Phys. Rev. B* **53** (1996) 5259–5267.
- [60] D. Bonn, S. Tanase, B. Abou, H. Tanaka and J. Meunier, “Laponite: aging and shear rejuvenation of a colloidal glass”, *Phys. Rev. Lett.* **89** (2002) 015 701.
- [61] D. Bonn, H. Tanaka, P. Coussot and J. Meunier, “Ageing, shear rejuvenation and avalanches in soft glassy materials”, *J. Phys.-Condens. Matter* **16** (2004) S4987–4992.
- [62] H. A. Kramers, “Brownian motion in a field of force and the diffusion model of chemical reactions”, *Physica* **7** (1940) 284–304.
- [63] A. J. Liu and S. R. Nagel, “Nonlinear dynamics - jamming is not just cool any more”, *Nature* **396** (1998) 21–22.
- [64] A. Widmer-Cooper, P. Harrowell and H. Fynewever, “How reproducible are dynamic heterogeneities in a supercooled liquid?”, *Phys. Rev. Lett.* **93** (2004) 135 701.
- [65] G. Tarjus, S. A. Kivelson, Z. Nussinov and P. Viot, “The frustration-based approach of supercooled liquids and the glass transition: a review and critical assessment”, *J. Phys.-Condens. Matter* **17** (2005) R1143–1182.

- 
- [66] G. Biroli and J. P. Bouchaud, “Critical fluctuations and breakdown of Stokes-Einstein relation in the mode-coupling theory of glasses”, arXiv:cond-mat/0609705v1 (2006).
- [67] J. P. Bouchaud, “Granular media: some ideas from statistical physics”, arXiv:cond-mat/0211196v2 (2002).
- [68] J. T. Bendler, J. J. Fontanella and M. F. Shlesinger, “The defect diffusion model and the properties of glasses and liquids”, *J. Non-Cryst. Solids* **352** (2006) 4835–4842.
- [69] A. Reiser and G. Kasper, “On the pressure dependence of fragility”, *Europhys. Lett.* **76** (2006) 1137–1143.
- [70] E. W. Fischer, “Light-scattering and dielectric studies on glass-forming liquids”, *Physica. A* **201** (1993) 183–206.
- [71] P. G. de Gennes, “A simple picture for structural glasses”, *C. R. Phys.* **3** (2002) 1263–1268.
- [72] K. Schröter and E. Donth, “Comparison of shear response with other properties at the dynamic glass transition of different glass formers”, *J. Non-Cryst. Solids* **307** (2002) 270–280.
- [73] D. R. Reichman and P. Charbonneau, “Mode-coupling theory”, *J. Stat. Mech.-Theory Exp.* **2005** (2005) P05 013.
- [74] R. Zondervan, T. Xia, H. van der Meer, C. Storm, F. Kulzer, W. van Saarloos and M. Orrit, “Soft glassy rheology of supercooled molecular liquids”, *Proc. Natl. Acad. Sci. U. S. A.* **105** (2008) 4993–4998 (Chapter 2 of this thesis).
- [75] K. Schröter, S. A. Hutcheson, X. Shi, A. Mandanici and G. B. McKenna, “Dynamic shear modulus of glycerol: Corrections due to instrument compliance”, *J. Chem. Phys.* **125** (2006) 214 507.
- [76] J. L. Cox (ed.), “Natural Gas Hydrates : Properties, Occurrence, and Recovery”, Butterworth (1983).
- [77] R. C. Weast (ed.), “Handbook of Chemistry and Physics”, The Chemical Rubber Co. (1968).
- [78] Y. H. Jeong, “Frequency-dependent shear modulus of glycerol near the glass-transition”, *Phys. Rev. A* **36** (1987) 766–773.



- [79] G. Tammann and E. Jenckel, “Die Kristallisationsgeschwindigkeit und die Kernzahl des Glycerins in Abhaengigkeit von der Temperatur”, *Z. Anorg. Allg. Chem.* **193** (1930) 76–80.
- [80] A. Ha, I. Cohen, X. L. Zhao, M. Lee and D. Kivelson, “Supercooled liquids and polyamorphism”, *J. Chem. Phys.* **100** (1996) 1–4.
- [81] I. Cohen, A. Ha, X. L. Zhao, M. Lee, T. Fischer, M. J. Strouse and D. Kivelson, “A low-temperature amorphous phase in a fragile glass-forming substance”, *J. Chem. Phys.* **100** (1996) 8518–8526.
- [82] H. Tanaka, R. Kurita and H. Mataka, “Liquid-liquid transition in the molecular liquid triphenyl phosphite”, *Phys. Rev. Lett.* **92** (2004) 025 701–025 704.
- [83] R. Kurita and H. Tanaka, “Critical-like phenomena associated with liquid-liquid transition in a molecular liquid”, *Science* **306** (2004) 845–848.
- [84] A. Hédoux, Y. Guinet, P. Derollez, O. Hernandez, R. Lefort and M. Descamps, “A contribution to the understanding of the polyamorphism situation in triphenyl phosphite”, *Phys. Chem. Chem. Phys.* **6** (2004) 3192–3199.
- [85] R. Kurita, Y. Shinohara, Y. Amemiya and H. Tanaka, “Microscopic structural evolution during the liquid-liquid transition in triphenyl phosphite”, *J. Phys.: Condens. Matter* **19** (2007) 152 101.
- [86] M. M. Hurley and P. Harrowell, “Kinetic structure of a 2-dimensional liquid”, *Phys. Rev. E: Stat. Phys., Plasmas, Fluids, Relat. Interdiscip. Top.* **52** (1995) 1694–1698.
- [87] R. S. Miller and R. A. MacPhail, “Ultraslow nonequilibrium dynamics in supercooled glycerol by stimulated Brillouin gain spectroscopy”, *J. Chem. Phys.* **106** (1997) 3393–3401.
- [88] R. S. Miller and R. A. MacPhail, “Physical aging in supercooled glycerol: evidence for heterogeneous dynamics?”, *J. Phys. Chem. B* **101** (1997) 8635–8641.
- [89] S. Reinsberg, X. H. Qiu, M. Wilhelm, H. W. Spiess and M. D. Ediger, “Length scale of dynamic heterogeneity in supercooled glycerol near  $T_g$ ”, *J. Chem. Phys.* **114** (2001) 7299–7302.

- 
- [90] H. Jinnai, H. Yoshida, K. Kimishima, Y. Funaki, Y. Hirokawa, A. E. Ribbe and H. Hashimoto, “Observation of fine structures in bicontinuous phase-separated domains of a polymer blend by laser scanning confocal microscopy”, *Macromolecules* **34** (2001) 5186–5191.
- [91] H. Aoki, Y. Sakurai, S. Ito and T. Nakagawa, “Phase-separation structure of a monolayer of binary polymer blend studied by fluorescence scanning near-field optical microscopy”, *J. Phys. Chem. B* **103** (1999) 10 553–10 556.
- [92] Y. Hirokawa, H. Jinnai, Y. Nishikawa, T. Okamoto and T. Hashimoto, “Direct observation of internal structures in poly (N-isopropylacrylamide) chemical gels”, *Macromolecules* **32** (1999) 7093–7099.
- [93] C. A. Helm, H. Möhwald, K. Kjaer and J. Als-Nielsen, “Phospholipid monolayers between fluid and solid states”, *Biophys. J.* **52** (1987) 381–390.
- [94] T. Baumgart, S. T. Hess and W. W. Webb, “Imaging coexisting fluid domains in biomembrane models coupling curvature and line tension”, *Nature* **425** (2003) 821–824.
- [95] S. L. Veatch and S. Keller, “Separation of liquid phases in giant vesicles of ternary mixtures of phospholipids and cholesterol”, *Biophys. J.* **85** (2003) 3074–3083.
- [96] R. Zondervan, F. Kulzer, S. B. Orlinskii and M. Orrit, “Photoblinking of rhodamine 6G in poly(vinyl alcohol): radical dark state formed through the triplet”, *J. Phys. Chem. A* **107** (2003) 6770–6776.
- [97] R. Kurita, K. Murata and H. Tanaka, “Control of fluidity and miscibility of a binary liquid mixture by the liquid-liquid transition”, *Nat. Mater.* **7** (2008) 647–652.
- [98] A. Donald, “Food for thought”, *Nat. Mater.* **3** (2004) 579–581.
- [99] H. Tanaka, “General view of a liquid-liquid phase transition”, *Phys. Rev. E* **62** (2000) 6968–6976.
- [100] J. Carpenter, M. Agamalian, K. Littrell, P. Thiyagarajan and C. Rehm, “Time-of-flight implementation of an ultra-small-angle neutron scattering instrument”, *J. Appl. Crystallogr.* **36** (2003) 763–768.

## References

---

- [101] T. Mason, M. Arai and K. Clausen, “Next-generation neutron sources”, *MRS Bull.* **28** (2003) 923–928.
- [102] Y. B. Melnichenko and G. D. Wignall, “Small-angle neutron scattering in materials science: Recent practical applications”, *Journal of Applied Physics* **102** (2007) 201 101.
- [103] A. Dupuis, G. Zaccai and M. Satre, “Neutron small-angle scattering studies of ribonuclease in mixed aqueous solutions and determination of the preferentially bound water”, *Biochemistry* **22** (1984) 5951–5956.
- [104] G. Zaccai, G. Bunick and H. Eisenberg, “Denaturation of a halophilic enzyme monitored by small-angle neutron scattering”, *J. Mol. Biol.* **192** (1986) 155–157.
- [105] A. VanHook, “Crystallization: Theory and Practice”, Reinhold Publishing Corporation (1961).
- [106] M. Massa, M. Lee and K. Danlnoki-Veress, “Crystal nucleation of polymers confined to droplets: Memory effects”, *J Polym Sci , Part B: Polym Phys* **43** (2005) 3438–3443.
- [107] B. E. Schwickert, S. R. Kline, H. Zimmermann, K. M. Lantzky and J. L. Yarger, “Early stages of glacial clustering in supercooled triphenyl phosphite”, *Phys. Rev. B* **64** (2001) 045 410.
- [108] S. B. Smith, L. Finzi and C. Bustamante, “Direct mechanical measurements of the elasticity of single DNA molecules by using magnetic beads”, *Science* **258** (1992) 1122–1126.
- [109] S. B. Smith, Y. Cui and C. Bustamante, “Overstretching B-DNA: the elastic response of individual double-stranded and single-stranded DNA molecules”, *Science* **271** (1996) 795–799.
- [110] M. D. Wang, H. Yin, R. Landick, J. Gelles and S. M. Block, “Stretching DNA with optical tweezers”, *Biophys. J.* **72** (1997) 1335–1346.
- [111] M. Rief, H. Clausen-Schaumann and H. Gaub, “Sequence dependent mechanics of single DNA molecules”, *Nat. Struct. Mol. Biol.* **6** (1999) 346–349.
- [112] M. Kellermayer, S. Smith, H. Granzier and C. Bustamante, “Folding-unfolding transition in single titin molecules characterized with laser tweezers”, *Science* **276** (1997) 1112–1116.

- 
- [113] L. Tskhovrebova, J. Trinic, J. Sleep and R. Simmons, “Elasticity and unfolding of single molecules of the giant muscle protein titin”, *Nature* **378** (1997) 308–312.
- [114] A. Oberhauser, P. Marszalek, H. Erickson and J. Fernandez, “The molecular elasticity of the extracellular matrix protein tenascin”, *Nature* **393** (1998) 181–185.
- [115] B. Brower-Toland, C. Smith, R. Yeh, J. Lis, C. Peterson and M. Wang, “Mechanical disruption of individual nucleosomes reveals a reversible multistage release of DNA”, *Proc. Natl. Acad. Sci. U. S. A.* **99** (2002) 1960–1965.
- [116] B. Brower-Toland, D. A. Wacker, R. M. Fulbright, J. T. Lis, W. L. Kraus and M. D. Wang, “Specific contributions of histone tails and their acetylation to the mechanical stability of nucleosomes”, *J. Mol. Biol.* **346** (2005) 135–146.
- [117] M. Kruihof, F.-T. Chien, A. Routh, C. Logie, D. Rhodes and J. van Noort, “Single-molecule force spectroscopy reveals a highly compliant helical folding for the 30-nm chromatin fiber”, *Nat. Struct. Mol. Biol.* **16** (2009) 534–540.
- [118] F.-T. Chien and J. van Noort, “10 years of tension on chromatin: results from single-molecule force spectroscopy”, *Curr. Pharm. Biotechnol.* **10** (2009) 474–485.
- [119] A. Hards, C. Zhou, M. Seitz, C. Bräuchle and A. Zumbusch, “Simultaneous AFM manipulation and fluorescence imaging of single DNA strands”, *ChemPhysChem.* **6** (2005) 534–540.
- [120] S. Hohng, R. Zhou, M. K. Nahas, J. Yu, K. Schulten, D. M. J. Lilley and T. Ha, “Fluorescence-force spectroscopy maps two-dimensional reaction landscape of the Holliday junction”, *Science* **318** (2007) 279–283.
- [121] A. Gaiduk, R. Kühnemuth, S. Felekyan, M. Antonik, W. Becker, V. Kudryavtsev, C. Sandhagen and C. Seidel, “Fluorescence detection with high time resolution: From optical microscopy to simultaneous force and fluorescence spectroscopy”, *Microscopy Research and Technique* **70** (2007) 433–441.
- [122] J. van Mameren, M. Modesti, R. Kanaar, C. Wyman, E. Peterman and G. Wuite, “Counting rad51 proteins disassembling from nucleoprotein filaments under tension”, *Nature* **457** (2009) 745–748.

- [123] X. Michalet, A. Kapanidis, T. Laurence, F. Pinaud, S. Doose, M. Pflughoeft and S. Weiss, “The power and prospects of fluorescence microscopies and spectroscopies”, *Annu. Rev. Biophys. Biomol. Struct.* **32** (2003) 161–182.
- [124] M. Böhmer and J. Enderlein, “Fluorescence spectroscopy of single molecules under ambient conditions: Methodology and technology”, *Chem Phys Chem* **4** (2003) 792–808.
- [125] G. Haran, “Topical review: Single-molecule fluorescence spectroscopy of biomolecular folding”, *J. Phys.: Condens. Matter* **15** (2003) R1291–R1317.
- [126] S. de Keijzer, A. Sergé, F. van Hemert, P. Lommerse, G. Lamers, H. Spaink, T. Schmidt and B. Snaar-Jagalska, “A spatially restricted increase in receptor mobility is involved in directional sensing during *Dictyostelium discoideum* chemotaxis”, *J. Cell Sci.* **121** (2008) 1750–1757.
- [127] B. Schuler, E. A. Lipman and W. A. Eaton, “Probing the free-energy surface for protein folding with single-molecule fluorescence spectroscopy”, *Nature* **419** (2002) 743–747.
- [128] J. R. Lakowicz, “Principles of fluorescence spectroscopy (Third edition)”, Springer (2006).
- [129] E. Boukobza, A. Sonnenfeld and G. Haran, “Immobilization in surface-tethered lipid vesicles as a new tool for single-biomolecule spectroscopy”, *J. Phys. Chem. B* **105** (2001) 12 165–12 170.
- [130] C. Wu, R. Komoroski and L. Mandelkern, “The observation of *cis* residues in poly(l-proline) in aqueous solution.”, *Macromolecules* **8** (1975) 635–637.
- [131] S. Doose, H. Neuweiler, H. Barsch and M. Sauer, “Probing polyproline structure and dynamics by photoinduced electron transfer provides evidence for deviations from a regular polyproline type II helix”, *Proc. Natl. Acad. Sci. U. S. A.* **104** (2007) 17 400–17 405.
- [132] R. Best, K. Merchant, I. Gopich, B. Schuler, A. Bax and W. Eaton, “Effect of flexibility and *cis* residues in single-molecule FRET studies of polyproline”, *Proc. Natl. Acad. Sci. U. S. A.* **104** (2007) 18 964–18 969.

- 
- [133] N. Helbecque and M. Loucheux-Lefebvre, “Critical chain length for polyproline-II structure formation in H-Gly-(Pro)<sub>n</sub>-OH”, *Int. J. Pept. Protein. Res.* **19** (1982) 94–101.
- [134] J. Jacob, B. Baker, R. Bryant and D. Cafiso, “Distance estimates from paramagnetic enhancements of nuclear relaxation in linear and flexible model peptides”, *Biophys. J.* **77** (1999) 1086–1092.
- [135] C. Grathwohl and K. Wüthrich, “NMR studies of the rates of proline *cis*–*trans* isomerization in oligopeptides”, *Biopolymers* **20** (2004) 2623–2633.
- [136] L. P. Watkins, H. Y. Chang and H. Yang, “Quantitative single-molecule conformational distributions: A case study with poly-(L-proline)”, *J. Phys. Chem. A* **110** (2006) 5191–5203.
- [137] H. Sahoo, D. Roccatano, A. Hennig and W. Nau, “A 10-Å spectroscopic ruler applied to short polyprolines”, *J. Am. Chem. Soc.* **129** (2007) 9762–9772.
- [138] B. Valeur, “Molecular fluorescence: principles and applications”, Wiley–VCH (2002).
- [139] B. Müller, E. Zaychikov, C. Bräuchle and D. Lamb, “Pulsed interleaved excitation”, *Biophys. J.* **89** (2005) 3508–3522.
- [140] A. Kapanidis, N. Lee, T. Laurence, S. Doose, E. Margeat and S. Weiss, “Fluorescence-aided molecular sorting: Analysis of structure and interactions by alternating-laser excitation of single molecules”, *Proc. Natl. Acad. Sci. U. S. A.* **101** (2004) 8936–8941.
- [141] P. Bodis, R. Timmer, S. Yeremenko, W. J. Buma, J. S. Hannam, D. A. Leigh and S. Wouterson, “Heterovibrational interactions, cooperative hydrogen bonding, and vibrational energy relaxation pathways in a rotaxane”, *J. Phys. Chem. C* **111** (2007) 6798–6804.
- [142] P. Bodis, M. R. Panman, B. H. Bakker, M. Prato, W. J. Buma, A. M. Brouwer, E. R. Kay, D. A. Leigh and S. Wouterson, “Two-dimensional vibrational spectroscopy of rotaxane-based molecular machines”, *Acc. Chem. Res.* **42** (2009) 1462–1469.

## *References*

---

## Samenvatting

In dit proefschrift komen twee verschillende onderwerpen aan bod. Het eerste onderwerp is de structuur van de glasvormer glycerol bij temperaturen boven het glaspunt. In hoofdstuk 2-5 onderzochten we deze structuur met verschillende methoden en keken in het bijzonder naar de heterogeniteit van structuren die op grote schaal blijkt te bestaan. Een tweede onderwerp van studie is de dynamica van enkele moleculen. In hoofdstuk 6 bestudeerden we de dynamica van conformaties van enkele polyproline moleculen in een dunne glycerol film met onze recent voorgestelde temperatuurcycli microscopie. In deze studie konden de conformaties van het polyproline bekeken worden via de fluorescentie van twee fluorescerende moleculen (fluoroforen) die aan de uiteinden van het polyproline bevestigd waren.

## Heterogeniteit in onderkoelde vloeistoffen

Begrijpen hoe een vloeistof een glas wordt is het centrale onderwerp in de studie van glasvormers. In oudere modellen van glasvorming wordt het bestaan van gebieden die zich al samenwerkend herordenen (cooperatively rearranging regions) gepostuleerd. Gedacht wordt dat deze gebieden in nauw verband staan met de heterogeniteit en het karakter van de glasovergang. Het begrijpen van heterogeniteit is daarom een essentiële stap naar een volledige structurele beschrijving van de glasovergang. Gemotiveerd door eerdere enkele molecuul studies naar onderkoeld glycerol, die ontdekten dat bij temperaturen ruim boven het glas punt heterogene structuren ontstaan die verrassend lang kunnen blijven bestaan, bestudeerden we de heterogeniteit in glycerol met rheometrie, fluorescentie microscopie en verstrooiing experimenten met neutronen.

In hoofdstuk 2 beschreven we onze eerste rheologische metingen aan glycerol and *ortho*-terphenyl, respectievelijk. De experimentele opstelling was een zelfgemaakte rheometer gebaseerd op een Couette cell. Deze opstelling stelde ons in staat om kleine en constante schuifkrachten (rond de 100 Pa) op het sample aan te brengen en de mechanische respons te bekijken als functie van de tijd. We hebben in beide materialen een gedrag gevonden als van een vaste stof, bij temperaturen ruim boven hun respectievelijke glas punten, waar de materialen zich volgens het huidige begrip van glasvormers als vloeistoffen



zouden moeten gedragen. We vonden dat een bepaalde thermische behandeling noodzakelijk was om zulk gedrag waar te nemen. Deze thermische behandeling bestond onder meer uit een initiële afkoeling tot een temperatuur slechts een paar graden boven het glas punt, gevolgd door een annealing van enkele uren bij deze temperatuur, en een verharding bij een hogere temperatuur. We realiseerden ons dat de thermische behandeling die gebruikt werd in de rheologische metingen zeer vergelijkbaar was met de thermische behandeling in eerdere studies aan enkele moleculen, waar de rotaties van de moleculen in hun omgeving van glycerol werden gevolgd als functie van de temperatuur. Net als in de eerdere studies met de enkele moleculen in glycerol concluderen we uit de macroscopische rheologie metingen dat in het ondergekoelde glycerol de vloeistof fase wordt doordrenkt met een netwerk van een vaste fase, en dat dit vaste netwerk blijft bestaan tot temperaturen ruim boven het glas punt. Dit netwerk wordt met de tijd stijver, reageert elastisch op kleine schuifkrachten en breekt bij grote schuifkrachten, wat laat zien dat het glycerol geen eenvoudige vloeistof meer is, maar zich goed laat beschrijven met alle bekende eigenschappen van de rheologie van zachte glasvormers, zoals aging, yield-stress, and shear thinning.

In hoofdstuk 3 breidden we het werk aan supergekoeld glycerol in hoofdstuk 2 uit met het gebruik van een commerciële rheometer. Deze rheometer stelde ons in staat tot het doen van oscillerende metingen met zeer kleine vervormingen. Dit was nodig om tijdens de metingen beschadigingen aan het fragiele vaste netwerk zo veel mogelijk te voorkomen. Eerst reproduceerden we het vast worden van het glycerol in een Couette cell zoals waargenomen in hoofdstuk 2. We vonden dat een initiële langzame koeling (5 K/h) voorafgaand aan de annealing bij hogere temperatuur cruciaal was voor de initiatie van de vaste matrix. De wachttijd nodig voor deze initiatie nam af bij toenemende temperatuur. Het vaste glycerol smolt bij verhitting bij het smeltpunt van kristallijn glycerol. Vanwege de vervorming van het meetapparaat zelf kan de stijfheid van glycerol in de geometrie van de Couette cel slechts gemeten worden tot ongeveer  $10^7$  Pa, twee ordes van grootte kleiner dan de stijfheid van kristallijn glycerol. Om uit te kunnen sluiten dat het vaste netwerk eenzelfde stijfheid had als kristallijn glycerol veranderden we de geometrie van het experiment naar een plaat-plaat geometrie, waar de grootte van de platen en de afstand ertussen zo gekozen werd dat de vervorming van het meetapparaat verwaarloosbaar was. Een bijkomend voordeel was dat we in deze configuratie het sample met een camera konden bekijken. Tot onze verrassing konden we in de plaat-plaat geometrie de vorming van een vaste fase in het glycerol niet betrouwbaar reproduceren met het thermisch profiel dat we gebruikten in de

Couette cell. We vonden een vaste-stofachtig gedrag van het glycerol slechts in één van de zes uitgevoerde metingen. In deze meting groeide een sponsachtige fase van de bovenste plaat, met de groeisnelheid van de kristallijne fase. De schuif modulus van deze sponsachtige fase was echter twee ordes van grootte kleiner dan de schuif modulus van de kristallijne fase, die we maten in een seeded sample.

In hoofdstuk 4 bestudeerden we een dunne glycerol film met daarin een lage concentratie fluorescerende moleculen met de techniek van fluorescentiemicroscopie. In deze techniek is de intensiteit van fluorescentie op een gegeven plek in het sample een maat voor de lokale concentratie van de fluoroforen en geeft daarmee informatie over de structuur van het sample. We vonden twee verschillende heterogene patronen van fluorescentieintensiteit, afhankelijk van de snelheid van de afkoeling van het sample. Een sample dat langzaam werd afgekoeld liet een patroon zien als een gatenkaas, met donkere gaten van micrometer grootte in een heldere achtergrond. In een sample dat snel afgekoeld werd zagen we een patroon met vele heldere eilanden van micrometer grootte verstrooid in een donkere matrix. Deze twee heterogene patronen, gevormd door een inhomogene verdeling van fluorescerende moleculen in de glycerol film, bleven onveranderd gedurende enkele dagen als het sample niet significant verhit werd. Dit suggereert vorming van stabiele dichtheidsfluctuaties van micrometer grootte in onderkoeld glycerol.

De resultaten uit de hoofdstukken 2 en 3 brengen een belangrijke vraag naar voren: wat is de structuur van de waargenomen vaste-stofachtige toestand van glycerol? Het lijkt erop dat het waargenomen viscoelastische gedrag te maken heeft met de groei van een kristallijne structuur in onderkoeld glycerol. Immers, de vaste structuren groeiden met min of meer dezelfde snelheid als het kristal en smolten bij het smeltpunt van kristallijn glycerol. Daartegenover staat dat de gemeten stijfheid van het vaste glycerol twee ordes van grootte kleiner is dan dat van kristallijn glycerol. Daarnaast leken de metingen in hoofdstuk vier te wijzen op een afwezigheid van grote microkristallen, ongeacht de snelheid van afkoeling van het glycerol.

In hoofdstuk 5 probeerden we meer te leren over de vaste toestand van glycerol door het doen van verstrooiingsexperimenten met neutronen. We voerden metingen uit aan twee samples van glycerol, met thermische preparatie vergelijkbaar met die in hoofdstuk 2. Slechts in een van beide samples zagen we het ontstaan van vaste structuren, waargenomen zowel via de verstrooiingsspectra van de neutronen als via inspectie met het blote oog. Een nieuwe piek in de spectra, gecentreerd rond  $0.1 \text{ \AA}^{-1}$ , is het teken aan de wand voor deze vaste toestand, aangezien deze piek duidelijk afwezig is bij glycerol in de volledig

vloeibare toestand en bij het kristal bij dezelfde temperatuur. Maar, aangezien het gekozen meetbereik (van 0.008 tot 0.431 Å<sup>-1</sup>) niet het bereik omvatte waar normaal de Braggpieken van de kristallijne structuur waargenomen worden (van 0.5 tot 5 Å<sup>-1</sup>), konden we niet bevestigen of de vaste vorm van glycerol kristallijn van nature is. Toekomstige metingen in dit meetbereik zullen meer inzicht geven in de precieze structuur van de vaste toestand van glycerol.

## **Temperatuurcycli van polyprolines gelabeld met een enkel paar van fluoroforen**

Het is de droom van iedere experimentele natuurkundige die met fluorescentiemicroscopie van enkele moleculen werkt om het signaal van een enkel molecuul oneindig lang te kunnen observeren en de snelle bewegingen van dit molecuul in alle detail te kunnen volgen. Tegenwoordig is het mogelijk om een enkel geïmmobiliseerd fluorescerend molecuul in een oplossing bij kamertemperatuur gedurende enkele minuten te bekijken door het toevoegen van triplet quenchers en zuurstof “scavengers”. De tijdsresolutie van dit soort experimenten is echter nog steeds gelimiteerd tot enkele milliseconden, de tijd die nodig is om uit dit molecuul genoeg fotonen te verzamelen om een redelijke signaal-ruis verhouding te bereiken. Om een langere observatietijd mogelijk te maken zonder moleculen te hoeven immobiliseren en tegelijkertijd snelle bewegingen van de moleculen te kunnen volgen op tijdschalen van enkele microseconden hebben we onlangs een nieuwe methode van temperatuurcycli microscopie voorgesteld.

In hoofdstuk 6 lieten we zien hoe deze methode gebruikt kan worden om de conformatiedynamica van polyprolines te bestuderen. De conformaties van het polyproline kunnen indirect bekeken worden via Förster Resonant Energy Transfer (FRET) tussen twee fluoroforen die bevestigd zijn aan de beide uiteinden van het polyproline molecuul. FRET is een niet radiatieve energie overdracht tussen een donor en een acceptor molecuul. De efficiëntie van de overdracht is een functie van de spectrale overlap tussen het emissiespectrum van de donor en het absorptiespectrum van de acceptor, en de relatieve oriëntatie en afstand tussen beide moleculen. In een experiment kan deze efficiëntie gemeten worden door de fluorescentie van beide fluoroforen te detecteren. Omdat de efficiëntie van de energie overdracht afhangt van de afstand tussen de moleculen, kan FRET worden gebruikt om afstanden te meten op moleculaire schaal, als de eigenschappen van het acceptor en donor molecuul bekend zijn. Eerst maten we de statische FRET efficiency van bevroren polyproline 6 and polyproline 20 bij lage temperatuur in glycerol. Beide metingen lieten een

brede distributie van FRET efficiënties zien. Deze verbreding ontstond door de grote spreiding in de orientatiefactor en de spreiding in de afstand tussen de fluorescerende moleculen. We bestudeerden de mogelijke variaties in signalen van het donor molecuul en het acceptor molecuul in het FRET paar door het fluorescentiesignaal van enkele paren gedurende een langere tijd te meten. We namen drie typen gebeurtenissen waar. (1) Een correlatie tussen de twee signalen, dat wil zeggen een intensiteit van het acceptorsignaal dat positief gecorreleerd is met de intensiteit van de donor, zagen wij als de donor in een donkere toestand verkeerde of gebleekt was. (2) Een afwezigheid van correlatie, dat wil zeggen een intensiteit van de acceptor die onafhankelijk is van de intensiteit van de donor, zagen we als de acceptor in een niet fluorescerende toestand was waarin nog steeds de donor gequenched kan worden. Deze situatie ontstaat waarschijnlijk doordat de acceptor absorptiespectrum niet veranderd is, hoewel zijn fluorescentie uitgeblust is. De energieoverdracht tussen de moleculen blijft dus zo efficiënt als in de fluorescerende toestand van de acceptor. (3) Een anti-correlatie tussen het donor- en het acceptor signaal werd waargenomen als één van de niet fluorescerende vormen van de acceptor de opgenomen energie van de donor niet meer kan ontvangen. Dat kan worden veroorzaakt door een blauwverschuiving van het acceptorabsorptiespectrum na zijn photobleaching.

We voerden onze eerste metingen met temperatuurcycli uit op het polypropylene6 en waren in staat om de reoriëntaties van de labels als gevolg van de temperatuurcycli te detecteren door het meten van de FRET efficiëntie. Deze eerste metingen laten zien dat de door ons voorgestelde methode van temperatuurcycli aan enkele moleculen in combinatie met FRET enkele moleculen mogelijkheden biedt voor het bestuderen van de dynamica van eiwitvouwing op het niveau van een enkel molecuul.



## List of Publications

- M. E. Möbius, T. Xia, W. van Saarloos, M. Orrit, and M. van Hecke “Aging and solidification of supercooled glycerol”, *submitted to J. Phys. Chem. B*.
- F. Kulzer, T. Xia, and M. Orrit, “Single molecules as optical nanoprobe for soft and complex matter”, *Angew. Chem. Int. Ed.* **49** (2010) 854–866.
- T. Xia, L. Xiao, and M. Orrit, “Micro-sized structure in a thin glycerol film revealed by fluorescent probes”, *J. Phys. Chem. B* **113** (2009) 15724–15729.
- T. Xia, M. Orrit, C. Storm, and W. van Saarloos, “Verrassend gedrag van onderkoeld glycerol boven de glasovergang”, *Nederlands Tijdschrift voor Natuurkunde* **74-10** (2008) 340.
- R. Zondervan, T. Xia, H. van der Meer, C. Storm, F. Kulzer, W. van Saarloos, and M. Orrit, “Soft glassy rheology of supercooled molecular liquids”, *Proc. Natl. Acad. Sci. USA* **13** (2008) 4993–4998.

---

## Curriculum Vitae

Ted (Tie) Xia, born in Dalian (Liaoning, China) on 25<sup>th</sup> June, 1977.

Ted Xia completed his BSc degree in medicine at Beijing College of Acupuncture and Orthopedics (now Beijing University of Chinese Medicine since August 2000) from September 1995 to July 2000. He then worked as a technical support, first in Beijing PUSRY Biological Technology Ltd from December 2000 to November 2001 and then in Pel-Freez Biotechnology (Beijing) Ltd (now Invitrogen Beijing Office since 2005) from December 2001 to September 2003. During these periods he was mainly responsible for HLA (human leukocyte antigen) genotyping kits based on sequence-based typing (SBT) and reference strand conformational analysis (RSCA). In September 2003, he came to The Netherlands and started his Master study (Biomolecular Sciences) at Utrecht University and got his MSc degree in Chemistry in August 2005. During this period, he conducted two Master projects at Utrecht University. The major one entitled “Identification of plasma membrane associated gene products upregulated at infection sites in *Arabidopsis thaliana* by *Hyaloperonospora parasitica*” was carried out in the Molecular Genetics Group led by Dr. Guido Van den Ackerveken. The minor one on “Study *Drosophila melanogaster* polybromo with NMR spectroscopy” was performed in the Department of NMR spectroscopy and was supervised by Prof. Rolf Boelens.

He joined the Institute of Physics at Leiden University as a PhD candidate in September 2005 under the supervision of Prof. Michel Orrit. He worked on probing heterogeneity in supercooled liquids and temperature-cycle microscopy of single-molecule FRET in polyprolines. The results of this work are presented in this thesis. During his PhD period, he assisted the second-year Bachelor practical course on “Michelson interferometer” and supervised two Master projects. In May 2010, he will start a postdoctoral appointment in the group of Prof. Fang Xiaohong in the Key Laboratory of Molecular Nanostructure and Nanotechnology, Institute of Chemistry, The Chinese Academy of Sciences (CAS).



---

## Nawoord

At the end of this thesis, I would like to acknowledge the people involved in my scientific and nonscientific lives during my stay in Leiden. Without them, this work would not be possible.

I am very grateful to Michel Orrit for offering me the possibility to make the transition from molecular biology to molecular physics and for his guidance, experience, and patience. Rob Zondervan and Florian Kulzer, two important people in the beginning of my PhD period, taught me how to work with optics and electronics in the lab. Although they left one after another, their support has never stopped; especially Florian, who always answered my questions in great detail. My thanks also go to other former members: Clemens Hofmann, Meindert van Dijk, and Alexander Wirtz were always ready to help me. Aurélien Nicolet, who rejoined the group as a Postdoc, helped me solve a lot of L<sup>A</sup>T<sub>E</sub>X-related problems during the preparation of this thesis. In the last two years, I shared an office with Alexander Gaiduk and Paul Ruijgrok. I very much enjoyed the cosy and pleasant atmosphere they created. Alexander, an expert in Labview programming, helped me improve the control software for my experiments. Paul, a very good English-to-Dutch translator, did an excellent job with the *Samenvatting* of this thesis. I am very thankful for the endless amounts of the advice and help that I received from these two roommates. I am also deeply indebted to Haifeng Yuan, a talented Master student (now a PhD candidate in the group since September 2009), who contributed a lot to the snapshot project. Without his presence, this thesis would not have been finished on time. I want to thank Liantuan Xiao, a visiting professor from Shanxi University (China), for his contribution to the work presented in Chapter 4 and for the helpful discussions we had during his stay about the field of single-molecule optics in China.

It is difficult to forget the other members of the group: Harmen van der Meer and Jos Disselhorst, two dedicated technicians, whose work is always effective and professional, Peter Gast, who often keeps me posted about what has happened in China during the lunch break, Robin Purchase, who taught me how to use English in an English way, Silvia Sottini, for organizing soccer games on Thursday afternoon in the past (I miss those games), Henriëtte van Leeuwen, who makes sure that we can focus on scientific work without

---

nonscientific distractions, Edgar Groenen, Silvia Völker, and Martina Huber for their help to improve my thesis.

I want to thank Arno van Amersfoort for rescuing my computer many times, Matthias Möbius for sharing satisfying moments in “torturing” glycerol on the seventh floor, and Fan-Tso Chien for many enjoyable discussions about sciences and personal life.

I am thankful to Mrs. Somer, my landlady, for her hospitality and kindness during my stay in Wassenaar. I am also grateful to the Tang family for wonderful Chinese meals every Tuesday evening and the joyful time I had at their place and Kamlung Cheng for being my closest friend during the last six years. Finally, I would like to thank my mom for her encourage and unconditional support and my wife for her love and understanding through the years.